AMERICAN UNIVERSITY OF BEIRUT

OPTIMIZATION OF A SOLAR PHOTOVOLTAIC MICRO GRID FOR ELECTRICITY AND DESALINATED WATER SUPPLY

by
ADNAN ALI ZEIN

A dissertation
submitted in partial fulfillment of the requirements
for the degree of Doctor of Philosophy
to the Department of Electrical and Communication Engineering
of the Maroun Samaan Faculty of Engineering and Architecture
at the American University of Beirut

Beirut, Lebanon
August 2023

AMERICAN UNIVERSITY OF BEIRUT

OPTIMIZATION OF A SOLAR PHOTOVOLTAIC MICRO GRID

FOR ELECTRICITY AND DESALINATED WATER SUPPLY

by
ADNAN ZEIN

Approved by:

_____
Dr. Sami Karaki, Professor   Advisor
Electrical and Computer Engineering, AUB

_____
Dr. Riad Chedid, Professor   Committee Chair
Electrical and Computer Engineering, AUB

_____
Dr. Rabih Jabr, Professor   Member of Committee
Electrical and Computer Engineering, AUB

_____
Dr. Mahmoud Al-Hindi, Associate Professor   Member of Committee
Chemical Engineering and Advanced Energy, AUB
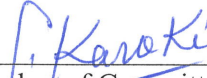
_____
Dr. Hadi Kanaan, Professor   on his behalf.   Member of Committee
ESIB, University Saint Joseph (External)

_____
Dr. Francesco Calise, Professor   on his behalf   Member of Committee
Industrial Engineering, University of Naples Federico II (External)

Date of dissertation defense: August 28, 2023

2

AMERICAN UNIVERSITY OF BEIRUT

DISSERTATION RELEASE FORM

Student Name: Zein_____Adnan_____Ali_____
                 Last   First   Middle

I authorize the American University of Beirut, to: (a) reproduce hard or electronic copies of my dissertation; (b) include such copies in the archives and digital repositories of the University; and (c) make freely available such copies to third parties for research or educational purposes:

☒ As of the date of submission

☐ One year from the date of submission of my dissertation.

☐ Two years from the date of submission of my dissertation.

☐ Three years from the date of submission of my dissertation.

_____07/09/2023_____
Signature   Date

ACKNOWLEDGEMENTS

ABSTRACT
OF THE DISSERTATION OF

Adnan Ali Zein   for   Doctor of Philosophy
                                     Major: Electrical and Computer Engineering

Title: Optimization of a Solar Photovoltaic Micro Grid for Electricity and Desalinated Water Supply

Renewable energy is promising to become a major resource for future communities, while water scarcity is becoming a major threat. The use of solar photovoltaic (PV) to power reverse osmosis (RO) plants and produce water will enhance the sustainability of water supplies in several dry coastal areas. Varying the operating power level of the RO plant has been proposed in the literature as a solution to accommodate intermittent PV power sources. Such variable operation is intended to match the RO load to the available PV power. Nevertheless, such operation has not been used outside research laboratories and small pilot plants. In this work, different case studies to evaluate the benefit of using variable operation and its effects on system design, system operation and levelized cost of water (LCOW) were investigated. A simulation model for the optimal operation of the system is developed using three-dimensional dynamic programming (DP) to determine the power levels of the PV generators, battery, diesel generator, and RO plant while optimal sizing of these plants and associated water tanks was solved using an ordinal optimization (OO) approach. Simulations are performed under a MATLAB environment. The use of OO permitted the examination of a large design search space quickly but exhaustively using a simple model. The different designs were then ranked in increasing cost order and assessed a reduced number of these using an accurate model to simulate the system operation on an hourly basis for all the days of the year. This approach relies on the fundamental tenet of OO: "order is robust to the noise introduced by the simple model". Different power modulation strategies are investigated, and their implications on the hydraulic operating parameters are presented. The operation of the RO system at varying power levels and different sizes of backup systems (battery and diesel generator) was investigated. This ability to vary the RO operating level helped in a better matching of the system load to the available, yet variable, PV power, even when the backup and storage systems were at a minimum. Operating an RO plant with PV and backup systems is found to be far more cost effective than operating it without backup systems, reducing costs by 37-57% for the case studies considered.

Keywords: Variable Operation, Reverse Osmosis, Renewable Energy, Dynamic Programming, Ordinal Optimization.

TABLE OF CONTENTS

ILLUSTRATIONS

TABLES

ABBREVIATIONS

A_j Annuity factor of component j with 5% rate

B_i Battery power

B_{min} Minimum operation level of the battery

B_{max} Maximum operation level of the battery

BSS   Battery Storage System

D_i Dumped power at time i

DG   Diesel Generator

DP   Dynamic Programming

E_B Battery capacity

E_{life} Total expected battery energy over its lifetime

G_i Diesel generator power

G_{max} Maximum power operation level of the generator

G_{min} Minimum power operation level of the generator

I_j Initial investment cost of component j

LCOW   Levelized Cost Of Water

NDOD   Expected battery number of cycles at given DOD

NV   Total number of PV panels

OO   Ordinal Optimization

P_i Power delivered by the PV generator at time i

PV   Photovoltaic

$P(STC)$ Nominal PV power at STC

QD_i Flow of water out of tank at time i

QP_i Flow of water into tank at time i

R_i Reverse osmosis load

R_{max} Maximum operation level of the RO

R_{min} Minimum operation level of the RO

RO   Reverse Osmosis

S_i Solar Irradiance level at time i

SOC_{max} Maximum state of charge

SOC_{min} Minimum state of charge

T_i PV Module temperature at time i

T_{year}	Number of hours per year 8760
W_{max}	Maximum operating volume level of the RO
W_{min}	Minimum operating volume level of the RO
WST	Water Storage Tank
δ_B	Measure of battery degradation
Δ_h	Duration of one time period, equals 1 hour
$\varphi_G(G_i)$	Diesel fuel consumption as a quadratic function
γ	PV panel power temperature coefficient

I would like to dedicate this research to my greatest supporter, my beloved wife,

Africa de Robert.

CHAPTER 1

INTRODUCTION

This chapter is a general introduction to the work done in this thesis. Section 1.1 exposes the background that led us to work on this topic. Section 1.2 presents the dissertation contributions, and section 1.3 describes the structure of this document.

1.1. Background

Renewable energy is becoming an important player in the energy sector and is promising to become a major resource for future communities. With increasing populations and water requirements for human activities, water scarcity is growing, especially in areas with high solar irradiation. The utilization of renewable energy for fresh water production in desalination plants is currently attracting significant research effort (Castro et al., 2020), (Borge-Diez et al., 2021) (Giovanni et al., 2021) (Nassrullah et al., 2020) (Ghazi et al., 2022) (Rosales-Asensio et al., 2022).

The primary challenge in utilizing renewable energy (RE) for RO desalination systems lies in its intermittent nature. Despite the cost reductions and improved efficiencies of lithium-ion battery storage systems (BSS) in recent years, their integration still requires a significant investment. When faced with extended periods of adverse weather conditions, system designers have two options for meeting the load requirements: either oversized BSS to accommodate the worst days of the year or incorporate backup diesel generators. For islands, remote areas, or military bases, reducing the dependence on such backup diesel generators is a strategic objective as it comes at a higher cost than that of standalone solar systems. For this reason, researchers proposed a different approach for overcoming RE intermittencies: by varying the power level of the RO plant to match it with solar or wind resources. Thus, large amounts of water are

desalinated during high RE production times and the resulting potable water is stored in water storage tanks (WST) for later use.

Stand-alone PV-RO systems suffer from the impossibility of balancing the sizes of solar generators and water demand. On the one hand, a small solar generator can only supply enough power to an RO system for a limited amount of time during day hours, on the other hand, increasing the size of the solar generator results in wasting larger portions of available but unused solar power (when available solar power surpasses the maximum operation power of the RO). If a steady state (fixed power level) operation regime is considered, this balancing challenge strongly affects RO running time, as the operation window is restricted to the periods of the day where available solar power is equal or greater than the needed fixed power level. If a variable operation regime is considered instead, this dilemma still affects running time, but to a lesser extent, as variable operation requires a certain minimum level of power supply to keep system parameters within the safe operation window (SOW) of the RO membranes. Combining RO plants with PV generators, a battery storage system (BSS), a water storage tank (WST) and a diesel generator (DG) introduces a much-needed flexibility into the system and is here demonstrated to strongly reduce the overall cost of water. In fact, the main contribution of this work is to show that integrating backup systems (DG, BSS, and WST) always leads to lower levelized cost of water (LCOW).

Conventional RO plants operate with quasi-constant feed pressure and quasi-constant flow rate, while direct coupling to Renewable Energy (RE) sources require modulation of power consumption and thus modulation of hydraulic parameters. In fact, manufacturers of RO membranes usually give guarantees for their products under recommended steady conditions (Dow Chemicals, 2022). Despite these manufacturers restrictions, researchers have tested power modulation on pilot projects, and their conclusions ranged from no deterioration (Abufayed, 2003) (Latorre et al., 2015) to improved performance (Subiela et al., 2009) (Al-Bastak & Abbas,

1998) of the membranes under variable operation. This improved performance is explained by improved diffusion and reduced concentration polarization resulting from increased turbulence caused by fluctuating pressure and flow rates inside the membranes. An investigation by (Richards et al., 2015) evaluated the effects of irradiation transients on the RO performance, by varying the solar input power level and transient occurrence frequency. They reported good overall performance, noting positive effects of a varying feed pressure level on the membrane's performance. (Ruiz-García & Nuez, Long-term intermittent operation of a full-scale BWRO desalination plant, 2020) analyzed the operation data over 14-years, for about 9 hours per day, of an intermittently operated RO plant and concluded that daily shutdowns and start-ups did not cause additional problems in the desalination plant, indicating that intermittent operation of BWRO desalination plants is feasible over the long term. The permeability of RO membranes declines with usage, (Freire-Gormaly & Bilton, Impact of intermittent operation on reverse osmosis membrane fouling for brackish groundwater desalination systems, 2019) compared intermittent and continuous operations with regards to RO membrane fouling for brackish water and concluded that the decline of the membrane permeability can be reduced in intermittent operation with a permeate water rinse before shutdown period. The same authors studied the effect of components sizing of a PV-RO system (Freire-Gormaly & Bilton, Design of photovoltaic powered reverse osmosis desalination systems considering membrane fouling caused by intermittent operation, 2019) and concluded that neglecting membranes fouling in such studies would result in under-sized systems. In this work, fouling simulation was not included as it does not align with the main objectives of this research and would not impact a variable RO system more than a constant operation RO system.

The modulation of RO power requires the operation of the reverse osmosis membranes in varying pressure and flow conditions. The study of these variable conditions leads to the concept of safe operating window (SOW), which was first proposed by Feron back in 1985 (Feron,

1985). In a more in-depth analysis, (Pohl et al., 2009) used the ROSA software (predecessor of the software WAVE) to build the SOW of a commercial membrane by varying its operating conditions. Pohl et al. found out that a constant permeate recovery strategy would be the best choice for a variable RO operation, as it allows low specific energy consumption (SEC) values over a large power operating range, while constant feed pressure strategy is only beneficial when the system operates around its nominal power. (Richards et al., 2014) detailed a method to construct experimentally the SOW for any membrane and any feed water salinity and compared different operating strategies. Although the authors' measurements confirmed that a constant recovery strategy is the most efficient one as suggested by (Pohl et al., 2009), they argued that such operation strategy increases system complexity. (Mito et al., 2022) installed a test rig using an RO system with a split-feed flow configuration. They tested different strategies and concluded that constant brine flow strategy offers the widest operation range and lowest SEC, contrary to previous studies. Differences between these results are explained by the fact that different number of membranes per pressure vessel are considered, and variations in membrane characteristics studied, including permeability coefficients and feed spacer geometries affect optimization results as noted in (Ruiz-García & Nuez, Simulation-based assessment of safe operating windows and optimization in full-scale seawater reverse osmosis systems, 2022).

More recent studies have tackled variable RO operation conditions. (Modarresi et al., 2020) coupled a portable nano-filtration unit with PV panels, batteries, and a water tank, and compared variable pressure operation with fixed pressure, and concluded that there is a 20% reduction in yearly costs using variable operation. From the design side of the problem, the authors pre-designed some of the system elements, fixing the battery capacity, NF system size, and only optimizing the number of PV panels used. (Heihsel et al., 2019) analyzed the economic benefit of installing intermittently operated RO plants coupled with renewable energies in coastal areas of Australia and concluded that desalination plants are particularly suitable for load-shifting and

may reduce both, the LCOE by 43% and the required utility grid capacity by 29%. A thorough study presented by (Carta & Cabrera, 2021) assesses the cost effectiveness of using wind turbines with a flywheel to operate a standalone RO system with hourly water requirements. The authors modulated the RO operation such that permeate water concentration was fixed and concluded that variable operation reduces water cost by about 14% compared to an on-off strategy.

1.2. Dissertation Contributions

Research papers published on the topic of variable RO operation have predominantly focused either on the short term (transients, hours) operation of a stand-alone PV-RO (and sometimes storage) (Mito et al., 2022) (Jiang et al., 2015) (Leijon et al., 2020) without including it in a full techno-economic context with seasonal variations or have focused on system economics (Loutatidou et al., 2017), omitting detailed operation parameters. As a result, it is not yet clear if and where variable operation of RO systems is actually beneficial. The work done in this dissertation tries to fill this gap by offering both a detailed technical simulation model, while taking into consideration the main economic indicators.

(Zein et al., 2018) studies a microgrid supplying both water and electricity to a remote community, where the RO specific power consumption represented an average value of about 2.28 kWh/m^3. The RO plant was operated using a rule-based controller, i.e., turning it on when excess solar energy is available, or when the water level inside the tank drops below minimum. In this work, a flexible and accurate RO system model that accounts for hydraulic and mechanical variability affecting power consumption and cost estimation was developed. The RO plant model was integrated with models of a PV plant, a battery, and a diesel generator using the method of dynamic programming (DP) to determine the hourly level of operation over a year. The two-dimensional method (Karaki et al., 2015), applied for the design of fuel-cell car

components, was extended to calculate the power mix of three subsystems: The RO plant, the diesel generator, and the battery. This facilitated the assessment of the variable operation of the RO system as presented in this work. The objective is to minimize the cost of system operation accounting for diesel fuel usage, and battery degradation. Ordinal optimization (OO) was used to examine the design search space of different sizes of the RO, PV, water tanks, and diesel generator, and select the ones that yield a minimum levelized cost of water. The design search space is large, but it is quickly and exhaustively examined using a simple model. The different designs are thus assessed and then ranked in increasing cost order. A reduced number of designs, as predicted by the OO theory, are then simulated using an accurate model on an hourly basis for all the days of a year and an accurate system cost is computed. This approach relies on the fundamental tenet of OO, which states that order obtained through the simple model is robust to noise introduced by the model simplification. The simple model samples the year using only 48 days and allows three operational levels of the RO plant and three levels of the diesel generator (DG). The accurate model allows for more DG and RO power levels, e.g., 5 to 7 levels for each. By utilizing OO, the number and complexity of the simulation runs needed to obtain a system design are significantly reduced. The optimal sizing and operational results are presented for five different case studies, with the objective of minimizing the yearly cost of operation of water production.

1.3. Dissertation structure

This dissertation is presented in six chapters.

Chapter 1 is a general introduction on utilization of renewable energy systems in desalination plants, a literature review focusing on PV-RO, and a review of the challenges and gaps in the variable RO operation methods, the main research objectives, innovations, and dissertation structure.

Chapter 2 presents the general design of the system, a proposed strategy to simulate it, and the method used to find its optimal solution, highlighting in particular the Ordinal Optimization and Dynamic Programming techniques.

Chapter 3 outlines the system model, describing the different approximations and equations used to represent all the system components (Solar system, battery storage, reverse osmosis plant, diesel generator, and the water storage. An emphasis is given to the RO system model developed.

Chapter 4 gives the simulation results obtained and analyzes the energy dynamics and system sizing considerations and efficiencies of a solar based reverse osmosis system.

Chapter 5 summarizes the Dissertation and concludes with corresponding challenges to address in future work.

Chapter 6 lists bibliographic citations for the whole Dissertation.

CHAPTER 2

PROBLEM FORMULATION AND OPTIMIZATION TECHNIQUES USED

This chapter describes the system topology and methods used to develop the simultion model. Section 2.1 provides the solar powered reverse osmosis system topology used. Section 2.2 describes the ordinal optimization technique used in optimal sizing of the system components, while section 2.3 describes the dynamic programing technique used to find optimal hourly operation steps. Section 2.4 describes how both optimization techniques where coupled together for simultaneous sizing and operation optimization.

2.1. Introduction – Solar powered RO

A solar-powered reverse osmosis (RO) system utilizes solar energy to power the desalination process and produce fresh water from seawater or brackish water sources. The operation of a solar-powered RO system involves several key components and processes:

Solar Photovoltaic (PV) Panels: PV panels are used to capture sunlight and convert it into electricity. These panels consist of multiple solar cells made of semiconducting materials that generate direct current (DC) electricity when exposed to sunlight.

Energy Conversion and Storage: The DC electricity generated by the PV panels is converted into alternating current (AC) electricity using an inverter. This AC electricity can be directly used to power the RO system. Additionally, energy storage systems such as batteries can be integrated into the system to store excess electricity generated during peak sunlight hours for use during periods of low solar irradiation.

Diesel Generator units: stand by diesel generators can also be used to directly provide AC power to the system whenever necessary.

Sea Water Intake: typically consists of various elements designed to ensure the efficient and sustainable extraction of seawater while minimizing the intake of debris, organisms, and sediments that could potentially affect the performance of the RO system.

Pre-Treatment: Before entering the RO system, the feed water undergoes pre-treatment processes to remove particulates, sediments, and other impurities. Pre-treatment typically involves filtration, sedimentation, and disinfection to ensure the water meets the required quality standards and protect the RO membranes from fouling or damage.

Reverse Osmosis Process: The heart of the system is the reverse osmosis process, where the feed water is pressurized and passed through a semi-permeable membrane. This membrane selectively allows water molecules to pass through, while rejecting dissolved salts, minerals, and other contaminants. The applied pressure helps overcome the osmotic pressure, allowing the production of purified water, known as permeate, and a concentrated brine stream.

Energy Recovery Devices (ERDs): systems that enable the recovery and reuse of energy from the concentrated brine stream generated during the desalination process. Since RO systems operate under high pressures, a significant amount of energy is required to pump water through the membrane and generate fresh water. These devices work by transferring the pressure energy from the brine to the incoming feed water. The primary purpose of using ERDs in RO systems is to improve overall energy efficiency and reduce operational costs.

Post-Treatment: The permeate from the RO process may undergo post-treatment processes to further improve its quality and ensure it meets the required standards for various applications. Post-treatment can include remineralization, pH adjustment, disinfection, and other processes to optimize water quality for specific uses.

Water Storage Tank: simple water collection tanks used as a buffer between the production flow and consumption flow.

System Monitoring and Control: A solar-powered RO system incorporates monitoring and control mechanisms to optimize performance and ensure efficient operation. This includes monitoring solar irradiation levels, energy production, water flow rates, pressure, and other parameters. Automated control systems can adjust operating parameters, such as feed water flow rates, based on real-time solar energy availability and water demand to maximize system efficiency.

Overall, a solar-powered reverse osmosis system combines the use of solar energy, advanced membrane technology, and water treatment processes to provide a sustainable and environmentally friendly solution for freshwater production from saline or brackish water sources. The operation of the system involves harnessing solar energy, treating the feed water, passing it through RO membranes, and ensuring the quality of the produced water through pre- and post-treatment processes.

The topology of the proposed system is shown in Figure 1. The system consists of a microgrid with the following components: a diesel generator (DG), a battery storage system (BSS), an RO plant, a PV generator, and a water storage tank (WST).
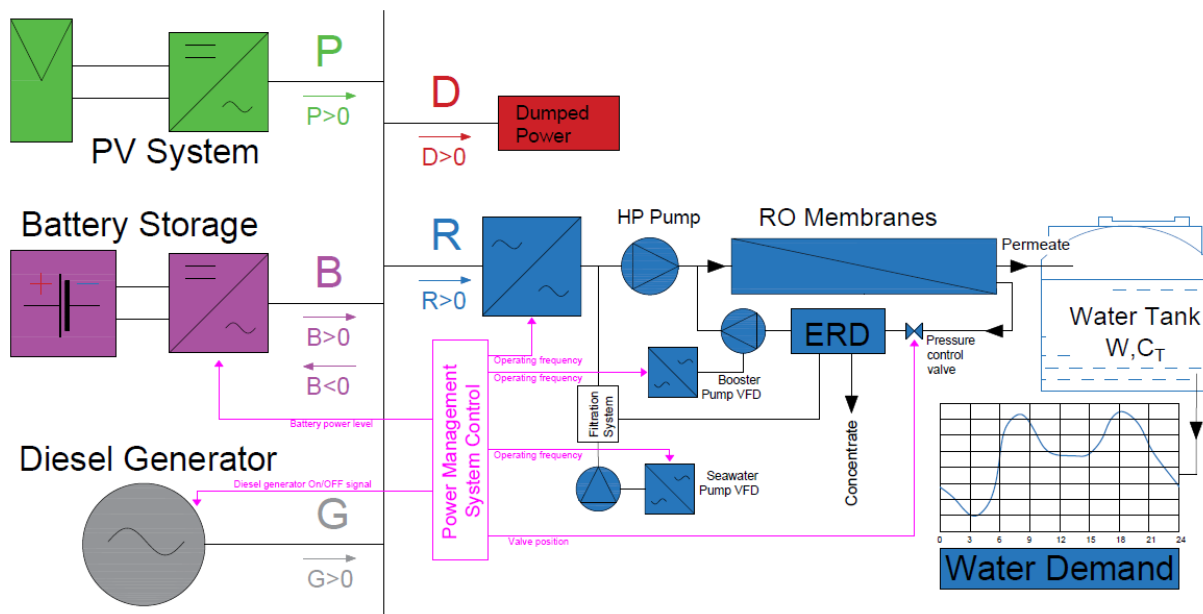
Figure 1. Topology of system with power control signals

The proposed hybrid system is composed of a variety of complex components, with non-linear operation regimes, varying efficiencies, and restrictions on allowable operating ranges. To name a few, safe RO system operation is limited to a window of input/output conditions that restricts operating range. The set of pumps included in the RO system have varying efficiencies depending on the chosen hydraulic operating points, which in turn have an effect on the desalted water output flow and salinity. In addition, the shutdown and startup of RO systems should respect minimum up and down times for the sake of membranes longevity and to allow backwash cleaning of the membranes. Diesel generators and battery storage systems have non-linear efficiencies, while solar radiation variability adds an additional layer of complexity.

In order to make realistic evaluations of such a system, the use of detailed models of its components is essential. The detailed models of the various components, which are described below, were integrated into the DP-based simulation using hourly data points.

A power management and control system is used to operate the BSS, the RO plant, and the DG. The electric power level consumed by the RO system is controlled through a variation of the operating frequency of its pumps, and by controlling the position of the concentrate pressure valve. This controller also manages the charging and discharging powers of the battery and turns on or off the diesel generator in a way to guarantee system stability and to minimize costs. If the BSS is full, the excess solar energy is dumped (not produced by shifting the MPPT voltage of the PV plant).

2.2. Ordinal Optimization for Components Sizing (OO)

Sustainable management of freshwater along coastal aquifers is imperative to protect the economic, social, and environmental security of coastal communities as large populations rely on these reservoirs. Enforcing a well-founded management strategy requires an understanding of the dynamic of SWI in response to the factors influencing the intrusion.

The OO theory provides a probabilistic framework for reducing the search space and the computational effort involved in ranking the different alternatives. OO is based on the idea that the relative order of different alternatives in a decision problem is robust with respect to estimation noise. This implies that if a set of alternatives is very approximately evaluated and ordered according to this approximate evaluation, then there is high probability that the actual good alternatives can be found in the top-s estimated good choices.

(Jabr & Pal, 2009) used OO to locate and size distributed generators on power distribution-grid nodes. The OO formulation used in this work is closely based on their approach. A similar approach was used by (Karaki et al., 2015) in sizing the components of a fuel cell car. The overall sizing optimization logic is summarized in Figure 2. The steps for OO implementation are described in the following paragraphs.
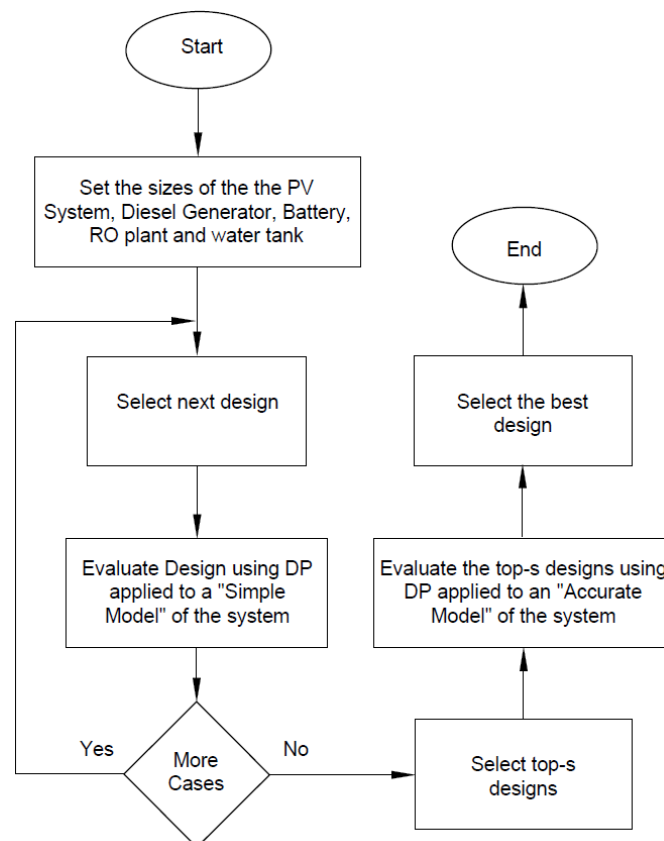
Figure 2. Ordinal Optimization of components sizes for minimum cost

Reduce the Search Space: let Θ represent the population of all designs, and Λ represents the population of the top α-percent designs in Θ. If we randomly pick N designs in Θ, the probability that at least one of these designs is in Λ is $1 - (1 - \alpha)^N$. If this probability is desired to be at least P, then N should be chosen as follows: (Luo et al., 2001)

2.
$$N \geq \frac{\ln(1-P)}{\ln(1-\alpha)} \tag{1}$$

Choosing $P = 99.9\%$, and $\alpha = 0.3\%$, then N should be at least 2300. In reality, the choice of the N alternatives is enhanced by a heuristic choice based on knowledge of the water and electricity needs and associated component sizes. Thus, N is an upper limit for the number of designs that respect P.

Rank the Alternative Designs: a simple model of the system is applied on all N alternative designs of the reduced search space, then these are ranked according to their year costs.

Find the Size of the top-s Designs: let S denote the subset of the top-s alternative designs among the above ordered N designs using the simple model and let the actual top-g designs denote the good enough subset G, that is, the truly good enough designs are the top-g alternatives among the accurately ordered N designs. By assuming an infinite variance of the estimation noise of the simple model relative to the accurate model, it is possible to compute the value s such that at least k truly good enough alternatives are in S with a given value of the alignment probability:

$$3. \quad AP(k) = Prob(|G \cap S| \geq k) = \sum_{i=k}^{\min(g,s)} \frac{\binom{g}{i}\binom{N-g}{s-i}}{\binom{N}{s}} \tag{2}$$

If $k = 1$ is chosen, the value of s that gives $AP(1) \geq 0.975$ is the number of top-s designs to be chosen among the N designs, ordered using the simple model, with a 97.5% chance that at least 1 of these s-designs is among the truly top-g designs. Choosing N= 2304 and g= 115 (5% of N), the s value for $AP(1) \geq 0.975$ is 72 designs.

Rank the Top-s Designs with an Accurate Model: now that we have a small set of designs to test (top-s designs), we will use an accurate model to determine the cost of operation for each and finally pick the best of the top-s designs.

2.3. Operation Optimization

With a given mix of component sizing, different operating power levels of the battery storage, the diesel generator, and the RO system can be used to optimize costs. The objective is to minimize the yearly cost of the system defined as follows:

$$\min_{n=1...N} \left\{ \sum_j A_j I_j(n) + O_c(n) + M_c(n) \right\} \tag{3}$$

$$O_c(n) = \min \left\{ \sum_{i=1}^{T} [\varphi_G(G_i) + \varphi_B(B_i)] \right\} \tag{4}$$

where $\varphi_G(G_i)$ is a quadratic curve relating fuel consumption costs and electric power generated, and $\varphi_B(B_i)$ is a cost measure of battery degradation. Both functions are defined in Chapter 3 below. The term $\sum_j A_j I_j(n)$ is the sum of the annualized investment costs of each of the system components, $O_c(n)$ is the yearly operation cost and $M_c(n)$ is the yearly maintenance cost for design n. The above objective function is subject to the following constraints. The power balance equation is given by:

$$G_i + B_i + P_i = R_i + D_i \tag{5}$$

The battery state of charge and the water volume in the tank are given by:

$$SOC_i = SOC_{i-1} - \frac{Q_B(B_i)}{C_{bat}} \Delta \tag{6}$$

$$W_i = W_{i-1} + (Q_{Pi} - Q_{Di})\Delta t \tag{7}$$

where $Q_B(B_i)$ is the internal energy rate change of the battery when the battery is delivering a power B_i, and the rest of the variables defined in the diagrams of Figure 1 and Figure 7 . A set of inequality constraints arising from the physical limitations of the components are given by:

$$SOC_{min} \leq SOC_i \leq SOC_{max} \tag{8}$$

$$G_{min} \leq G_i \leq G_{max} \tag{9}$$

$$B_{min} \leq B_i \leq B_{max} \tag{10}$$

$$R_{min} \leq R_i \leq R_{max} \tag{11}$$

$$W_{min} \leq W_i \leq W_{max} \tag{12}$$

$$D_i \geq 0 \tag{13}$$

Constraint (8) is the upper and lower limitation on the state of charge (SOC) of the battery. Constraints (9), (10) and (11) represent the upper and lower power limits of the diesel generator, the battery inverters, and the total reverse osmosis system respectively. Constraint (12) is the upper and lower limits of the water level inside the water storage tank. Constraint (13) simply expresses that curtailed (dumped) solar power can only by positive or null (negative dumped power is meaningless).

The diesel generator and RO system power levels, G_i and R_i, are both discretized in the 3D dynamic programming approach. For each pair of values, the required power from the battery is calculated from the power balance equation (5). The dumped power D_i is usually zero unless the BSS is fully charged. To solve the problem using a 3D DP, solar power P_i is calculated for the 8760h of the year proportionally to PV generator size chosen and simulated solar production. Then cost and effect of each stage of (B_i and R_i) combination is simulated, and using power balance equation (5), G_i and corresponding battery and water storage tank levels are calculated. The objective function (3) will be calculated for all the possible states of the first hour of the year. Then for each state of subsequent hours (i.e., i=2 to 8760), the pssible transitions from states of the previous stage i-1 are identified, and the minimum cumulative cost of reaching each

state is built recursively. When the last stage is reached, the state with minimum cost is recognized, and the preceding states leading to it are identified by a trace-back procedure. each hour of the year. Then for each state of subsequent

2.4. Combined Sizing and Operation Optimization

The problem may be viewed as two interrelated optimization tasks, one being the sizing choices of the components mix, and the other being the search for the best operation corresponding to each particular mix. A large pool of system components sizes is chosen, and a simple model calculation is performed, first using hourly data of 48 days to represent the whole year, and very rough discretization of the diesel generator and RO system power levels, with only 3 different levels allowed (0%, 50%, and 100%). The 48-day simple model is built by reducing the 365 days to 48 days, averaging every 7 to 8 consecutive days into one day, keeping seasonal variations.

Even though an interval of smaller length than 48 days could be used as simple model, this length was chosen in order to account for battery state of charge and its effects on sizing. In fact, if a much smaller number of days is used as a simple model, the initial state of charge of the BSS and the WST (both set to 50%) will artificially reduce the system operation costs, resulting in a bad choice of top-s designs. These top-s designs, representing a limited set of the best component mixes identified using the simple model, are now simulated with the accurate model, using hourly data of 365 days, and 5 different power levels, before being ranked according to total yearly costs. This formulation provides a probabilistic framework that greatly reduces the computation time needed without affecting the final chosen solution.

To validate the choice of the simple model simulations were performed using the 48-day simple model first, the designs were then ranked. All trhe design were then simulated using the accurate model, and it was determined that the simple model ranking gave results that are very

26

close to the accurate model results. In Table 2-1, the ranks of the top-10 system size combinations in the simple and accurate models are shown for Fixed and Variable RO operations. For example, the top design in the accurate model simulation (No. 1) appeared in the simple model simulation as No. 3 in the Fixed RO operation and as No. 2 in the Variable RO operation. The rank number allocated in the simple model is compared to that allocated by the accurate model, using both a variable RO operation mode and a fixed operation mode. We note that system designs highly ranked in the simple model are also being highly ranked in the accurate model, validating the OO approach used.

Table 2-1 Simple and Accurate Model Ranking Comparisons

Rank in Accurate Model	1	2	3	4	5	6	7	8	9	10
Rank in Simple Model – Fixed RO	3	1	2	5	4	6	7	9	8	10
Rank in Simple Model – Variable RO	2	3	4	1	5	7	6	9	8	10

This good alignment demonstrates that the ranking made using the simple model is reliable and allows the relaxation of the percentage of good-enough subset that should be accurately simulated.

The choice of using Dynamic Programming (DP) and Ordinal Optimization (OO) to solve this problem instead of Genetic Algorithms (GA), Particle Swarm Optimization (PSO), or Mixed-Integer Nonlinear Programming (MINLP) is justified as follows:

- DP help us find the optimal operation of a given system design and appropriately determine its cost of operation in a significantly less complex formulation than a MINLP. Formulating the operational problem using MINLP over a year may result in a very large problem of three variables, the powers of the batteries (BT), diesel generator (DG), and RO plant to be evaluated for 8760 hours leading to a problem of about 26280 variables. This leads to a very large problem formulation that is not necessary as power levels in one week are not strongly related to power in other weeks

of the year. Another advantage of using DP is the ability to control the discretization the power levels of the three variables. Thus, we used a larger granularity when simulating the operation of the system using a simple model to speed up the solution and examine a large number of alternative designs efficiently but with moderate accuracy. A smaller granularity was used when simulating the system using an accurate model for the small number of alternative good-enough designs. Finally, the problem solved has clear progression in time, with well-defined state space and transition dynamics, and for such problems DP is very efficient.

- Rather than using GA or PSO, we opted in this research to use OO since it allowed us to clearly define ranges for the variables characterizing a particular design. These variables were the sizes of PV panels, diesel generator (DG), battery storage system (BSS), water storage tanks (WST), and reverse osmosis (RO) plant. Right from the start of the design process, we selected commercially available sizes for the mentioned five subsystems, which cover the whole design search space. We were able through the simple model simulation to evaluate all the designs of search space very efficiently. For the search space of 5 variables each having 6 values, the number of simulations is given by $5^6 = 15625$. GA and relies on the use genetic operators to examine the search space, which however is a much slower process than OO. The PSO approach is slightly more efficient in terms of computation as it sends random agents to examine different parts of the solution search space and focus on the regions of lower costs. The OO approach is conceptually similar to PSO as both rely on operational simulation that may be done using the DP approach. However, OO has a clear advantage over PSO as it is able to exhaustively examine all the regions of the search space using the simple model and then find the good enough solutions to be later examined using the accurate model. The

number of good-enough solutions to be examined by the accurate model is relatively small in the order of 30 to 70 but depends on the accuracy of the simple model.

The inputs of the DP simulation program, which are the same for the simple or accurate model operations, are as follows:

- A selected size from the search space for each of the subsystems, i.e., PV, DG, BSS, WST and RO.

- Unit subsystem prices, fuel cost of DG, unit maintenance costs, initial BSS and WST states, the minimum up time and down times required of DG and RO plant, and the annuity factors.

- The hourly water load values, the solar irradiation, and the water temperature. For the simple model, these hourly values are over selected periods of the year representing one week in each season. For the accurate model simulation, the hourly values are those of the whole year.

- Lookup tables describing the specific power production of the PV panels, the charge-discharge curve of the BSS, the fuel consumption of DG, and the power required by the RO systems for different operating regimes.

- Number of system combinations to be simulated in the accurate model.

The outputs from the DP operational simulation model are the different subsystem combinations and their associated costs sorted in increasing yearly operational costs. These yearly costs account for the annuity on investment for each subsystem, the diesel fuel cost, maintenance costs, and battery degradation cost. The DP program provides also detailed hourly power values of the best design provided by PV, BSS, DG, and RO as well as the SOC of the BSS and the water level in the WST.

CHAPTER 3

SYSTEM MODELING

This chapter describes the mathematical models used for each system component. Section 3.1describes the photovoltaic system. Section 3.2 describes the battery storage system. Section 3.3 describes the diesel generator. Section 3.4 describes the reverse osmosis train used. Section 3.5 delves deeper into the different RO operation strategies simulated.

3.1. Photovoltaic System (PV)

In the preliminary study of the system, an empirical model of the PV generator was used where the DC power of the solar generator can be modeled as a linear source with respect to irradiance and PV panel temperature as expressed in the following equations:

$$P_{PV} = N_{PVs}N_{PVp}\left[P_{STC}\frac{S_i}{1000}[1 - \gamma(T_i - 25)]\right] \tag{1}$$

$$T_i = T_{amb} + \frac{S_i}{800}(NOCT - 20) \tag{2}$$

P_{PV}: DC MPP power

N_{PVs}: number of PV panels in series

N_{PVp}: number of PV panels in parallel

P_{STC}: nominal PV panel power at STC

S_i: irradiance level at time i

γ: temperature coefficienct of PV panel

T_i: PV cell temperature

T_{amb}: ambient temperature

$NOCT$: Normal operating conditions temperature

The parameters of a typical commercial polycrystalline PV panel are given as $P_{STC} = 320W$, $\gamma = -0.41\%/°C$, $NOCT = 45°C$. STC conditions are: irradiance 1000 W/m2, cell temperature 25 °C, AM=1.5. More details about the above-described PV model are provided in (Zein et al., 2018). Even though such approach gives good enough results, a more accurate simulation, which takes into consideration all details of a typical solar systems such as module temperature variations, light induced degradation, mismatching between solar panels, cabling voltage drops, inverter efficiencies, low light performance, and soiling, was finally adopted as described below.

Using a state-of-the-art solar PV system simulator (PVSyst, 2020), a simulation was done using a 1000kWp system facing south and tilted to optimal year-round production (20 degrees tilt), and irradiation and weather data for Beirut-Lebanon. The output of the simulation was tabulated as MPPT current and MPPT voltage as a function of irradiation and ambient temperature, using conventional solar ground-mount systems. Impp and Vmpp values are drawn from a PVSyst simulation of a 300Wp commercial PV panel.

Table 3-1 Lookup table for Impp and Vmpp of a 300Wp PV panel

Cell Temp	1200 W/m2		1000 W/m2		800 W/m2		600 W/m2		400 W/m2		200 W/m2	
	V_{mpp}	I_{mpp}	V_{mpp}	I_{mpp}	V_{mpp}	I_{mpp}	V_{mpp}	I_{mpp}	V_{mpp}	I_{mpp}	V_{mpp}	I_{mpp}
0	39.774	9.916	40.095	8.255	40.331	6.592	40.492	4.924	40.392	3.266	39.888	1.611
10	38.207	9.938	38.657	8.235	38.821	6.588	38.999	4.917	38.848	3.265	38.268	1.612
25	35.919	9.946	36.280	8.270	36.540	6.598	36.580	4.942	36.517	3.273	35.793	1.622
40	33.529	9.970	33.995	8.276	34.152	6.621	34.249	4.950	34.058	3.289	33.390	1.626
55	31.209	9.960	31.644	8.287	31.829	6.623	31.849	4.962	31.673	3.294	30.889	1.634
70	28.829	9.953	29.343	8.275	29.463	6.626	29.488	4.962	29.251	3.299	28.450	1.636

This table is used to create a rectangular 2D-grid structure in MATLAB, using the "ndgrid" function, which is then used in the simulations in scaled up or down formats as per the different solar system sizes considered, using interpolation between data points. The weather data used should include irradiance and cell temperature data. A simple interpolation allows an instantaneous calculation of DC PV power output, without the need to use any solar equations.

The above values were provided by PVSyst simulation considering the following simulation parameters:

- Array soiling 3%,
- thermal loss factor Uc (constant) 29 $Wm^{-2}K^{-1}$ and Uv (wind) 0 $Wm^{-2}K^{-1}$,
- light induced degradation 2%,
- module quality loss -0.8%,
- module mismatch losses 2%,
- string mismatch loss 0.2%,
- wiring ohmic losses 2%.

A typical efficiency curve of a commercial solar inverter is shown in Figure 3 (Sunny Tripower Core1, 2022)
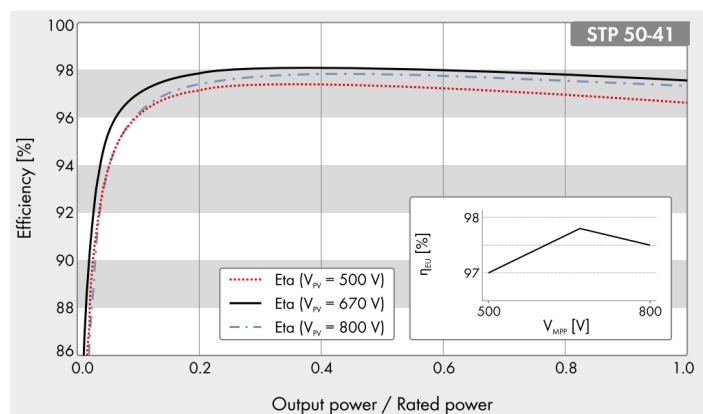
Figure 3 Inverter Efficiency

The efficiency curve may be modeled as simple mathematical function in case needed, although it can be roughly considered to be constant (~97.5% for 800VDC) for operations above 20% of nominal power.

Using the above, a 1MWp solar PV system would be able to produce about 1751MWh the first year if none of the available solar power is dumped. In reality, production figures will be lower as significant portions of the PV power are usually lost due to recurring full BSS states. Production values are expected to decrease by about 0.5% each year, following the PV panels yearly degradation.
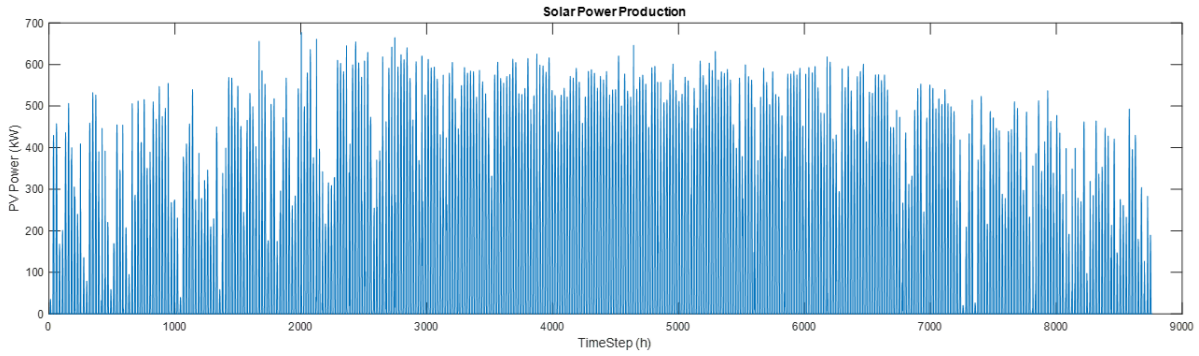
Figure 4 Simulated solar power production from a 650kWp solar system

3.2. Battery Storage System (BSS)

A battery model has been developed by (Karaki et al., 2015) for the simulation of a fuel cell hybrid electric vehicle. The model uses the equivalent circuit of a lithium ion battery, featuring the internal battery voltage and its series resistance to produce an internal charge rate curve. The same model has been used after scaling it up or down as needed in our simulations. The curve shown in Fig. 2 is the internal charge curve of a 1MW battery with 5MWh capacity for a varying operating power.
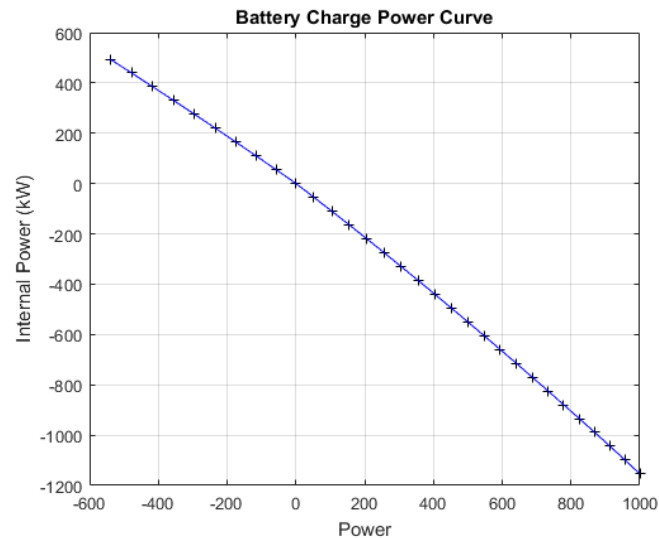
Figure 5 Battery charge power curve

The ageing model of the battery system can be made more or less complex as per the required details needed in the simulation. (Weitzel et al., 2018) described a sophisticated modeling method for battery ageing that divides battery ageing into two components: the total amount of

33

energy cycled through the battery, and battery calendrical ageing, both being a function of the depth of discharge (DOD). Weitzel's model requires the simulation of a plethora of battery parameters such as temperature, charge rate and DOD. In the work presented here, we opted for a simpler, yet representative model, which considers that half of the battery investment is lost in calendrical ageing, and the other half is lost in energy cycling.

The total expected battery energy over its lifetime (E_{life}) is calculated using the battery capacity (E_B) expressed in kWh, the DOD and the expected number of cycles (N_{DOD}) at the given DOD published by battery manufacturer:

$$E_{life} = E_B \ DOD \ N_{DOD} \tag{3}$$

The cyclical ageing (δ_B), in per unit, is calculated as the sum of the delivered energy by the battery (positive output power only) divided by E_{life}:

$$\delta_B = \frac{\sum_{i=1}^{T_{year}} max(B_i, 0) \ \Delta h}{E_{life}} \tag{4}$$

The cost of cyclical ageing φ_B is calculated as the per unit loss times half of the battery investment cost (C_B) while the cost of the calendrical ageing is calculated as annuity factor ($A_{battery}$) times half of C_B.

$$\varphi_B = (\delta_B + A_{battery}) \frac{C_B}{2} \tag{5}$$

3.3. Diesel Generator (DG)

Backup diesel generators fuel consumption can be modeled by a quadratic fit to manufacturer data.

$$\varphi_G(G_i) = a_0 + a_1 \ G_i + a_2 G_i{}^2$$

Where a_j, with j = 0, 1, 2 are the quadratic fitting coefficients.

Consumption levels are usually given by manufacturers for operation at 50%, 75% and 100% of nominal power. Table 3-2 shows consumption data taken for different sizes of diesel

generators. It is straight forward to notice that different diesel generators have different specific consumption values (L/kWh), and that smaller diesel generators have higher specific consumption that bigger ones. Figure 6 shows the fuel consumption of a CAT 600kVA, 480kW diesel generator based on manufacturer data (CAT DG C18-600, 2023). The specific consumption value (L/ kWh) is minimal at around 85% of nominal power. The yearly investment cost of the diesel generators is annualized using A_{10}. Different diesel generator sizes are considered in the simulations using scaled up or down consumption parameters.

Table 3-2 Fuel consumption figures of typical DG sets (manufacturer datasheets)

DG Size		Fuel Consumption (L/h) at different operation levels			Fuel Consumption (L/kWh) at different operation levels		
KVA	kW	50%	75%	100%	50%	75%	100%
40	36	7.2	9.5	12.1	0.40	0.35	0.34
100	90	16.4	21.9	27.4	0.36	0.32	0.30
275	220	36	49.9	64.2	0.33	0.30	0.29
400	320	43.2	61.8	82	0.27	0.26	0.26
455	364	51.5	71.8	94.5	0.28	0.26	0.26
500	400	54	76.2	102	0.27	0.25	0.26
550	440	58.8	83.9	111	0.27	0.25	0.25
600	480	63.9	91.9	122.7	0.27	0.26	0.26
1000	800	108.6	155.6	206.6	0.27	0.26	0.26
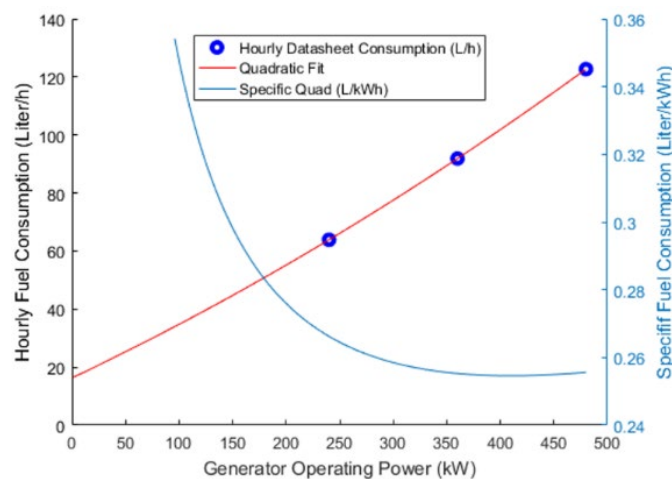
Figure 6 Diesel generator fuel consumption

We may also note here that manufacturers of diesel generators provide special lines of DG units optimized for low load operation. These generators often employ variable speed motors that allow them to adjust their operating speed based on the required load, allowing them to operate

efficiently at reduced power levels (Mobarra et al., 2022). Despite running at low loads, they provide reliable performance and have features that promote longevity and ease of maintenance. They find applications in various settings with fluctuating or consistently low power demands. For our study, we considered the use of a conventional DG unit and not one of these low load DGs.

3.4. Reverse Osmosis (RO)

RO systems are typically designed in a one-pass configuration for normal domestic water use. However, they can also be designed in two-pass configurations to achieve higher water quality, particularly for specific industrial processes. In this study, a detailed model of the RO plant has been developed, encompassing most of the essential elements of the system. The model takes into consideration energy losses in the filtration system and incorporates efficiency curves of various pumps to accurately represent the diverse operational levels of the RO plant and their impact on water quality, quantity, and cost. To ensure realistic simulations, commercially available equipment commonly utilized in industrial RO plants has been carefully selected, and their technical specifications have been integrated into the model.

A one-stage RO system consists of several components that work together to desalinate seawater. The system includes a seawater intake (SWI) pump responsible for drawing in the seawater from a source, such as the Mediterranean Sea. The seawater then passes through a filtration system, which removes large particles and impurities, preparing it for the subsequent stages. After filtration, the pre-treated seawater enters a high-pressure (HP) pump, which pressurizes the water to the required level for the reverse osmosis process. The high-pressure pump delivers the seawater to pressure vessels that contain multiple RO membranes each. Within the pressure vessels, the reverse osmosis membranes selectively allow water molecules to pass through to the permeate stream, while rejecting the majority of salts and impurities which

stay in the concentrate stream. This separation process results in the production of a low pressure desalinated water permeate stream, and a high pressure concentrate stream. The permeate is collected in a water storage tank (WST) for storage and distribution. A pressure exchanger (PX) is incorporated as an energy recovery device (ERD), enabling the transfer of energy from the concentrated brine to the incoming seawater, improving overall system efficiency. A booster pump (BP) is used to equalize the pressure of the seawater leaving the ERD with that of the high-pressure pump. This booster pump is relatively small as it only has to offset the the pressure lost in the pressure vessels and the piping losses. The seawater then joins the flow from the high-pressure pump to form the membrane feed flow.

To control the system pressure and maintain optimal operating conditions, a motorized concentrate valve is employed. This valve regulates the flow of the concentrated brine, allowing for precise control over the system pressure. To control the flow rate of water through the system, all the pumps, including the seawater intake pump, high-pressure pump, and booster pump, are equipped with variable frequency motor drives. These motor drives allow for precise control of the pump speeds and, consequently, the water flow rate.

A one-stage RO system unit, consisting of 10 pressure vessels, each containing 8 RO membranes, is shown in Figure 7 . The RO membrane chosen is a membrane used for single pass designs, and high rejection rates. It has an active area of 41 m^2, maximum operating pressure of 83 bar, and a nominal permeate flow rate of 37.5 m^3/h (Lenntech). The high pressure pump is chosen to operate at 60 m^3/h and 50 bar (FLOWSERVE, 2019), and the booster pump at 50 m^3/h and 2 bar (FLOWSERVE, 2019). The SWI pump needed is a 110 m^3/h and 4 bar (FLOWSERVE, 2019), and a rotary pressure exchanger is used as energy recovery device capable of handling 45 to 70 m^3/h. In the pressure exchanger element, the pressurized brine comes in direct contact with the low-pressure feed stream where the energy is transferred to the feed stream at a very high efficiency (92% to 98% depending on manufacturers (Danfoss, 2021)

(energy recovery, 2021)). The brine stream is at a lower pressure than the feed water stream, and some additional pressure losses occur across the pressure exchanger, compensated for by the booster pump.
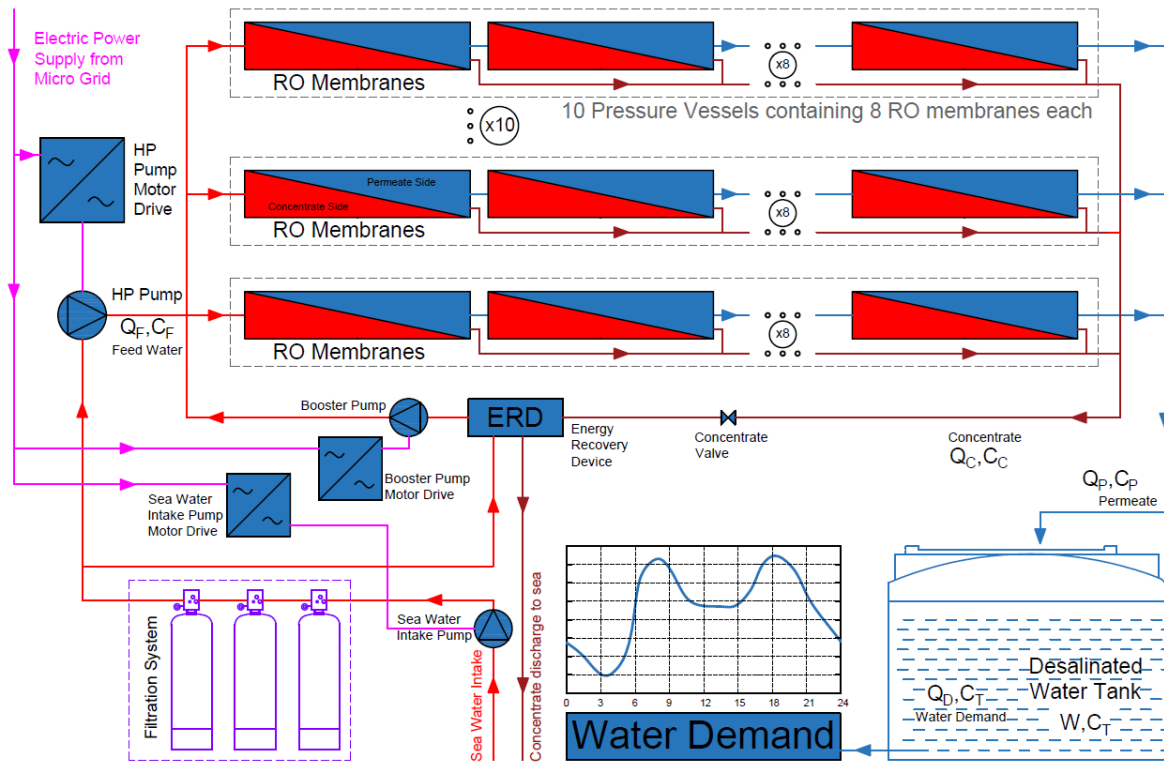
Figure 7 Simulated RO system design

WAVE (Dupont, 2021), a free water treatment simulation software, was used to obtain tabulated operating variables.

The input-output data of the membranes are simulated at different operation levels of feed flow, feed pressure and input water temperatures. Some of the input parameters used in WAVE are summarized in the following Figure 8. Note that 1000 PV vessels were simulated instead of 10 in order to get numerical results with more digits. In fact, WAVE's interface limits the results displayed to one fractional digit only. Scaling down to 10 PV vessels as per our design is easily done. Each of the PV vessels was simulated with 8 membrane elements.

Figure 8 Parameters used in WAVE simulations

Standard seawater, with a total dissolved solids (TDS) content of 35,000 mg/L, constitutes the largest amount of water worldwide. It possesses a nearly uniform composition across the globe. Nevertheless, the actual TDS content may vary considerably, ranging from 7,000 mg/L in the Baltic Sea to as high as 45,000 mg/L in the Red Sea and Arabian Gulf. The specific compositions of seawater can be estimated proportionally based on the standard seawater composition. However, water from seashore wells can differ significantly in salinity and composition due to factors such as soil conditions, inland influx, and other local influences, setting it apart from water directly taken from the sea. A predefined water composition provided in WAVE as "Seawater TDS 32000" was used in the simulations.

Cations

Symbol	mg/L	ppm CaCO₃	meq/L
NH₄	0.00	0.00	0.00
K	373.40	477.94	9.55
Na	10,087.30	21,957.77	438.77
Mg	1,201.07	4,945.96	98.83
Ca	385.55	962.83	19.24
Sr	7.44	8.50	0.17
Ba	0.00	0.00	0.00

Total Cations: 12,054.76   566.57

Anions

Symbol	mg/L	ppm CaCO₃	meq/L
CO₂	15.44	25.75	0.51
HCO₃	96.06	78.79	1.57
NO₃	0.00	0.00	0.00
Cl	18,134.63	25,598.12	511.52
F	1.22	3.20	0.06
SO₄	2,537.72	2,644.01	52.83

Total Anions: 20,785.07   566.50

Neutrals

Symbol	mg/L
SiO₂	0.91
B	4.20
CO₂	0.35

Total Neutrals: 5.47

Figure 9 Seawater composition

For every set of feed flow, pressure and temperature, WAVE gives us operating parameters such as in Table 3-3 below

Table 3-3 RO Pressure-Flow Table, sample WAVE output

Stage	Elements	#PV	#Els per PV	Feed Flow (m³/h)	Recirc Flow (m³/h)	Feed Press (bar)	Boost Press (bar)	Conc Flow (m³/h)	Conc Press (bar)	Press Drop (bar)	Perm Flow (m³/h)	Avg Flux (LMH)	Perm Press (bar)	Perm TDS (mg/L)
1	SW30XLE-440i	1000	8	9,977	0.00	49.7	0.0	5,236	48.1	1.6	4,752	14.5	0.0	172.3

Pass	Pass 1
Stream Name	Seawater - Salinity = 32000 - LarnacaTemps
Water Type	Sea Water (With conventional pretreatment, SDI < 5)
Number of Elements	8000
Total Active Area (m²)	327019
Feed Flow per Pass (m³/h)	9,977
Feed TDSª (mg/L)	32,939
Feed Pressure (bar)	50.0
Flow Factor	1.00
Permeate Flow per Pass (m³/h)	4,752
Pass Average flux (LMH)	14.5
Permeate TDSª (mg/L)	172.3
Pass Recovery	47.6 %
Average NDP (bar)	14.9
Specific Energy (kWh/m³)	3.66
Temperature (°C)	22.0
pH	8.2
Chemical Dose	
RO System Recovery	47.5 %
Net RO System Recovery	47.5%

Figure 10 shows the operating points of the RO system simulated in WAVE. These points were chosen based on a feed pressure discretization of 5 bar and feed flow discretization of 10 m3/h. The acceptable operating points are marked with an "×" symbol, while non-acceptable operating points are colored. The reason for non-feasibility of the colored operating points comes from hydraulic limitations and permeate quality requirements as explained in the legend.
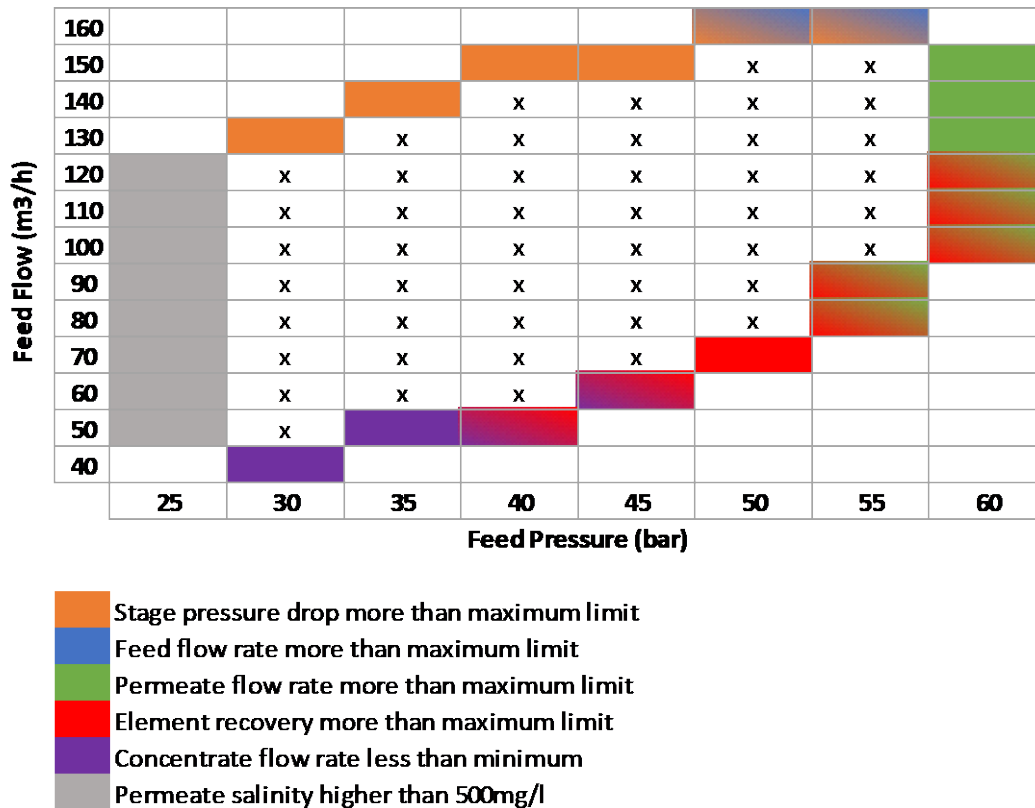
Figure 10 Operating points from WAVE

The values simulated in WAVE are shown in the following Table 3-4, Table 3-5 and Table 3-6 for different temperatures.

Table 3-4 Operation parameters at 22degC

Feed Flow (m³/h)	Feed Press (bar)	Conc Flow (m³/h)	Conc Press (bar)	Perm Flow (m³/h)	Perm TDS (mg/l)	Recovery (%)
5	30	3.91	29.2	1.09	531.9	21.7%
6	30	4.79	28.9	1.21	473.5	20.1%
6	35	4.13	34.0	1.87	348.0	31.1%
6	40	3.61	39.1	2.39	305.1	39.8%
7	30	5.69	28.6	1.31	433.3	18.7%
7	35	4.93	33.8	2.07	309.0	29.6%
7	40	4.31	38.9	2.69	266.4	38.4%
7	45	3.82	44.0	3.18	249.5	45.4%
8	30	6.62	28.3	1.38	405.1	17.3%
8	35	5.75	33.5	2.25	280.6	28.1%
8	40	5.04	38.6	2.96	237.8	37.0%
8	45	4.47	43.7	3.53	220.3	44.1%
8	50	4.01	48.9	3.99	213.6	49.9%
9	30	7.56	28.0	1.44	385.0	16.0%
9	35	6.60	33.2	2.40	259.3	26.7%
9	40	5.80	38.3	3.20	216.2	35.6%
9	45	5.14	43.5	3.86	198.0	42.8%
9	50	4.61	48.6	4.39	190.5	48.7%
10	30	8.52	27.6	1.48	370.8	14.8%
10	35	7.47	32.8	2.53	243.0	25.3%
10	40	6.58	38.0	3.42	199.4	34.2%
10	45	5.85	43.2	4.15	180.6	41.5%
10	50	5.25	48.3	4.75	172.3	47.5%
10	55	4.75	53.4	5.25	169.4	52.5%
11	30	9.49	27.3	1.51	361.1	13.7%
11	35	8.36	32.5	2.64	230.5	24.0%
11	40	7.39	37.7	3.61	186.2	32.8%
11	45	6.58	42.9	4.42	166.8	40.1%
11	50	5.91	48.0	5.09	157.8	46.3%
11	55	5.36	53.2	5.65	154.2	51.3%
12	30	10.48	26.9	1.52	355.0	12.7%
12	35	9.28	32.1	2.73	220.7	22.7%
12	40	8.23	37.3	3.77	175.6	31.4%
12	45	7.35	42.5	4.65	155.6	38.8%
12	50	6.61	47.7	5.40	146.1	45.0%
12	55	5.99	52.9	6.02	141.8	50.1%
13	35	10.21	31.7	2.79	213.0	21.5%
13	40	9.09	37.0	3.91	167.0	30.1%
13	45	8.14	42.2	4.86	146.5	37.4%
13	50	7.33	47.4	5.67	136.4	43.6%
13	55	6.65	52.5	6.36	131.6	48.9%
14	40	9.97	36.6	4.03	160.1	28.8%
14	45	8.95	41.8	5.05	139.0	36.1%
14	50	8.08	47.0	5.92	128.4	42.3%
14	55	7.33	52.2	6.67	123.1	47.6%
15	50	8.85	46.6	6.15	121.7	41.0%
15	55	8.05	51.8	6.95	116.0	46.3%

Table 3-5 Operation parameters at 27degC

Feed Flow (m³/h)	Feed Press (bar)	Conc Flow (m³/h)	Conc Press (bar)	Perm Flow (m³/h)	Perm TDS (mg/l)	Recovery (%)
5	30	3.91	29.2	1.09	691.1	21.7%
6	30	4.79	28.9	1.21	614.9	20.2%
6	35	4.13	34.0	1.87	453.6	31.2%
6	40	3.61	39.1	2.39	399.0	39.9%
7	30	5.69	28.6	1.31	561.8	18.8%
7	35	4.92	33.8	2.08	402.3	29.8%
7	40	4.30	38.9	2.70	348.3	38.6%
7	45	3.82	44.0	3.19	327.3	45.5%
8	30	6.60	28.3	1.40	523.6	17.5%
8	35	5.73	33.5	2.27	364.5	28.4%
8	40	5.02	38.6	2.98	310.6	37.3%
8	45	4.45	43.7	3.55	289.0	44.4%
8	50	4.00	48.9	4.00	281.0	50.0%
9	30	7.54	28.0	1.46	495.9	16.2%
9	35	6.56	33.2	2.44	335.8	27.1%
9	40	5.76	38.3	3.24	281.7	36.0%
9	45	5.11	43.5	3.89	259.4	43.2%
9	50	4.59	48.6	4.41	250.6	49.0%
10	30	8.49	27.6	1.51	475.9	15.1%
10	35	7.42	32.8	2.58	313.5	25.8%
10	40	6.53	38.0	3.48	259.1	34.8%
10	45	5.80	43.2	4.20	236.2	42.0%
10	50	5.20	48.3	4.80	226.5	48.0%
10	55	4.72	53.4	5.28	223.4	52.8%
11	30	9.46	27.3	1.55	461.5	14.0%
11	35	8.30	32.5	2.70	296.1	24.6%
11	40	7.32	37.7	3.69	241.0	33.5%
11	45	6.51	42.9	4.49	217.5	40.9%
11	50	5.84	48.0	5.16	207.1	46.9%
11	55	5.30	53.2	5.70	203.2	51.8%
12	30	10.43	26.9	1.57	451.8	13.1%
12	35	9.19	32.1	2.81	282.3	23.4%
12	40	8.13	37.3	3.87	226.5	32.3%
12	45	7.24	42.5	4.76	202.4	39.7%
12	50	6.51	47.7	5.49	191.3	45.8%
12	55	5.90	52.9	6.10	186.7	50.8%
13	35	10.11	31.7	2.89	271.4	22.2%
13	40	8.96	37.0	4.04	214.6	31.0%
13	45	8.00	42.2	5.00	189.9	38.5%
13	50	7.20	47.4	5.80	178.1	44.6%
13	55	6.53	52.5	6.47	172.9	49.8%
14	40	9.82	36.6	4.18	204.8	29.9%
14	45	8.79	41.8	5.22	179.5	37.3%
14	50	7.91	47.0	6.09	167.2	43.5%
14	55	7.19	52.2	6.82	161.3	48.7%
15	50	8.66	46.6	6.35	157.9	42.3%
15	55	7.86	51.8	7.14	151.6	47.6%

Table 3-6 Operation parameters at 17degC

Feed Flow (m³/h)	Feed Press (bar)	Conc Flow (m³/h)	Conc Press (bar)	Perm Flow (m³/h)	Perm TDS (mg/l)	Recovery (%)
5	30	3.92	29.2	1.09	405.3	21.7%
6	30	4.80	28.9	1.20	361.7	20.0%
6	35	4.15	34.0	1.85	264.5	30.9%
6	40	3.62	39.1	2.38	230.7	39.6%
7	30	5.71	28.6	1.29	332.4	18.4%
7	35	4.96	33.8	2.05	235.7	29.2%
7	40	4.34	38.9	2.66	201.8	38.0%
7	45	3.84	44.0	3.16	188.0	45.1%
8	30	6.64	28.3	1.36	312.2	17.0%
8	35	5.79	33.5	2.21	215.0	27.6%
8	40	5.09	38.6	2.91	180.7	36.4%
8	45	4.51	43.7	3.49	166.2	43.6%
8	50	4.04	48.9	3.96	160.4	49.5%
9	30	7.59	28.0	1.41	298.2	15.6%
9	35	6.66	33.2	2.34	199.7	26.0%
9	40	5.87	38.3	3.13	165.0	34.8%
9	45	5.21	43.5	3.79	149.9	42.1%
9	50	4.67	48.6	4.33	143.2	48.1%
10	30	8.56	27.6	1.44	288.8	14.4%
10	35	7.55	32.8	2.45	188.2	24.5%
10	40	6.68	38.0	3.32	153.0	33.2%
10	45	5.95	43.2	4.05	137.2	40.5%
10	50	5.34	48.3	4.66	129.9	46.6%
10	55	4.83	53.4	5.17	127.0	51.7%
11	30	9.54	27.3	1.46	282.8	13.2%
11	35	8.47	32.5	2.54	179.5	23.0%
11	40	7.52	37.7	3.48	143.6	31.6%
11	45	6.72	42.9	4.28	127.3	38.9%
11	50	6.04	48.0	4.96	119.4	45.1%
11	55	5.47	53.2	5.54	115.8	50.3%
12	30	10.54	26.9	1.46	279.6	12.2%
12	35	9.40	32.1	2.60	172.8	21.7%
12	40	8.39	37.3	3.61	136.2	30.1%
12	45	7.52	42.5	4.48	119.4	37.4%
12	50	6.77	47.7	5.23	111.0	43.6%
12	55	6.14	52.9	5.86	106.9	48.9%
13	35	10.35	31.7	2.65	167.8	20.4%
13	40	9.28	37.0	3.72	130.2	28.6%
13	45	8.34	42.2	4.66	113.0	35.8%
13	50	7.53	47.4	5.47	104.1	42.0%
13	55	6.84	52.5	6.16	99.5	47.4%
14	40	10.19	36.6	3.81	125.5	27.2%
14	45	9.19	41.8	4.81	107.7	34.3%
14	50	8.33	47.0	5.67	98.5	40.5%
14	55	7.58	52.2	6.43	93.5	45.9%
15	50	9.15	46.6	5.86	93.8	39.0%
15	55	8.34	51.8	6.66	88.4	44.4%

The output of WAVE simulation is tabulated in MATLAB and subsequently coupled with the detailed simulation of the RO plant.

Seasonal variation in the seawater temperature directly affects the efficiency of the RO system. The higher the water temperature, the higher the recovery rate under the same feed pressure and flow (and thus same power consumption). For example, in the Mediterranean Sea, water temperature varies between 12°C in January and 27°C in August (Richardson et al., 1999) as shown in Figure 11. To estimate the effect of these variations, simulations in WAVE were performed at temperatures of 12, 22 and 27°C. The energy consumption difference between a feed water of 27 and 12°C was determined to be around 2.9%, and that between 27 and 22°C to be 1.1%. These values represent the average from all SOW. For the nominal conditions (120m3/h flow and 50bar feed pressure), the difference in energy consumption between 27 and 12°C becomes 3.8%, while that between 27 and 22°C becomes 2.4%. These variations can be integrated into the system simulation in the future but have not been taken into consideration in this work. All data shown in this work corresponds to an average feed water temperature of 22°C. In (Koutsou et al., 2020), the authors analyzed the effects of using the feed water of the RO plant to cool down the PV panels, increasing both PV and RO systems efficiencies. They concluded that every 1% increase in RO feed temperature results in 1% reduction of required RO pressure. Another way of increasing RO system efficiency would be to utilize whatever excess solar PV power is available to heat up the feedwater stream if there is no better use for such excess power.
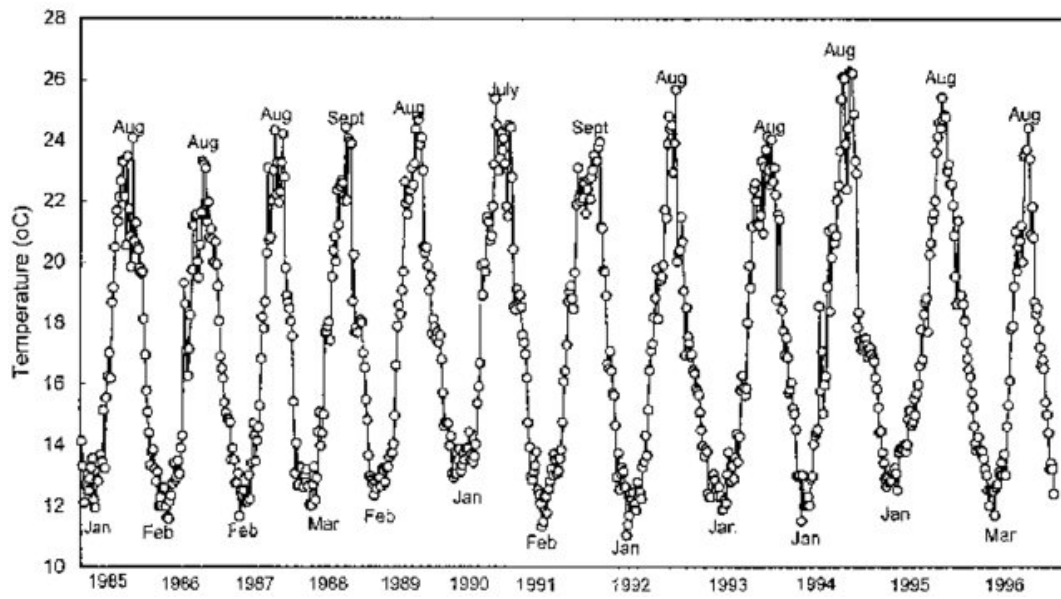
Figure 11 Mediterranean seawater temperature (Richardson et al., 1999)

3.5. RO Plant Operation Strategies

The total RO system power is equal to the sum of HP, BP and SWI required powers, which are calculated separately for each operation level. The following power equation is used for all pumps to calculate required electric pump power:

$$P_{elec} = \frac{\rho g H Q}{3.6 \times 10^6 \ \mu_p \ \mu_d}$$ (6)

where

P_{elec}: AC electric power supplied to the pump motor (kW)

ρ: density of sea water (1025 kg/m³)

g: gravitational constant

H: total dynamic head (m)

Q: water flow in (m³/h)

μ_p: pump efficiency (as per efficiency curve)

μ_d: motor drive efficiency (94%)

46

Given that solar available power is variable, pumps that are directly and solely powered by solar PV are operated at variable speeds (mainly found in orchards for irrigation or in municipal water supplies). Pump efficiencies and head-flow (H-Q) curves of the pumps are usually only given by suppliers at rated speed (equivalent to 50Hz). Affinity laws can be used to deduce the power and H-Q curves at different rotational speed values. In fact, the effect of varying the frequency is essentially the same as the effect of varying the speed. If the speed of a pump is changed, the flow, head, power, and efficiency will change according to the well-known Affinity laws that compare pumping characteristics at two different speed values n_1 and n_2:

$$\frac{Q_1}{Q_2} = \left(\frac{n_1}{n_2}\right) \quad ; \quad \frac{H_1}{H_2} = \left(\frac{n_1}{n_2}\right)^2 \quad ; \quad \frac{P_1}{P_2} = \left(\frac{n_1}{n_2}\right)^3 \tag{7}$$

These equations show that the flow is proportional to the speed and the head is proportional to the square of the speed. The hydraulic efficiency, however, does not change with the speed. The shaft power is therefore proportional to the cube of the speed.

The following mass and power balance relations are used:

- The flow supplied by the HP pump is equal to the RO system feed flow minus the ERD flow (which is in turn equal to the concentrate flow),

- HP Pump head is equal to the pressure vessel input pressure minus the HP pump suction pressure.

- Booster pump flow is equal to the ERD flow as the two elements are working in series.

- Booster pump head is equal to the feed pressure minus the recovered pressure from the concentrate minus the booster pump suction pressure (pressure at the output of the filter)

- SWI pump flow is equal to the pressure vessels feed flow

- SWI pump head is equal to the input pressure of the filtration system.

With the above mass and power balance equations, we can calculate the operating flow and pressure of each of the water pumps. The filtration system's pressure drop is considered to be a constant at a 2 bar value. Given those calculated operating points, we can now calculate power consumption using equation (6).

Interpolation was used to characterize the system operation parameters between the simulated operating points detailed in Table 3-4. Figure 12 shows isolines of the RO plant's electric power consumption. Figure 13 shows isolines of specified water recovery ratios with steps of 5%. Figure 14 shows the calculated isolines of specific energy consumption in kWh/m^3, by dividing the plant's power consumption in kW by the corresponding permeate flow rate in m^3/h.
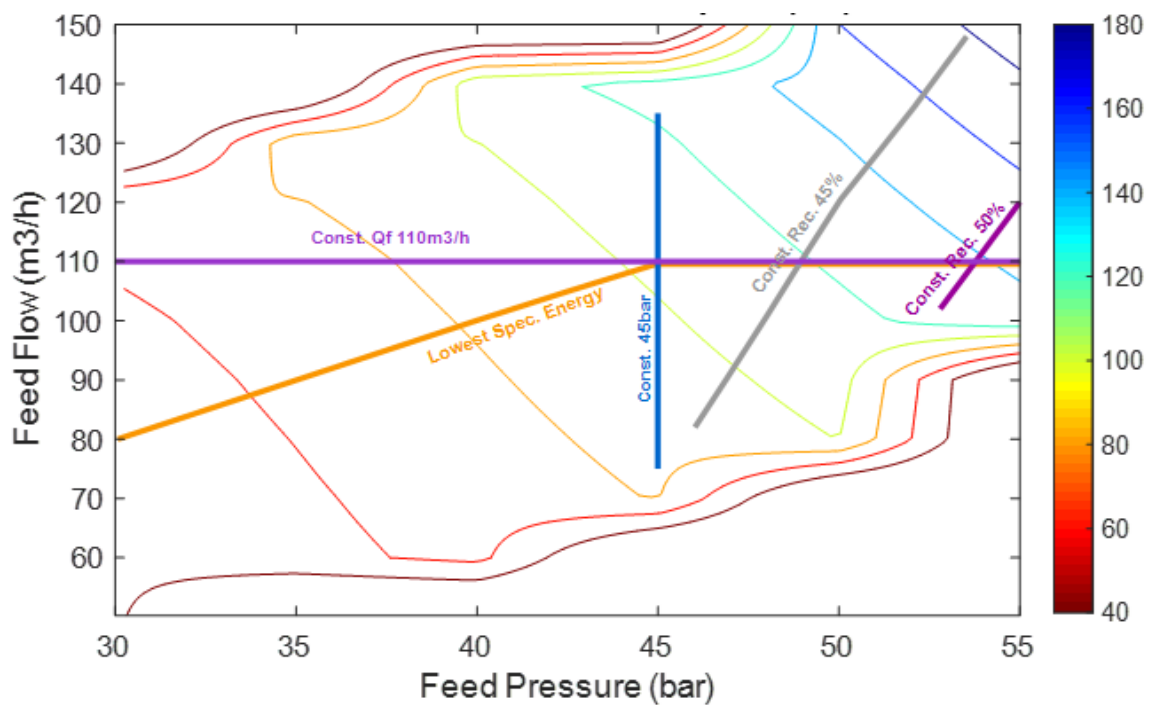
Figure 12 Isolines of power consumption with strategy lines overlay (kW)
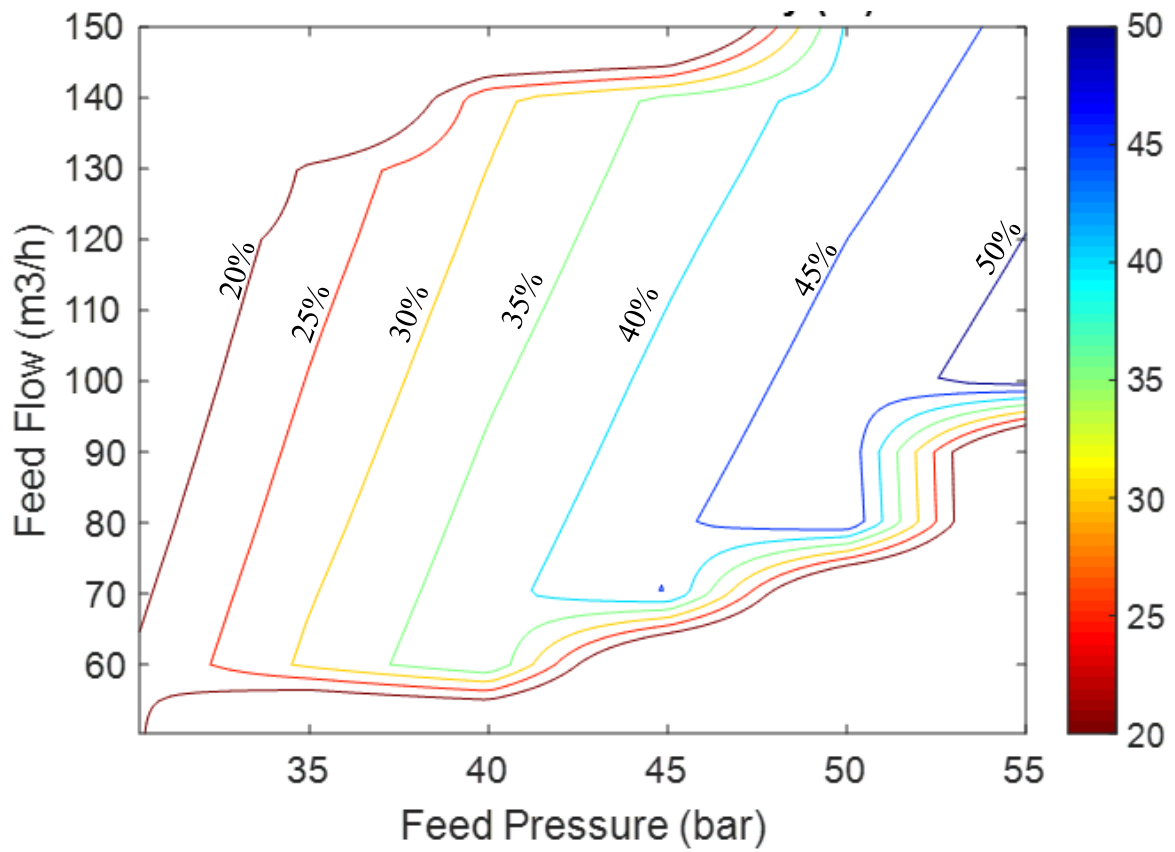
Figure 13 Isolines of water recovery (%)
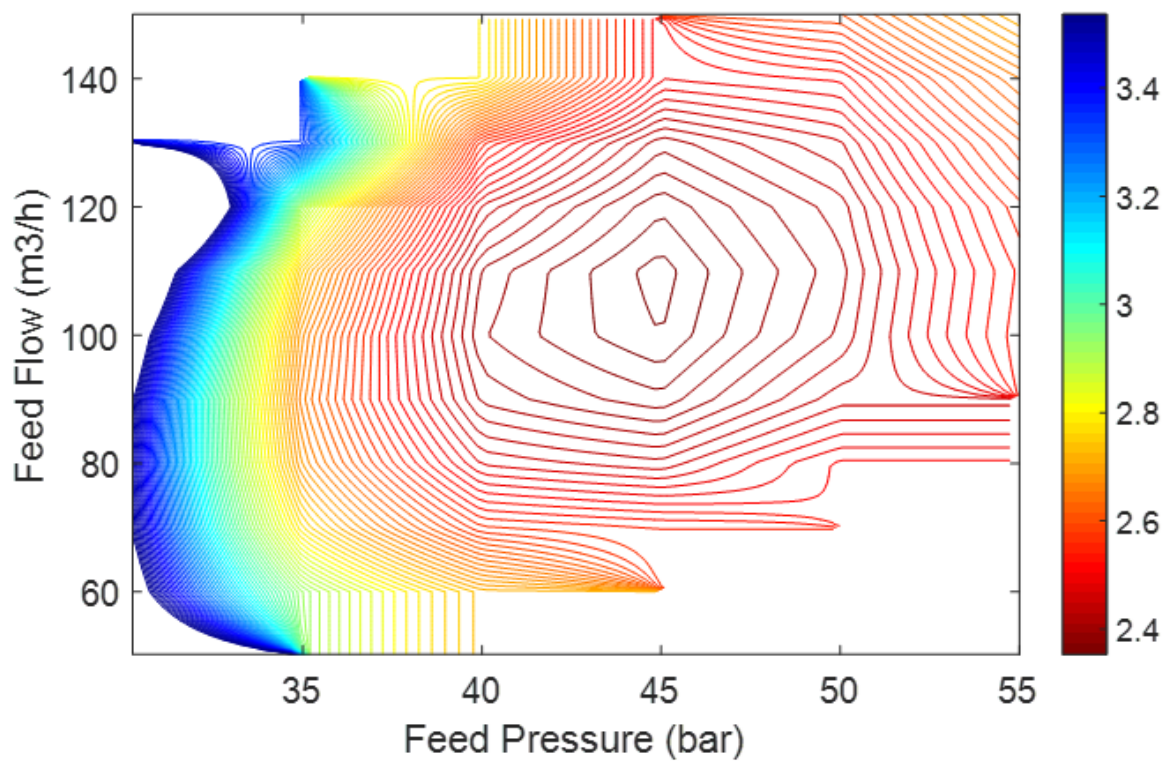
Figure 14 Isolines of specific energy consumption (kWh/m3)

As shown in Figure 12, each power level of the RO plant can be associated with a continuum of feed water pressure and feed flow sets. Thus, we need to choose an operation strategy that associates each RO power level with a unique set of head-flow values. Once those strategies are defined, each power level of the RO system is translated to a unique set of hydraulic parameters, namely the feed pressure and flow, the permeate flow rate and concentration, among others. The different operating strategies are described below:

- **Constant feed pressure:** Membrane manufacturers highly insist on limiting operational pressure variations (Dow Chemicals, 2022), which would suggest a preference for constant pressure operation. Unfortunately, such a strategy results in small margins of power variation as shown in Figure 15. In this strategy, only the feed pressure is fixed to 45 bars while feed flow rate is varied according to allocated power level. Power variation within the SOW range from 85 to 120kW.

- **Minimum specific energy consumption**, allowing large power level variations, but also results in high variations of feed pressure as shown in Figure 16. In this strategy, all RO system states are varied in a way to follow the minimum SEC (normal to the isolines of Figure 14). Power variation within the SOW range from 80 to 180kW.

- **Constant RO water recovery rate**, a compromise strategy allowing large power variations with relatively low pressure modulation, as shown in Figure 17. In this strategy, only the RO recovery rate is fixed while feed pressure and flow rates are varied according to allocated power level. In practice, applying this strategy requires varying the speed of the water pumps to regulate flow rate while controlling the concentrate valve at the same time to regulate system pressure. Power variation within the SOW range from 90 to 180kW.

- **Constant Feed flow rate**, as shown in Figure 18, this strategy also allows large power modulation range, but this time ranging between 60kW and 145kW only. It has the

benefit of simplicity with regards to constant flow rates but does not allow good enough usage of the available RO system capacity.

Above mentioned strategies are summarized numerically in the following Table 3-7.

Table 3-7 Strategy curves

Constant feed pressure 45bars		Constant recovery rate 45%		Minimum SEC		Constant Feed Flow 110m3/h	
P (bar)	Q (m³/h)	P (bar)	Q (m³/h)	P (bar)	Q (m³/h)	P (bar)	Q (m³/h)
45	7.5	46.02	8.2	30.07	8	30	11
45	8.5	46.93	9.05	35.02	9	35	11
45	9.5	48.03	10.1	39.97	10	40	11
45	10.5	48.95	11	42.53	10.5	45	11
45	11.5	50.05	12.05	44.92	11	50	11
45	12.5	50.97	12.75	47.48	11	55	11
45	13.5	52.07	13.6	48.95	11		
		52.8	14.2	52.43	11		
		53.53	14.8	55	11		

For each of the strategies mentioned above, a strategy table can be prepared using the data points taken from WAVE and interpolating between those points wherever needed. The strategy tables prepared show the variables of interest: feed pressure, feed flow, permeate flow, permeate concentration (TDS), and power consumption, at each of the strategy's operating points. Table 3-8 shows the strategy table computed for the 45% recovery rate. Similar tables are prepared for the rest of the operating strategies considered.

Table 3-8 Strategy Table of Constant Recovery 45%

Feed Pressure (bar)	Feed Flow (m³/h)	Permeate Flow(m³/h)	TDS	RO Power (kW)
46.0	82	36.9	214.4	90.5
46.9	90.5	40.8	194.2	98.3
48.0	101	45.5	174.2	108.9
49.0	110	49.5	159.7	118.7
50.1	120.5	54.2	145.6	131.5
51.0	127.5	57.3	137.9	142.0
52.1	136	61.2	129.5	156.2
52.8	142	63.9	124.1	166.9
53.5	148	66.6	119.1	178.5
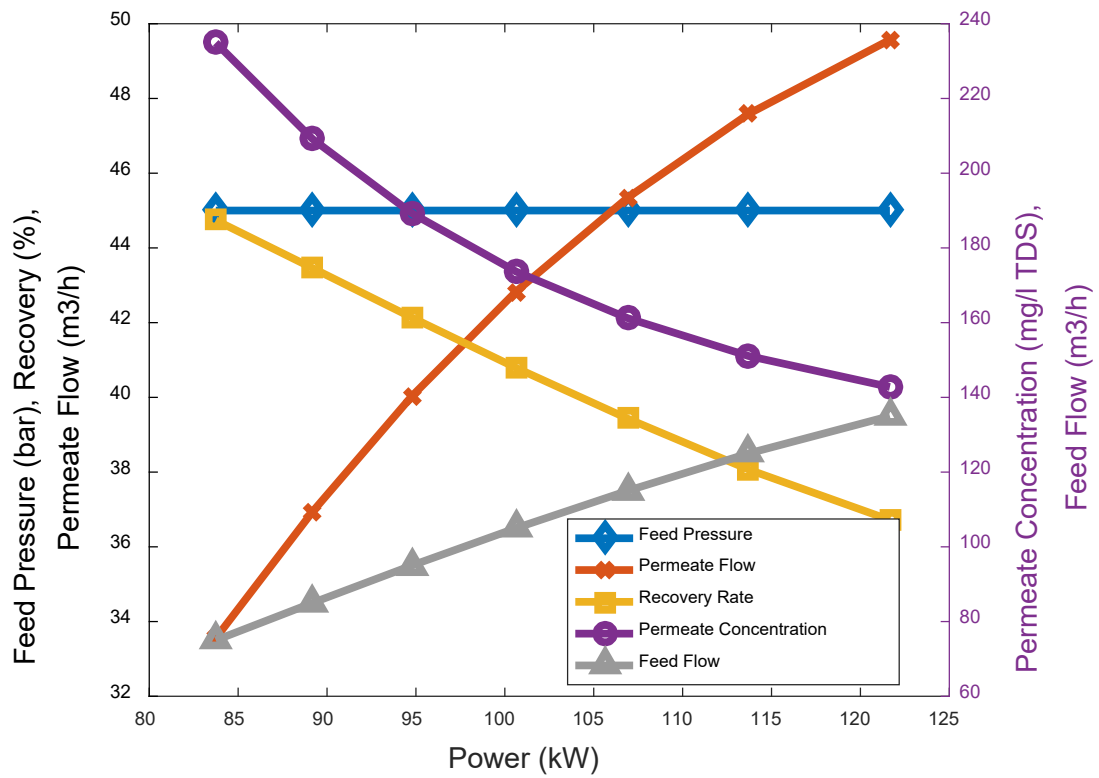
Figure 15 Constant Pressure 45bar
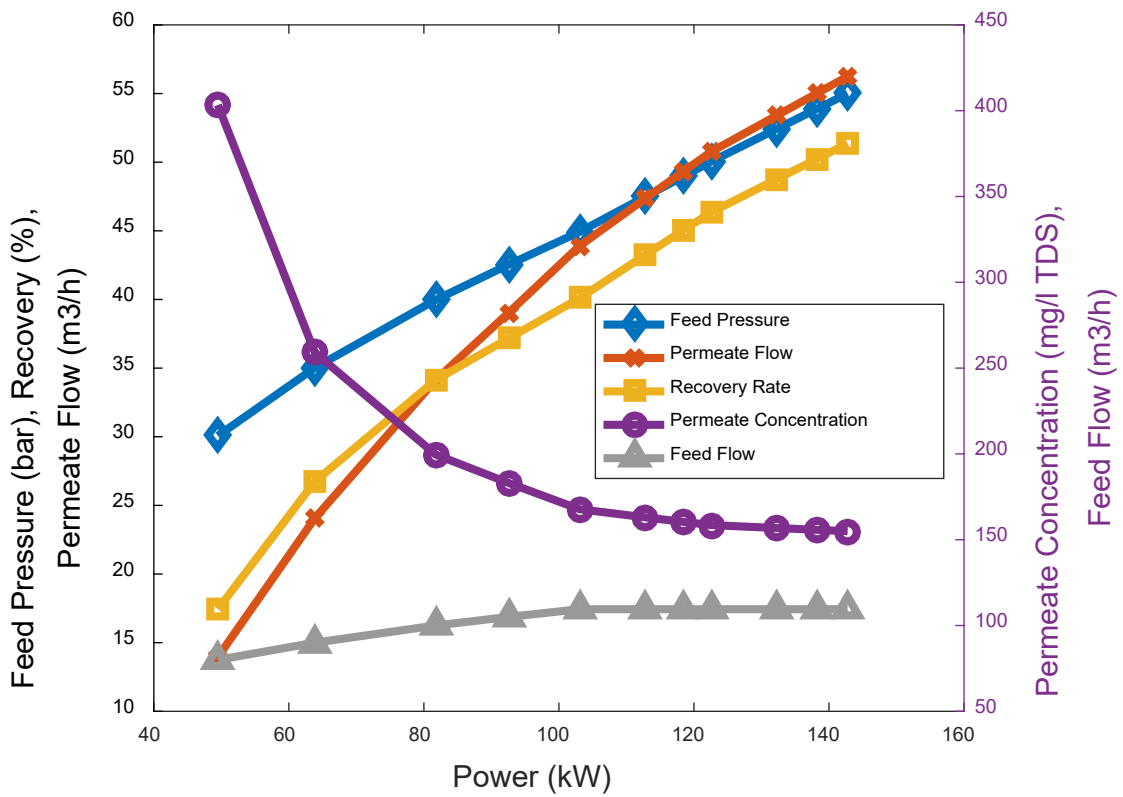
Figure 16 Lowest SEC
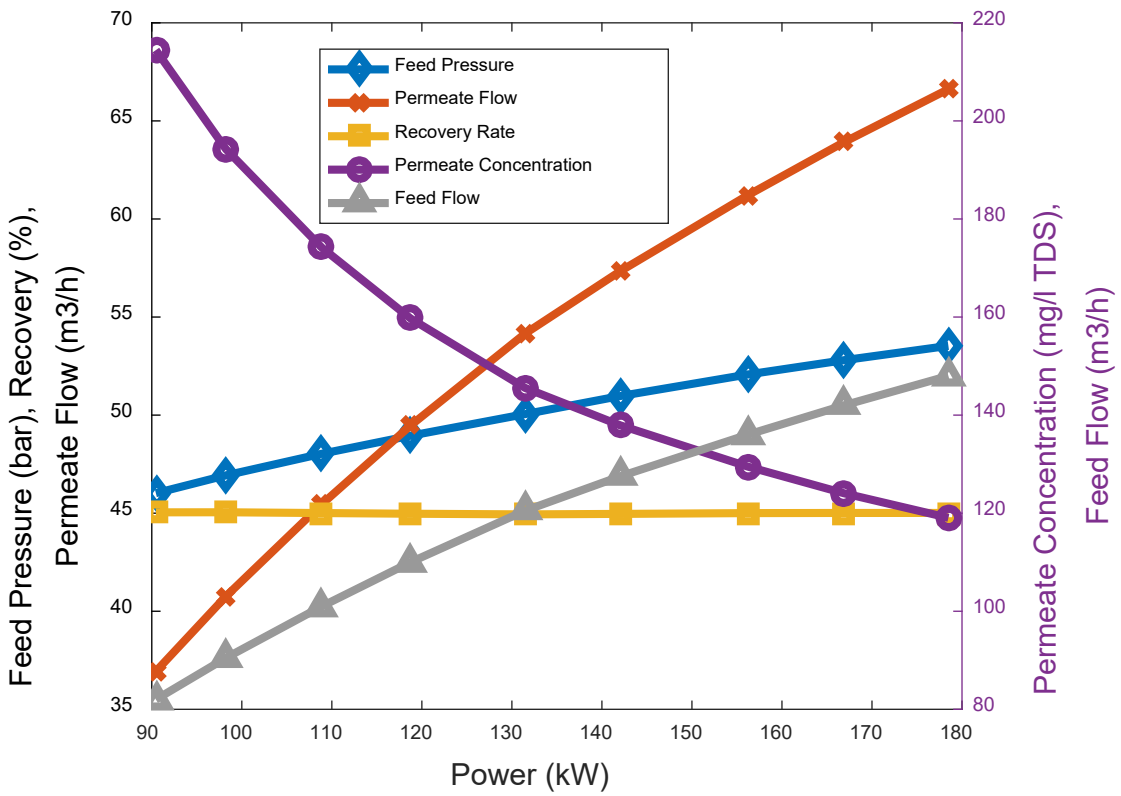
Figure 17 Constant Recovery Rate 45%
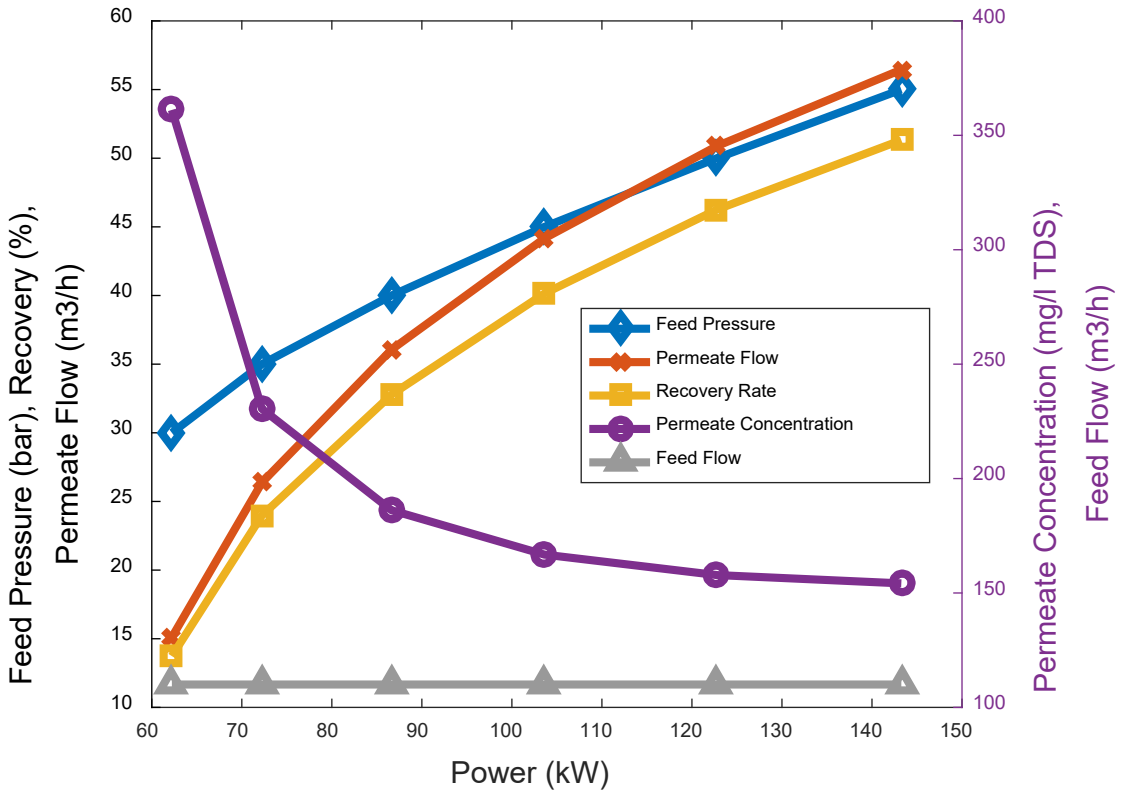
Figure 18 Constant Feed Flow 110m3/h

Figure 12 shows that the 50% constant recovery rate strategy restricts operational levels to only very high-power values, while the 45% constant recovery rate strategy allows large variations of power. A lower recovery rate is not considered as it results in higher water intake and filtration costs, and low usage level of the RO plant investment. As a result, the 45% fixed recovery rate strategy was chosen and used in subsequent sections.

One can argue that a recovery rate higher than 45% would be more adequate in summer as the seawater temperature will increase, and a different lower recovery rate value might be more suitable in the cold months of winter. While this is totally true, this does not directly affect the conclusions in this work regarding the RO's variable operation itself. The different operation strategies may be considered as a hybrid between minimum SEC for power values between 60kW and 145kW, and after that following a constant 54bar pressure with increasing flow. This last section of the curves would extend the operating window to higher power levels.

The RO plant's minimum uptime is fixed at 10 hours, and a minimum downtime of 10 hours is also set. This configuration ensures system stability and allows for the backwashing of the RO membranes. The diesel generator has a minimum uptime and downtime of 2 hours each. Using the constant recovery rate strategy of 45%, RO operation parameters are determined for each power level, including the permeate flow, which feeds the WST.

A fixed 94% efficiency is considered for the motor drives as a worst-case scenario efficiency for part-load operations (U.S. Department of Energy , 2012). A fixed 95% efficiency was used for the ERD (minimum efficiency warranted by ERD supplier). Considering fixed efficiencies for the ERD and motor drives is justified by the fact that the variation of their efficiencies is minimal. The initial state of charge of both BSS and WST are set to 50%.

In order to do a search for the best RO system size, the designed RO system was used a base case, and multiplication factors were employed to increase or decrease the simulated RO plant

size. The multiplication factors were carefully tailored to the plant's parameters. As an example, to simulate an RO plant that has double the designed system's capacity, the maximum and minimum RO power consumption, feed flow, permeate flow, and actual power consumption are multiplied by two, while pressure and TDS values are kept the same. Cost and maintenance costs are also scaled accordingly.

CHAPTER 4

SIMULATION RESULTS

In this chapter, section 4.1 describes the case studies used in the simulations, section 4.2 provides a detailed assessment of the presence or absence of different system components into the power mix. Finally, section 4.3 exposes a critical analysis of the merit of variable reverse osmosis operation compared to fixed power operation.

4.1. Case Studies

Different synthetic case studies were considered to cover different water profiles. A "residential" water profile where the water load is distributed throughout the day, peaking early in the morning and in the evening, and slightly lower during weekends. Weighting coefficients were used with the residential profile as shown in

Table 4-2. An "Industrial" profile adapted from (Li et al., 2018) representing water use in a large beef packing plant, where weekends have a very low water use compared to weekdays. A "constant" year-round water load represents a desalination plant that supplies a constant flow rate to a water network. A "Day only" profile where constant flow rate is supplied for 9h during daytime only (8am to 5pm) was considered to test if such water load shifting to day hours only would enhance the benefits of variable RO operation. Finally, an "Agricultural" water load profile was synthetically built in a way to mimic solar power profile on a typical sunny day, and was weighted with seasonal coefficients (

Table 4-2) adapted from a study representing irrigation of an olive orchards in the Mediterranean (Todde et al., 2019). These load profiles are plotted in Figure 19. It should be noted that all demand profiles were scaled in such a way that yearly consumption is exactly the same across all case studies, 730,000 m^3 per year (averaging 2000 m^3/d).

Table 4-1 Water demand profiles of different case studies considered

Demand profile	Description	Average Daily Load
Residential	Water demand peaking at 9am and 9pm, with a relatively low flat day use	2000 m^3
Industrial	High quasi constant load from 8am to 4am, with a small dip between 4am and 8am	2000 m^3
Constant	Constant all day and night	2000 m^3
Day Only	Constant for 9h only during daytime, zero at night	2000 m^3
Agricultural	A hypothetical irrigation load that follows typical solar power profile	2000 m^3

Table 4-2 Seasonal Weighting Coefficients for Residential and Agricultural Profiles

	JAN	FEB	MAR	APR	MAY	JUN	JUL	AUG	SEP	OCT	NOV	DEC
Residential	63%	60%	63%	66%	70%	75%	91%	100%	97%	88%	79%	70%
Agriculture	0%	0%	53%	65%	65%	82%	100%	100%	65%	53%	0%	0%
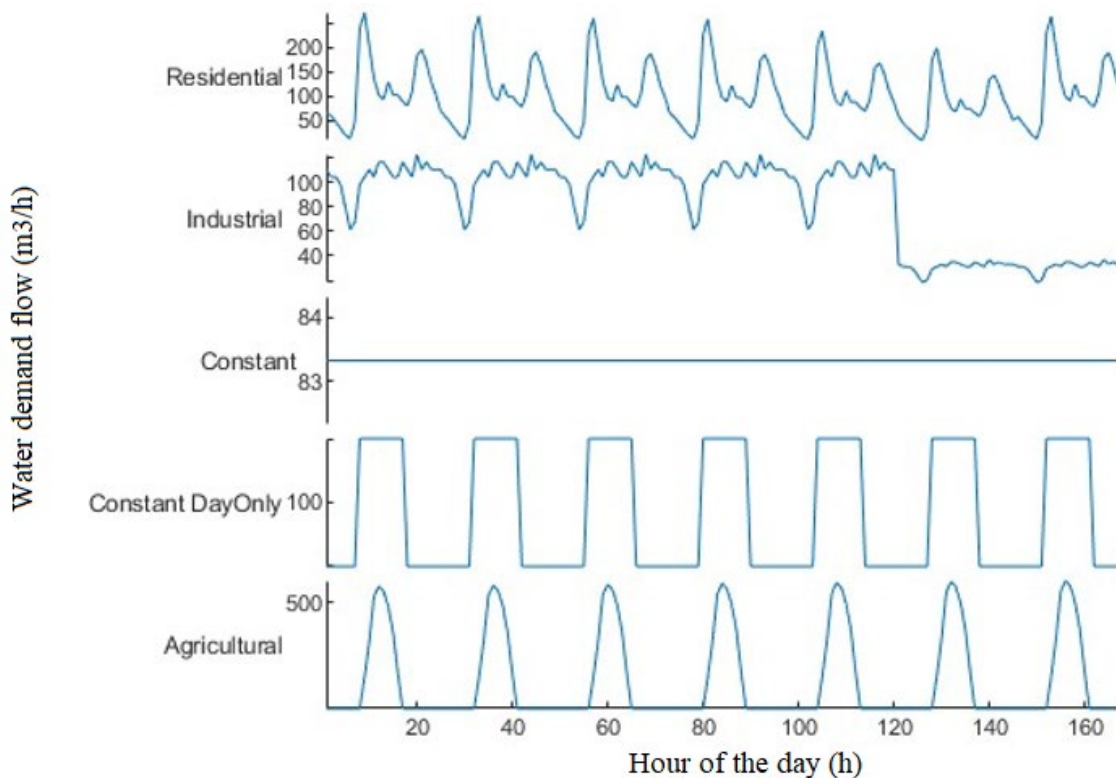
Figure 19 Plot of one week of the different water demand profiles

Investment costs for each of the system components are annualized over their expected lifetimes using an interest rate of 5%. The PV system, the water storage, and the battery (Saft Batteries, n.d.) systems are annualized over 25 years, while the diesel generator is annualized over 10 years and the RO system over 20 years. Capital investment costs, annuity factors and maintenance costs used in the simulation are given in Table 4-3.

Table 4-3 Investment, annuity factors and maintenance costs of the system components

Component	Units	Unit Cost (USD)	Annuity (Years / Rate)	Annuity Factor	Maintenance (USD)	Running Costs (USD)	References
Water Storage Tank	(m3)	220	(25/5%)	0.07095	1% of investment		(Carta & Cabrera, 2021)
Diesel Generator	(kW)	250	(10/5%)	0.1295	0.5$/h	Diesel Fuel 1.2$/L	(Masrur et al., 2020) (Mehrjerdi, 2020)
Battery Storage	(kWh)	400	(25/5%) half (cf. III-B)	0.07095	1% of investment	Degradation	(Rodríguez-Gallegos et al., 2018), market survey
Solar Generator	(kWp)	600	(25/5%)	0.07095	1% of investment		(Masrur et al., 2020), market survey
RO Nominal Permeate Flow	(m3/d)	2000	(20/5%)	0.08024	0.25$/m3		(Upeksha & Christian, 2017) (Carta & Cabrera, 2021) (Bhojwani et al., 2019)

4.2. Analysis of different component combinations

Each case study was simulated under five different compositions as detailed in Table 4-4.

Table 4-4 Different system combinations simulated

Combination Description	RO Fixed with DG, without BSS and without PV	RO Fixed with PV, without BSS and without DG	RO Variable with PV, without BSS and without DG	RO Fixed with BSS and DG and PV	RO Variable with BSS, DG and PV
Composition Tag	C1	C2	C3	C4	C5
With Solar Generator		X	X	X	X
With Battery Storage				X	X
With Diesel Generator	X			X	X
Fixed RO Operation	X	X		X	
Variable RO Operation			X		X

Graphical representations of all five combinations are shown in Figure 20 to Figure 22. The yearly costs of the optimal solutions found for each combination are shown in the stacked columns graphs for each case study Figure 23 to Figure 27 while LCOW values are shown in Figure 28. In all five case studies considered, the LCOW is the lowest using combinations C5 and C4, followed by C1, C3 and C2 respectively.
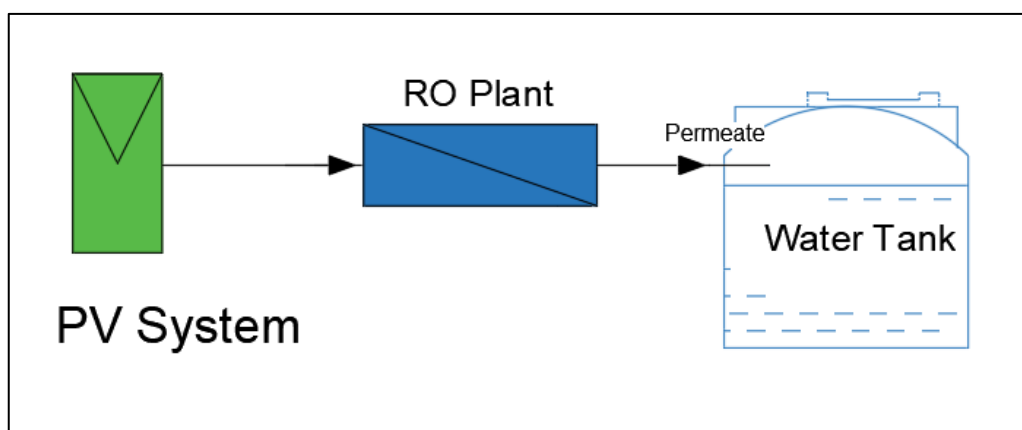
Figure 20 Graphical representation of C2 (fixed RO) and C3(variable RO)

In C2 and C3, the RO system relies solely on solar power from PV. Consequently, it can only function during daylight hours when there is a sufficiently high solar resource. In the fixed operation mode (C2), the RO plant remains inactive when the available solar power falls below the level required for its fixed nominal operating point. When the available solar power surpasses this nominal power threshold, the RO plant operates at its fixed nominal operating point, and any excess solar power is dumped. In the variable RO operation mode (C3), the RO plant operates at its minimum power level whenever the available solar power is adequate to cover that minimum requirement. In the 45% recovery rate strategy, this minimum power level is approximately 50% of the nominal operating power. After a slow start in the morning, the RO plant's operating power gradually increases in line with the available solar power until it reaches the nominal operating level. At this stage, any surplus solar power is dumped.

Taking into account that PV power gradually increases in the morning, reaches its peak at noon, and then diminishes, the optimal solutions found involve oversizing the RO, WST, and PV systems. This approach is necessary to accommodate the fluctuating and unstable solar resource during the limited periods of sunlight. However, this increase in system sizes has significant drawbacks, including excessively high annuity and maintenance costs. Consequently, the levelized cost of water (LCOW) values are quite high, ranging between 1.76 and $2.37 per cubic meter. Furthermore, this configuration suffers from a significant number of RO system startups per year, with occurrences ranging between 286 in the industrial case study and 411 in the agricultural case study.

Moreover, there is a considerable amount of available but unused solar energy, known as the dumped solar fraction, which ranges from 71% to 88%. This surplus solar energy results directly from the extensive oversizing of the PV system, except in the case of the agricultural study where this fraction ranges from 47% to 66%. Further discussion regarding the agricultural case study can be found below.
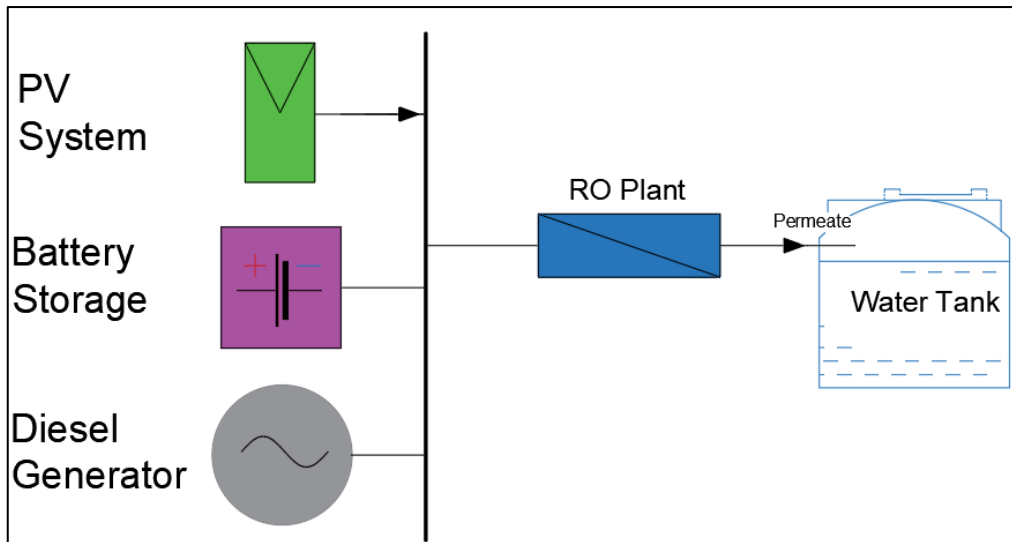
Figure 21 Graphical representation of C4 (fixed RO) and C5(variable RO)

In C4 and C5, the incorporation of backup energy systems (DG and BSS) into the power mix brings significant improvements. These additions allow for the utilization of a smaller RO system, WST, and PV generator, effectively mitigating the challenges posed by the PV power intermittency.

With C4 and C5, the sizes of the RO systems needed to meet the required water demand are reduced by 54% to 71% compared to C2 and C3. Similarly, PV system sizes are reduced by 59% to 80%, and WST sizes are diminished by 76% to 98% (excluding the agricultural case study). These substantial reductions in component sizes naturally result in lower LCOW values, ranging between 0.97 and $1.52 per cubic meter.

Additionally, the number of RO system startups is halved or even further reduced compared to C2 and C3. The fraction of energy supplied by diesel in C4 and C5 ranges between 10% and 13.5%, indicating that solar energy still accounts for 86.5% to 90% of the total RO energy consumption. The dumped solar fraction is decreased to a range between 35% and 43% (excluding the agricultural case study), indicating a significant reduction in unused solar energy.
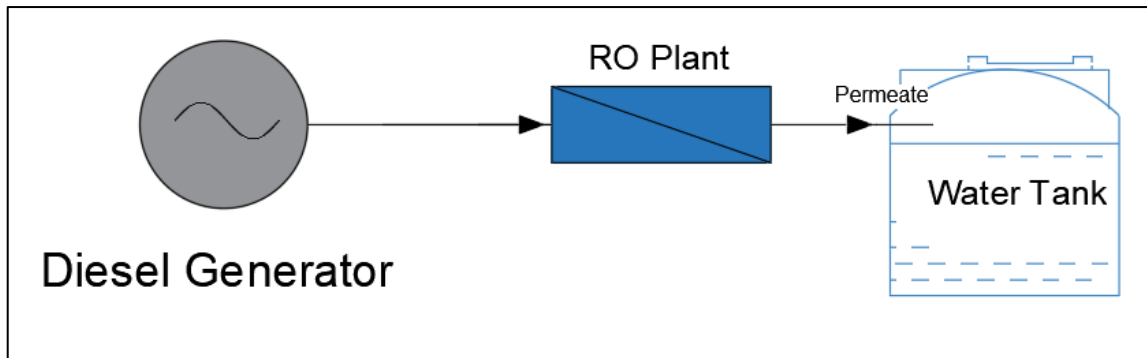
Figure 22 Graphical representation of C1

In C1, the RO system relies solely on a diesel generator for power, without the inclusion of PV systems. This setup enables the RO system to operate at any time of the day, following a steady state (fixed) regime. As a result, the RO system size is at its minimum, reducing the RO annuity and maintenance cost. However, the cost of diesel fuel is at its maximum.

In C1, diesel fuel cost ranges between 51 and 56% of the total yearly cost (except in the agricultural case study where it is 41%). LCOW ranges between 1.44 and $1.60/m^3 (except in agricultural case study where it is $1.98/m^3). The number of RO system startups is similar to that of C4 and C5.

Regarding the agricultural case study, irrigation of orchards is not required during January, February, November, and December, while irrigation demand peaks during the summer months. Given that the total yearly water volumes are similar across all case studies, the RO system size for agricultural use should be much larger than in other scenarios. This is necessary to produce the entire yearly volume within a shorter time frame of 8 months instead of 12. The high water demand in summer aligns with abundant solar resources, resulting in smaller WST, smaller BSS, and smaller fractions of dumped PV power. The increased costs associated with the larger RO system outweigh the benefits of smaller WST and BSS, leading to a significantly higher LCOW for this case study.

In conclusion, when considering energy supply to an RO plant without access to grid power, the combinations C4 and C5 are preferable. C4 offers cost savings ranging from 36% to 57%

compared to C2. Interestingly, C1 proves to be more cost-effective than C2 and C3. This implies that, in the absence of CO_2 emissions taxation, supplying an RO system with solar power alone, without the use of a diesel generator and battery storage, is more expensive than supplying it using diesel fuel, with costs ranging from 20% to 57% higher. These values are based on a diesel cost of $1.2 per liter and may vary if diesel prices change.
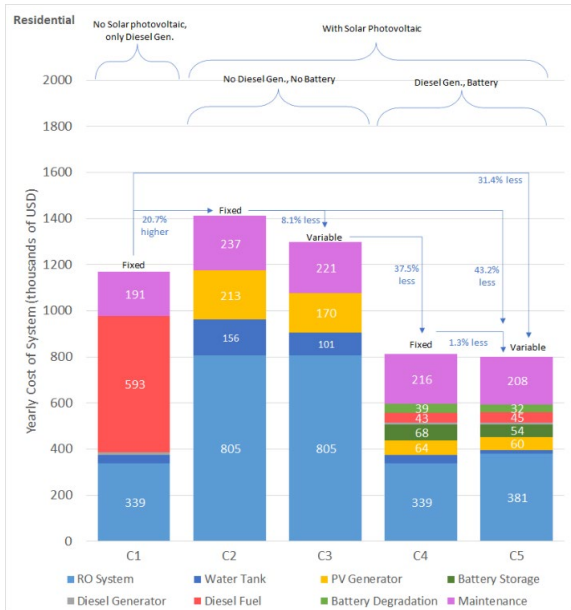
Figure 23 Residential yearly costs
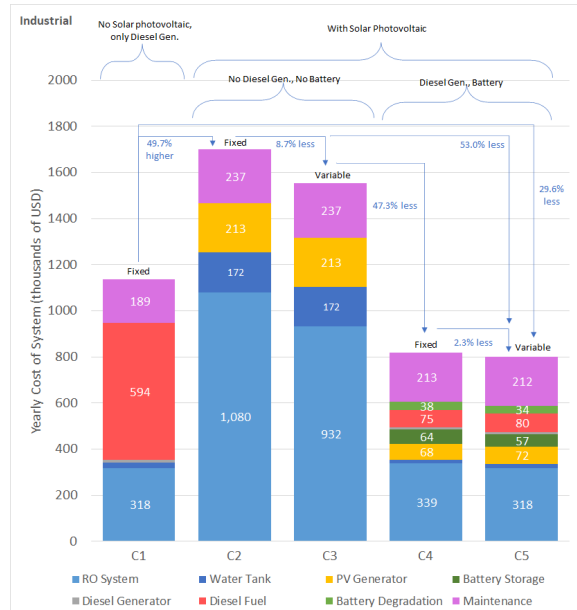
Figure 24 Industrial yearly costs
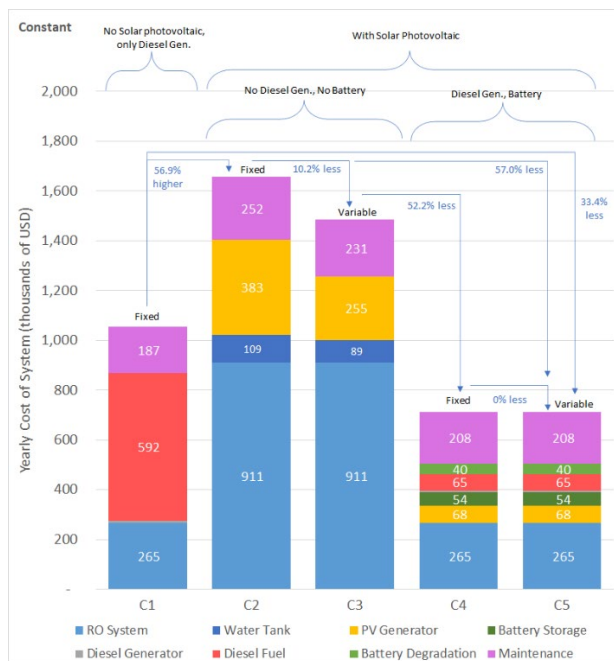
Figure 25 Constant flow yearly costs
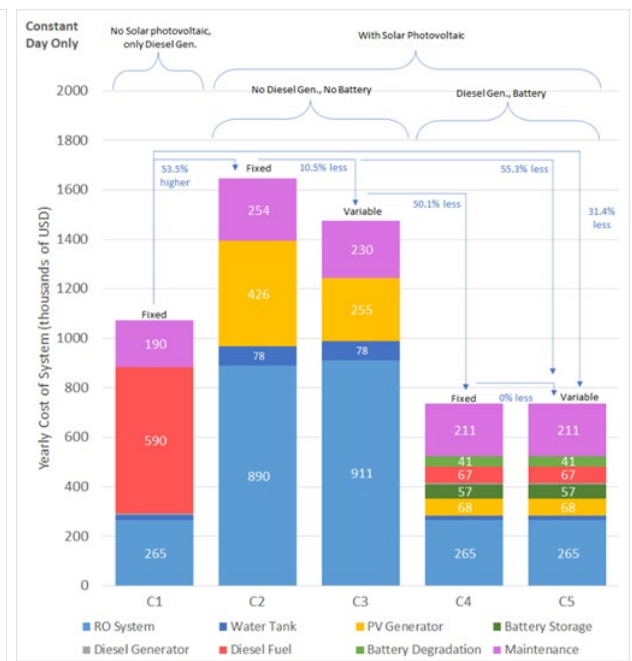
Figure 26 Constant flow day only yearly costs
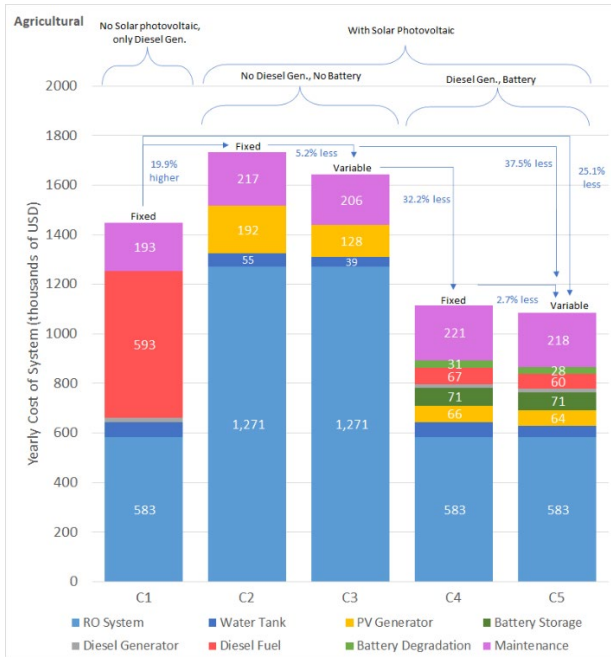
Figure 27 Agricultural yearly costs
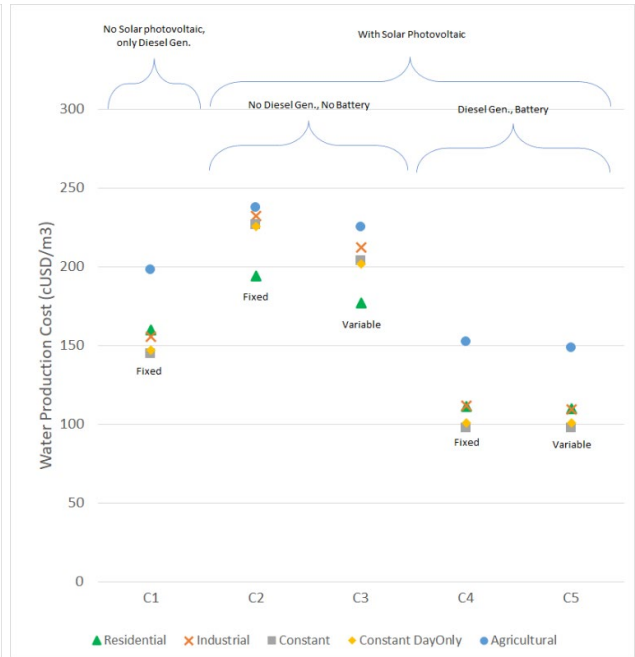
Figure 28 Levelized cost of water for the considered case studies

4.3. Analysis of variable RO Operation

The main distinction between C2 and C3 lies in the ability of C3 to vary the power level of the reverse osmosis (RO) system within the safe operating window, whereas C2 operates at a fixed power level equivalent to the nominal RO power. Yearly cost savings achieved through variable operation can be observed by comparing C2 to C3, where no diesel generator and battery storage are employed. The same comparison can be made between C4 and C5 when DG and BSS are utilized. These savings are summarized in Table 4-5.

Table 4-5 Savings on yearly costs resulting from variable operation

	Using C3 instead of C2	Using C5 instead of C4
Residential	8.1%	1.3%
Industrial	8.7%	2.3%
Constant	10.2%	0.0%
Constant day only	10.5%	0.0%
Agricultural	5.2%	2.7%

When energy backup systems are not utilized, modulating the RO power level significantly reduces yearly costs. These savings come from the fact that the RO plant will be modulating its

power level whenever solar resource is insufficient to operate at full power, yet enough to operate within its SOW, or else when the WST is full.

The typical behavior during winter and summer seasons is illustrated in Figure 29 for C3 in the constant case study. Looking at these graphs, it is clear that the benefit from variable RO operation is almost null during most of the day. In fact, the conditions needed for RO power modulation primarily occur during morning and evening hours and on cloudy days, but never during periods of intense sunlight. During strong sun hours, the RO plant operates at its nominal power level, especially that C3 always boosts an excessively oversized PV system as discussed in section 4.2 above.
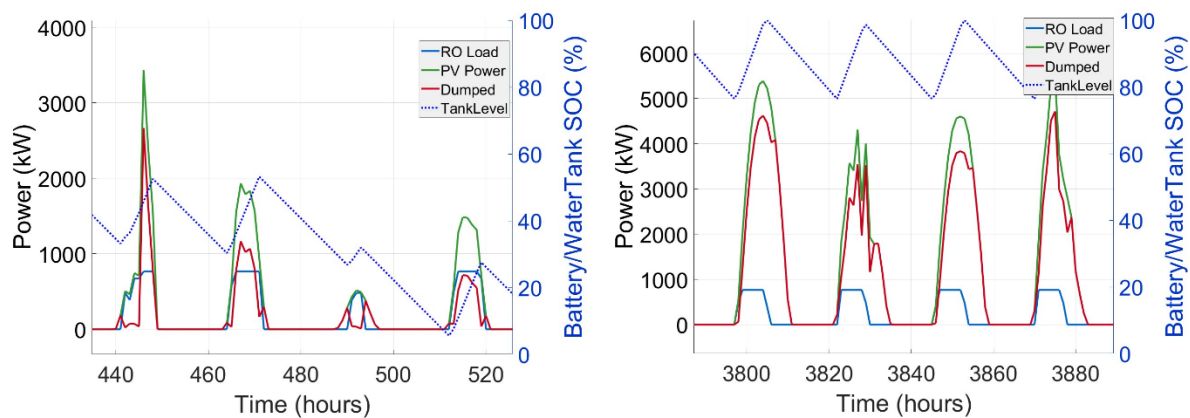
Figure 29 Extract of typical winter (left) and summer (right) days under C3 in the Constant case study

Figure 30 shows the frequency of RO operation levels for C2/C3, and for C4/C5 for all case studies considered. The large modular operation around 51% in constant day-only under C3 mostly represents reduction of power level during summer caused by a full tank condition and as such doesn't represent savings attributed to variable operation. Such condition doesn't show under the constant case study as the WST level is reduced during the nights, and then filled back up during the day.
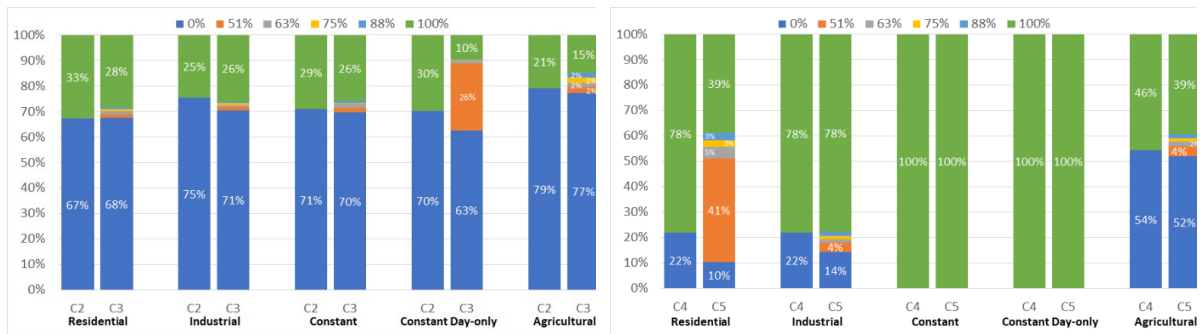
Figure 30 Frequencies of RO power operation levels under C2 and C3 (left) and under C4 and C5 (right)

Overall, savings shown in Table 4-5 between C2 and C3 are attributed to the reduction in required system component sizes in C3, either through a smaller solar generator, a smaller WST or a smaller RO system, or a combination thereof. The magnitude of these savings varies depending on daily and seasonal profiles of water demand. To gain further insight into the impact of demand profiles, Table 4-6 illustrates the RO system annuity cost portion out of the total yearly costs for all case studies and combinations considered. This portion is clearly the largest between all cost centers and directly stems from the substantial capital costs associated with the RO system.

Table 4-6 RO annuity portion of total yearly cost

	C1	C2	C3	C4	C5
Residential	29%	57%	62%	42%	48%
Industrial	28%	63%	60%	41%	40%
Constant	25%	55%	61%	37%	37%
Constant day only	25%	54%	62%	36%	36%
Agricultural	40%	73%	77%	52%	54%
Average	**29%**	**61%**	**64%**	**42%**	**43%**

In fact, with a value of $2000/ (m^{3}d^{-1}) as shown in Table 4-3, RO CAPEX is relatively very high compared to the CAPEX of other components, in a way that it becomes economically inefficient to install a large RO system and then modulate its power level to match solar resources. On the contrary, with the current affordability of PV systems, it becomes more optimal to oversize the PV generator in order to maximize the utilization of the RO plant. This observation helps explain the lower percentage of savings observed in the agricultural case study between C2 and C3. In this case, the RO CAPEX alone represents 77% of the costs in C3, in

addition to the lower utilization time (the RO plant being off during the 4 months of the rainy season).

The lack of significant savings between C4 and C5, as depicted in Table 4-5, can also be attributed to the relatively high RO CAPEX compared to other system components. The integration of a diesel generator and battery storage provides substantial operational flexibility, resulting in optimal solutions that aim to minimize the size of the RO system to a middle ground between the requirements for high-demand periods and low-demand periods throughout the year. This is particularly evident in the 0% savings between C4 and C5 in the constant and constant day-only case studies. Figure 31 illustrates a snapshot of winter and summer operation under C5 in the Constant case study. The optimal solution found under C5 entails running the RO plant at a fixed power level equal to nominal power level, leading to the same operational behavior as in C4. During winter, the diesel generator kicks in whenever the BSS level drops to 20% and then turns off when solar power is available. In summer, the diesel generator remains unused since the BSS stores enough power during the day to sustain the fixed full level operation of the RO plant.
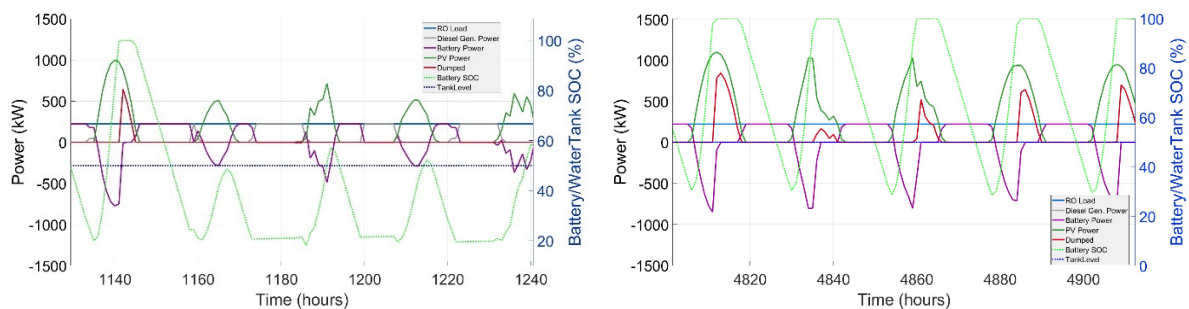
Figure 31 Extract of typical winter (left) and summer (right) days under C5 in Constant case study

The slight savings attributed to variable operation shown for agricultural, industrial, and residential case studies (2.7%, 2.3%, and 1.3% respectively) come from the minor RO oversizing caused by the seasonal variations in the agricultural and residential case studies (high in summer, lower in winter), and the weekend low load in the industrial case study. With a

67

slightly larger than needed RO plant during low load periods, variable operation kicks in and makes use of any small amount of solar power available. This is shown in the snapshot of 6 days in February in the residential case study in Figure 32.
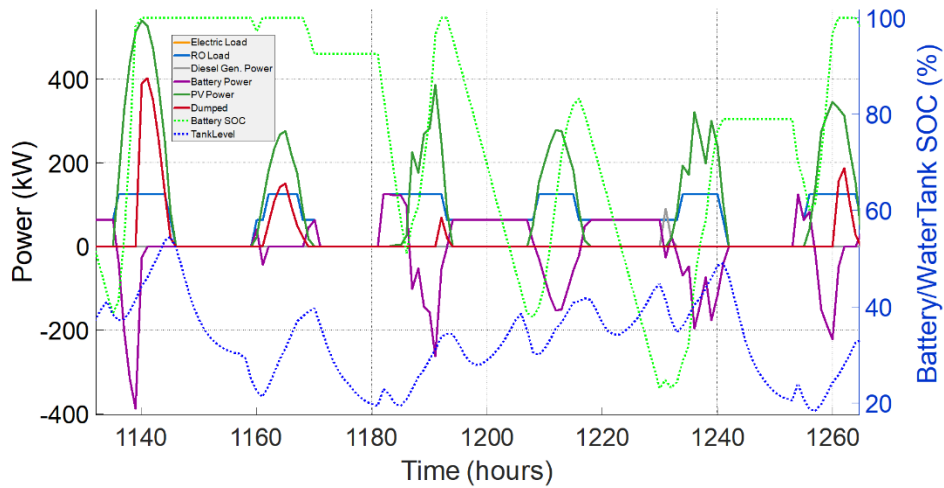
Figure 32 Snapshot of 6 days in February under C5 – residential

Simply put, the current CAPEX costs of RO systems are high enough not to permit variable operation from being economically attractive whenever backup energy sources are possible.

Following Table 4-7 provides the main results for all case studies under C5.

Table 4-7 Main results under C5

			Residential	Industrial	Constant	Constant Day only	Agricultural
Component Sizes	Water Storage Tank	(m3)	800	1,200	100	1,200	3,000
	Diesel Generator	(kW)	270	270	270	225	450
	Battery Storage	(kWh)	3,800	4,000	3,800	4,000	5,000
	Solar Generator	(kWp)	1,400	1,700	1,600	1,600	1,500
	RO Nominal Permeate Flow	(m3/d)	2,878	2,398	2,000	2,000	4,397
Annuity costs	Water Storage Tank	(1000 USD)	12.5	18.7	1.6	18.7	46.8
	Diesel Generator	(1000 USD)	8.7	8.7	8.7	7.3	14.6
	Battery Storage	(1000 USD)	53.9	56.8	53.9	56.8	71.0
	Solar Generator	(1000 USD)	59.6	72.4	68.1	68.1	63.9
	RO System	(1000 USD)	381.3	317.8	265.0	265.0	582.5
	Investment Annuity	(1000 USD)	516.0	474.4	397.3	415.9	778.7
	Investment Value	(1000 USD)	7,355.5	6,911.5	5,871.9	6,182.7	10,932.5
O&M Costs	Diesel Fuel Spent	(1000 USD)	44.8	80.0	65.4	67.2	59.5
	Battery Degradation	(1000 USD)	32.2	34.1	40.3	41.5	27.8
	Maintence Cost	(1000 USD)	208.3	212.0	208.1	211.4	218.4
	Yearly System Cost	(1000 USD)	**801.3**	**800.5**	**711.1**	**735.9**	**1,084.5**
Indicators	Count RO Yearly Startups	(Occurences)	176	76	-	-	421
	Generator Running Time	(Hours)	909	1,282	1,131	1,233	570
	Solar Fraction	(%)	92.5	86.8	89.1	88.7	90.1
	Diesel Fraction	(%)	7.7	13.5	11.0	11.2	10.0
	Dumped Solar	(%)	29.8	43.6	38.0	35.5	28.6
Water Cost	RO Energy Consumed	(MWh)	1,883	1,945	1,956	1,956	1,937
	Water Produced	(m3)	730,176	729,814	730,000	730,000	731,435
	Specific Energy Consumption	(kWh/m3)	2.58	2.67	2.68	2.68	2.65
	Energy Cost	(USD/MWh)	425.6	411.5	363.6	376.2	560.0
	LCOW	(USD/m3)	**1.10**	**1.10**	**0.97**	**1.01**	**1.48**

The Ordinal Optimization process ensures system reliability, which refers to the ability to meet the specified demand consistently throughout the operating period. During simulation, if a design fails to supply the required demand and results in a large amount of energy not supplied (ENS), it is penalized proportionally. Similarly, oversized designs incur higher costs and are also likely to be rejected in the ordinal optimization process as they rank low in the selection of the top designs.

4.4. Sensitivity analysis on system prices

Using an annual growth rate of 10% in global cumulative online saline water reverse osmosis (SWRO) capacity and a learning rate of 10%, (Upeksha & Christian, 2017) estimated an RO

cost of $1,603/m3/d in 2030 and $1,282/m3/d in 2040. In our sensitivity analysis, we varied RO capital costs between $2,000 and $1,000. Investment cost projections for battery energy storage systems range from $200 to $350, depending on different scenarios (Fleer et al., 2018). According to (Al-Bastak & Abbas, 1998), projected solar PV module prices should decrease by about 20% to 60%, depending on different scenarios and different markets. Such a decrease would result in about a 10% to 30% decrease in total solar system prices, and as such, we varied solar system prices between $600 and $300. The diesel fuel price trends vary significantly depending on considered scenarios, but we can estimate that the diesel market price will continue to increase as environmental pressures increase and CO_2 emission taxes are introduced. Diesel prices were varied between $1.2/L to $2.35/L.

Table 4-8 shows yearly system costs with increasing diesel fuel prices. We can see that a two-fold increase in diesel fuel price ($2.35/L) is required to make combination C1 more expensive than combination C2, while a diesel fuel price of $2.05/L is required to make combinations C1 more expensive than combinations C3. In all cases, with increasing diesel prices, C4 and C5 are still the most affordable combinations.

Table 4-9 shows yearly system costs with decreasing RO CAPEX. With an RO cost of $1500/m3/d, the variable operation now saves about 2.9% (instead of 1.3%) in the residential case between C2 and C3 and saves 9.4% (instead of %8.1) in the residential case between C4 and C5. Similar observations can be made on the other combinations. In general, we note that the cheaper the RO cost, the greater the benefit from the variable RO operation. Table 4-10 shows the effects of varying solar prices and battery storage system prices together. As these systems are both expected to see their prices reduced in the future, combinations relying on solar and BES without diesel become more and more affordable. As a result, C4 and C5 are still the best solutions with BESS prices of $200/kWh and PV prices of $300/kWp. We can also note that the merits of C4 and C5 over C2 and C3 and C1 is also bigger with decreasing BESS prices.

Table 4-8 Yearly costs with varying diesel fuel price

Diesel $1.2/L, BESS $400/kWh, Solar $600/kWp, RO $2000/m3/d

	C1	C2	C3	C4	C5
Residential	1,168,887	1,411,310	1,297,524	811,474	801,322
Industrial	1,136,321	1,701,574	1,553,335	819,052	800,467
Constant	1,054,716	1,655,031	1,486,334	711,148	711,148
Const. DayOnly	1,072,813	1,647,253	1,473,868	735,914	735,914
Agricultural	1,446,967	1,734,391	1,643,752	1,115,093	1,084,488

Diesel $1.6/L, BESS $400/kWh, Solar $600/kWp, RO $2000/m3/d

	C1	C2	C3	C4	C5
Residential	1,366,612	1,411,310	1,297,524	825,771	816,252
Industrial	1,334,332	1,701,574	1,553,335	844,000	827,136
Constant	1,252,147	1,655,031	1,486,334	732,961	732,961
Const. DayOnly	1,269,639	1,647,253	1,473,868	758,308	758,308
Agricultural	1,644,513	1,734,391	1,643,752	1,137,281	1,104,325

Diesel $2.35/L, BESS $400/kWh, Solar $600/kWp, RO $2000/m3/d

	C1	C2	C3	C4	C5
Residential	1,737,346	1,411,310	1,297,524	852,579	844,246
Industrial	1,705,602	1,701,574	1,553,335	890,778	877,141
Constant	1,622,330	1,655,031	1,486,334	773,860	773,860
Const. DayOnly	1,638,688	1,647,253	1,473,868	800,299	800,299
Agricultural	2,014,910	1,734,391	1,643,752	1,178,884	1,141,519

Table 4-9 Yearly costs with varying RO CAPEX

Diesel $1.2/L, BESS $400/kWh, Solar $600/kWp, RO $2000/m3/d

	C1	C2	C3	C4	C5
Residential	1,168,887	1,411,310	1,297,524	811,474	801,322
Industrial	1,136,321	1,701,574	1,553,335	819,052	800,467
Constant	1,054,716	1,655,031	1,486,334	711,148	711,148
Const. DayOnly	1,072,813	1,647,253	1,473,868	735,914	735,914
Agricultural	1,446,967	1,734,391	1,643,752	1,115,093	1,084,488

Diesel $1.2/L, BESS $400/kWh, Solar $600/kWp, RO $1500/m3/d

	C1	C2	C3	C4	C5
Residential	1,084,154	1,210,068	1,096,282	726,740	705,997
Industrial	1,056,884	1,431,486	1,320,318	734,319	721,029
Constant	988,465	1,427,310	1,258,613	644,897	644,897
Const. DayOnly	1,006,562	1,424,828	1,246,147	669,663	669,663
Agricultural	1,301,332	1,416,640	1,326,002	969,457	938,853

Diesel $1.2/L, BESS $400/kWh, Solar $600/kWp, RO $1000/m3/d

	C1	C2	C3	C4	C5
Residential	999,420	1,008,826	895,041	642,007	610,671
Industrial	977,446	1,161,398	1,087,301	649,585	641,591
Constant	922,214	1,199,589	1,030,892	578,646	578,646
Const. DayOnly	940,311	1,202,402	1,018,425	603,412	603,412
Agricultural	1,155,696	1,098,890	1,008,251	823,821	793,217

Table 4-10 Yearly costs with varying solar system and BES system prices

Diesel $1.2/L, BESS $400/kWh, Solar $500/kWp, RO $2000/m3/d

	C1	C2	C3	C4	C5
Residential	1,168,887	1,375,835	1,269,144	800,831	791,389
Industrial	1,136,321	1,666,099	1,517,860	807,700	788,405
Constant	1,054,716	1,591,176	1,443,764	699,796	699,796
Const. DayOnly	1,072,813	1,576,303	1,431,298	724,562	724,562
Agricultural	1,446,967	1,702,463	1,622,467	1,104,095	1,073,846

Diesel $1.2/L, BESS $400/kWh, Solar $400/kWp, RO $2000/m3/d

	C1	C2	C3	C4	C5
Residential	1,168,887	1,340,360	1,240,764	790,189	781,456
Industrial	1,136,321	1,630,624	1,482,385	796,348	776,344
Constant	1,054,716	1,527,321	1,401,194	688,444	688,444
Const. DayOnly	1,072,813	1,505,353	1,388,728	713,210	713,210
Agricultural	1,446,967	1,670,536	1,601,182	1,093,098	1,063,203

Diesel $1.2/L, BESS $400/kWh, Solar $300/kWp, RO $2000/m3/d

	C1	C2	C3	C4	C5
Residential	1,168,887	1,304,885	1,212,384	779,546	771,523
Industrial	1,136,321	1,595,149	1,446,910	784,996	764,282
Constant	1,054,716	1,463,466	1,358,624	677,092	677,092
Const. DayOnly	1,072,813	1,434,403	1,346,158	701,858	701,858
Agricultural	1,446,967	1,638,608	1,579,897	1,082,101	1,052,561

Diesel $1.2/L, BESS $300/kWh, Solar $500/kWp, RO $2000/m3/d

	C1	C2	C3	C4	C5
Residential	1,168,883	1,375,831	1,269,141	774,119	769,866
Industrial	1,136,318	1,666,095	1,517,856	782,264	765,684
Constant	1,054,713	1,591,173	1,443,760	676,244	676,244
Const. DayOnly	1,072,809	1,576,299	1,431,294	700,001	700,001
Agricultural	1,446,964	1,702,459	1,622,464	1,078,575	1,049,146

Diesel $1.2/L, BESS $200/kWh, Solar $500/kWp, RO $2000/m3/d

	C1	C2	C3	C4	C5
Residential	1,168,880	1,375,828	1,269,137	747,406	748,344
Industrial	1,136,314	1,666,091	1,517,853	756,828	742,962
Constant	1,054,709	1,591,169	1,443,757	652,693	652,693
Const. DayOnly	1,072,806	1,576,296	1,431,291	675,441	675,441
Agricultural	1,446,960	1,702,456	1,622,460	1,053,054	1,024,446

The above sensitivity analysis shows that the conclusions regarding the merits of different scenarios do not change much with varying prices, if price changes fall within a reasonable range. For instance, a twofold increase in Diesel prices would be required to make scenarios C2

or C3 more affordable than Scenario C1, which relies solely on DG operation. On the other side, even a 50% drop in the PV prices would keep the optimal designs of Scenarios C4 and C5 more favorable than those of C2 and C3.

Detailed results of each of the system compositions for every case study considered are given in Appendix A.

CHAPTER 5

CONCLUSIONS AND RESEARCH RECOMMENDATIONS

This last chapter summaries the main finding in section 5.1, while suggestions for future work are given in section 5.2.

5.1. Summary and findings

In this study, we developed a flexible and accurate RO system model and integrated it with models of a PV plant, a battery, and a diesel generator. Dynamic programming was employed to optimize the system operation and minimize costs, taking into account factors such as diesel fuel usage and battery degradation.

To efficiently explore the large design search space, we utilized ordinal optimization (OO), which allowed us to quickly and exhaustively rank the different designs. The OO approach involved initially using a simplified model to evaluate designs and establish their cost order. This simplified model sampled the year using only 48 days and considered only three operational levels for the RO plant and the diesel generator.

By applying the principle that order is robust to noise introduced by the simplified model, we ranked the designs and focused on assessing a reduced number of designs using a more accurate model. The accurate model simulated the system on an hourly basis for all days of the year, providing a detailed and realistic evaluation of the selected designs.

By combining the DP optimization approach, the integration of various system components, and the use of OO, we were able to analyze and compare the performance and cost-effectiveness of different system designs in a comprehensive and efficient manner. Using this technique, the

search space on each simulation was reduced from 2304 combinations (in the simple model) down to 72 combinations in the accurate model, saving tremendous amount of time.

The study presents optimal sizing and operational results for five different case studies aimed at minimizing the annual cost of water production. The focus is on the variable operation of a solar PV-powered reverse osmosis (RO) plant, which was found to reduce yearly costs by approximately 5% to 10% depending on the specific water demand profiles.

To further explore cost-saving measures, the study also considers the inclusion of a diesel generator and a battery storage system in the energy mix. Interestingly, while these additional components significantly reduce costs by 37% to 57%, they also diminish the effectiveness of variable operation. Consequently, the savings attributed to variable operation decrease to a range between 0% and 2.7%.

A sensitivity analysis on key parameters such as diesel fuel price, RO prices, solar system prices and BESS costs showed that the conclusion of this work would still be correct in the near future as per 2030 cost projections.

It is noteworthy that the study finds diesel fuel-based operation without solar to be more cost-effective compared to using solar and RO without backup energy systems. This indicates that, in the absence of backup energy systems, relying solely on diesel fuel for operation proves to be a better economical choice if CO_2 emissions are not penalized.

5.2. Study limitations and recommendations for future work

The results obtained in the simulation are subject to the specific cost factors and assumptions used. Considering factors such as seasonal variations in feed water temperature can further enhance the accuracy and realism of the simulation results. By incorporating the effects of temperature on system performance, a more comprehensive understanding of the system's behavior can also be obtained. Heating of the feed flow by any available excess solar power

75

might make the system more energy efficient and increase permeate water production. The effects of membrane fouling may also be assessed to identify any favorable or unfavorable operating regimes.

Furthermore, extending the application of the simulation to different locations with varying solar irradiance patterns would allow for a broader assessment of the system's performance under different environmental conditions. This analysis can help identify optimal system designs and operation strategies tailored to specific geographical locations. Lastly, exploring the impact of minimum startup and shutdown times on variable operation can provide insights into the system's flexibility and efficiency. By adjusting these parameters, it is possible to analyze how different operational constraints affect the overall cost-effectiveness and performance of the system.

APPENDIX A
DETAILED RESULTS OF ALL COMBINATIONS UNDER ALL CASE STUDIES

			Residential				
			C1	C2	C3	C4	C5
Component Sizes	Water Storage Tank	(m3)	2,200	10,000	6,500	2,200	800
	Diesel Generator	(kW)	360	-	-	270	270
	Battery Storage	(kWh)	1	1	1	4,800	3,800
	Solar Generator	(kWp)	-	5,000	4,000	1,500	1,400
	RO Nominal Permeate Flow	(m3/d)	2,558	6,076	6,076	2,558	2,878
Annuity costs	Water Storage Tank	(1000 USD)	34.3	156.1	101.5	34.3	12.5
	Diesel Generator	(1000 USD)	11.7	-	-	8.7	8.7
	Battery Storage	(1000 USD)	-	-	-	68.1	53.9
	Solar Generator	(1000 USD)	-	212.9	170.3	63.9	59.6
	RO System	(1000 USD)	338.9	805.0	805.0	338.9	381.3
	Investment Annuity	(1000 USD)	384.9	1,173.9	1,076.7	514.0	516.0
	Investment Value	(1000 USD)	4,798.4	15,232.4	13,862.4	7,595.5	7,355.5
O&M Costs	Diesel Fuel Spent	(1000 USD)	593.2	-	-	42.9	44.8
	Battery Degradation	(1000 USD)	-	-	-	38.7	32.2
	Maintence Cost	(1000 USD)	190.8	237.4	220.8	215.9	208.3
	Yearly System Cost	(1000 USD)	**1,168.9**	**1,411.3**	**1,297.5**	**811.5**	**801.3**
Indicators	Count RO Yearly Startups	(Occurences)	164	337	306	153	176
	Generator Running Time	(Hours)	6,852	-	-	644	909
	Solar Fraction	(%)	-	100.0	100.0	92.9	92.5
	Diesel Fraction	(%)	100.0	-	-	7.2	7.7
	Dumped Solar	(%)	-	77.9	70.8	31.2	29.8
Water Cost	RO Energy Consumed	(MWh)	1,956	1,947	1,942	1,956	1,883
	Water Produced	(m3)	730,233	727,542	733,310	729,914	730,176
	Specific Energy Consumption	(kWh/m3)	2.68	2.68	2.65	2.68	2.58
	Energy Cost	(USD/MWh)	597.6	724.8	668.1	414.9	425.6
	LCOW	(USD/m3)	**1.60**	**1.94**	**1.77**	**1.11**	**1.10**

			Industrial				
			C1	C2	C3	C4	C5
Component Sizes	Water Storage Tank	(m3)	1,500	11,000	11,000	900	1,200
	Diesel Generator	(kW)	360	-	-	270	270
	Battery Storage	(kWh)	-	-	-	4,500	4,000
	Solar Generator	(kWp)	-	5,000	5,000	1,600	1,700
	RO Nominal Permeate Flow	(m3/d)	2,398	8,154	7,035	2,558	2,398
Annuity costs	Water Storage Tank	(1000 USD)	23.4	171.7	171.7	14.0	18.7
	Diesel Generator	(1000 USD)	11.7	-	-	8.7	8.7
	Battery Storage	(1000 USD)	-	-	-	63.9	56.8
	Solar Generator	(1000 USD)	-	212.9	212.9	68.1	72.4
	RO System	(1000 USD)	317.8	1,080.4	932.1	338.9	317.8
	Investment Annuity	(1000 USD)	352.8	1,464.9	1,316.6	493.7	474.4
	Investment Value	(1000 USD)	4,380.4	18,884.4	17,036.4	7,249.5	6,911.5
O&M Costs	Diesel Fuel Spent	(1000 USD)	594.0	-	-	74.8	80.0
	Battery Degradation	(1000 USD)	-	-	-	37.9	34.1
	Maintence Cost	(1000 USD)	189.5	236.7	236.7	212.6	212.0
	Yearly System Cost	(1000 USD)	**1,136.3**	**1,701.6**	**1,553.3**	**819.1**	**800.5**
Indicators	Count RO Yearly Startups	(Occurences)	104	320	286	175	76
	Generator Running Time	(Hours)	7,305	-	-	1,098	1,282
	Solar Fraction	(%)	-	100.0	100.0	87.7	86.5
	Diesel Fraction	(%)	100.0	-	-	12.6	13.5
	Dumped Solar	(%)	-	76.6	77.0	39.0	43.6
Water Cost	RO Energy Consumed	(MWh)	1,956	1,961	1,948	1,956	1,945
	Water Produced	(m3)	729,960	732,498	732,408	730,873	729,814
	Specific Energy Consumption	(kWh/m3)	2.68	2.68	2.66	2.68	2.67
	Energy Cost	(USD/MWh)	581.0	867.8	797.5	418.7	411.5
	LCOW	(USD/m3)	**1.56**	**2.32**	**2.12**	**1.12**	**1.10**

			Constant				
			C1	C2	C3	C4	C5
Component Sizes	Water Storage Tank	(m3)	100	7,000	5,700	100	100
	Diesel Generator	(kW)	270	-	-	270	270
	Battery Storage	(kWh)	-	-	-	3,800	3,800
	Solar Generator	(kWp)	-	9,000	6,000	1,600	1,600
	RO Nominal Permeate Flow	(m3/d)	2,000	6,875	6,875	2,000	2,000
Annuity costs	Water Storage Tank	(1000 USD)	1.6	109.3	89.0	1.6	1.6
	Diesel Generator	(1000 USD)	8.7	-	-	8.7	8.7
	Battery Storage	(1000 USD)	-	-	-	53.9	53.9
	Solar Generator	(1000 USD)	-	383.1	255.4	68.1	68.1
	RO System	(1000 USD)	265.0	910.9	910.9	265.0	265.0
	Investment Annuity	(1000 USD)	275.3	1,403.3	1,255.3	397.3	397.3
	Investment Value	(1000 USD)	3,392.3	18,292.4	16,206.4	5,871.9	5,871.9
O&M Costs	Diesel Fuel Spent	(1000 USD)	592.3	-	-	65.4	65.4
	Battery Degradation	(1000 USD)	-	-	-	40.3	40.3
	Maintence Cost	(1000 USD)	187.1	251.7	231.0	208.1	208.1
	Yearly System Cost	(1000 USD)	1,054.7	1,655.0	1,486.3	711.1	711.1
Indicators	Count RO Yearly Startups	(Occurences)	-	364	289	-	-
	Generator Running Time	(Hours)	8,760	-	-	1,131	1,131
	Solar Fraction	(%)	-	100.0	100.0	89.1	89.1
	Diesel Fraction	(%)	100.0	-	-	11.0	11.0
	Dumped Solar	(%)	-	86.0	80.0	38.0	38.0
Water Cost	RO Energy Consumed	(MWh)	1,956	1,958	1,938	1,956	1,956
	Water Produced	(m3)	730,000	730,746	730,417	730,000	730,000
	Specific Energy Consumption	(kWh/m3)	2.68	2.68	2.65	2.68	2.68
	Energy Cost	(USD/MWh)	539.2	845.3	767.0	363.6	363.6
	LCOW	(USD/m3)	1.44	2.26	2.03	0.97	0.97

			Constant Day-Only				
			C1	C2	C3	C4	C5
Component Sizes	Water Storage Tank	(m3)	1,300	5,000	5,000	1,200	1,200
	Diesel Generator	(kW)	225	-	-	225	225
	Battery Storage	(kWh)	-	-	-	4,000	4,000
	Solar Generator	(kWp)	-	10,000	6,000	1,600	1,600
	RO Nominal Permeate Flow	(m3/d)	2,000	6,715	6,875	2,000	2,000
Annuity costs	Water Storage Tank	(1000 USD)	20.3	78.0	78.0	18.7	18.7
	Diesel Generator	(1000 USD)	7.3	-	-	7.3	7.3
	Battery Storage	(1000 USD)	-	-	-	56.8	56.8
	Solar Generator	(1000 USD)	-	425.7	255.4	68.1	68.1
	RO System	(1000 USD)	265.0	889.7	910.9	265.0	265.0
	Investment Annuity	(1000 USD)	292.6	1,393.5	1,244.4	415.9	415.9
	Investment Value	(1000 USD)	3,645.1	18,188.4	16,052.4	6,182.7	6,182.7
O&M Costs	Diesel Fuel Spent	(1000 USD)	590.5	-	-	67.2	67.2
	Battery Degradation	(1000 USD)	-	-	-	41.5	41.5
	Maintence Cost	(1000 USD)	189.7	253.8	229.5	211.4	211.4
	Yearly System Cost	(1000 USD)	1,072.8	1,647.3	1,473.9	735.9	735.9
Indicators	Count RO Yearly Startups	(Occurences)	1	368	362	-	-
	Generator Running Time	(Hours)	8,753	-	-	1,233	1,233
	Solar Fraction	(%)	-	100.0	100.0	88.7	88.7
	Diesel Fraction	(%)	100.0	-	-	11.2	11.2
	Dumped Solar	(%)	-	88.2	75.2	35.5	35.5
Water Cost	RO Energy Consumed	(MWh)	1,954	1,956	1,821	1,956	1,956
	Water Produced	(m3)	729,417	729,980	730,557	730,000	730,000
	Specific Energy Consumption	(kWh/m3)	2.68	2.68	2.49	2.68	2.68
	Energy Cost	(USD/MWh)	548.9	842.2	809.6	376.2	376.2
	LCOW	(USD/m3)	1.47	2.26	2.02	1.01	1.01

			Agricultural				
			C1	C2	C3	C4	C5
Component Sizes	Water Storage Tank	(m3)	4,000	3,500	2,500	4,000	3,000
	Diesel Generator	(kW)	495	-	-	450	450
	Battery Storage	(kWh)	-	-	-	5,000	5,000
	Solar Generator	(kWp)	-	4,500	3,000	1,550	1,500
	RO Nominal Permeate Flow	(m3/d)	4,397	9,593	9,593	4,397	4,397
Annuity costs	Water Storage Tank	(1000 USD)	62.4	54.6	39.0	62.4	46.8
	Diesel Generator	(1000 USD)	16.0	-	-	14.6	14.6
	Battery Storage	(1000 USD)	-	-	-	71.0	71.0
	Solar Generator	(1000 USD)	-	191.6	127.7	66.0	63.9
	RO System	(1000 USD)	582.5	1,271.0	1,271.0	582.5	582.5
	Investment Annuity	(1000 USD)	661.0	1,517.2	1,437.7	796.5	778.7
	Investment Value	(1000 USD)	8,264.2	19,310.4	18,190.4	11,182.5	10,932.5
O&M Costs	Diesel Fuel Spent	(1000 USD)	592.6	-	-	66.6	59.5
	Battery Degradation	(1000 USD)	-	0.0	-	31.1	27.8
	Maintence Cost	(1000 USD)	193.3	217.2	206.0	220.9	218.4
	Yearly System Cost	(1000 USD)	**1,447.0**	**1,734.4**	**1,643.8**	**1,115.1**	**1,084.5**
Indicators	Count RO Yearly Startups	(Occurences)	257	400	411	236	421
	Generator Running Time	(Hours)	4,019	-	-	628	570
	Solar Fraction	(%) -	0.2	100.0	100.0	90.8	90.1
	Diesel Fraction	(%)	100.2	-	-	11.1	10.0
	Dumped Solar	(%)	-	65.9	47.0	32.7	28.6
Water Cost	RO Energy Consumed	(MWh)	1,958	1,959	1,915	1,960	1,937
	Water Produced	(m3)	730,776	731,059	731,006	732,608	731,435
	Specific Energy Consumption	(kWh/m3)	2.68	2.68	2.62	2.68	2.65
	Energy Cost	(USD/MWh)	739.0	885.5	858.4	568.8	560.0
	LCOW	(USD/m3)	**1.98**	**2.37**	**2.25**	**1.52**	**1.48**

APPENDIX B
LIST OF PUBLICATIONS

1.   **A. Zein, S. Karaki, M. Al-Hindi,** Analysis of variable reverse osmosis operation powered by solar energy - *2023 Renewable Energy,*
http://dx.doi.org/10.1016/j.renene.2023.03.001

2.   **A. Zein, C. Ghabech and S. H. Karaki**, Optimization of a Solar Photovoltaic Micro Grid for Electricity and Desalinated Water Production, *2018 4th International Conference on Renewable Energies for Developing Countries (REDEC),* Beirut, Lebanon, pp. 1-6,
https://doi.org/10.1109/REDEC.2018.8597815

3.   **A. Zein and G. Bazzoun** Integration of photovoltaic generators into existing diesel mini-grids in Lebanon: Deir-Kanoun village case study *2013 25th International Conference on Microelectronics (ICM)* http://dx.doi.org/10.1109/ICM.2013.6734997

APPENDIX C
JOURNAL PAPER MANUSCRIPT
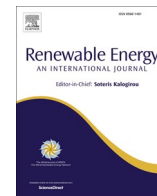
Analysis of variable reverse osmosis operation powered by solar energy

Adnan Zein [a,*], Sami Karaki [a], Mahmoud Al-Hindi [b]

[a] *Department of Electrical and Computer Engineering, American University of Beirut, Lebanon*
[b] *Department of Chemical Engineering and Advanced Energy, American University of Beirut, Lebanon*

ARTICLE INFO

ABSTRACT

The use of solar photovoltaic (PV) to power reverse osmosis (RO) plants and produce water will enhance the sustainability of water supplies in several dry remote coastal areas. Varying the operating power level of the RO plant has been proposed in the literature as a solution to accommodate intermittent PV power sources. Such variable operation is intended to match the RO load to the available PV power. Nevertheless, such operation has not been used outside research laboratories and small pilot plants. In this work, we used different case studies to evaluate the benefit of using variable operation and its effects on system design, system operation and levelized cost of water (LCOW). A simulation model for the optimal operation of the system is developed using three-dimensional dynamic programming (DP) to determine the power levels of the battery, diesel generator, and RO plant while optimal sizing of these plants and associated water tanks and PV generators was solved using an ordinal optimization (OO) approach. The use of OO permitted the examination of a large design search space quickly but exhaustively using a simple model. We then ranked the different designs in increasing cost order and assessed a reduced number of these using an accurate model to simulate the system on an hourly basis for all the days of a year. This approach relies on the fundamental tenet of OO: "order is robust to the noise introduced by the simple model". Different power modulation strategies are investigated, and their implications on the hydraulic operating parameters are presented. In this respect, we investigate the operation of the RO system at varying power levels and different sizes of backup systems (battery and diesel generator). This ability to vary the RO operating level helped in a better matching of the system load to the available, yet variable, PV power, even when the backup and storage systems were at a minimum. Operating an RO plant with PV and backup systems is found to be far more cost effective than operation without backup systems, reducing costs by 37–55% for the case studies considered.

1. Introduction

Renewable energy is becoming an important player in the energy sector and is promising to become a major resource for future communities. With increasing populations and water requirements for human activities, water scarcity is growing, especially in areas with high sun irradiation. Using renewable energy for the production of fresh water in desalination plants is currently attracting a lot of research effort [1-4].

The intermittent nature of RE is the most important hurdle to their usage in RO desalination systems. While recent developments in the lithium-ion technologies reduced the costs of battery storage systems (BSS) and increased round-trip storage efficiencies, the integration of a BSS is still a heavy investment. System designers have two alternatives for serving the loads under continuous bad weather conditions, either greatly oversizing the BSS to cover the worst days of the year or

integrating backup diesel generators. For islands, remote areas, or military bases, reducing the dependence on such backup diesel generators is a strategic objective as it comes at a higher cost than that from stand-alone solar systems. For this reason, researchers proposed a different approach for overcoming RE intermittencies: varying the power level of the RO plant to match it with solar and/or wind resources, desalinating large amounts of water during high RE production times and storing it in water storage tanks (WST) for later use.

Stand-alone PV-RO systems suffer from the impossibility of balancing solar generators sizes and water demand. On the one hand, a small solar generator can only supply enough power to an RO system for a limited amount of time during day hours, on the other hand, increasing the size of the solar generator results in wasting larger portions of available but unused solar power (when available solar power surpasses the maximum operation power of the RO). If a steady state (fixed power level) operation regime is considered, this balancing dilemma strongly

Nomenclature

P_i	Power delivered by the PV generator at time i	γ	PV panel power temperature coefficient
N_V	Total number of PV panels	Q_{Pi}	Flow of water into tank at time i
(STC)	Nominal PV power at STC	Q_{Di}	Flow of water out of tank at time i
S_i	Solar Irradiance level at time i	SOC_{min}	Minimum state of charge
T_i	PV Module temperature at time i	SOC_{max}	Maximum state of charge
$\varphi_B(G_i)$	Diesel fuel consumption as a quadratic function	G_{min}	Minimum power operation level of the generator
E_{life}	Total expected battery energy over its lifetime	G_{max}	Maximum power operation level of the generator
E_B	Battery capacity	B_{min}	Minimum operation level of the battery
N_{DOD}	Expected battery number of cycles at given DOD	B_{max}	Maximum operation level of the battery
$\delta(B_i)$	Measure of battery degradation	R_{min}	Minimum operation level of the RO
P_i	PV power	R_{max}	Maximum operation level of the RO
G_i	Diesel generator power	W_{min}	Minimum operating volume level of the RO
B_i	Battery power	W_{max}	Maximum operating volume level of the RO
L_i	Electric load	T_{year}	Number of hours per year 8760
R_i	Reverse osmosis load	A_j	Annuity factor of component j with 5% rate
D_i	Dumped power at time i	I_j	Initial investment cost of component j
		Δh	Duration of one time period, equals 1 h

affects RO running times, as the operation window is restricted to the periods of the day where available solar power is equal or greater than the needed fixed power level. If a variable operation regime is considered instead, this dilemma still affects running times, but to a lesser extent, as variable operation requires a certain minimum level of power supply to keep system parameters within the safe operation window (SOW) of the RO membranes. Combining RO plants with PV generators, battery storage system (BSS), water storage tank (WST) and a diesel generator (DG) introduces much flexibility into the system and is here demonstrated to strongly reduce the overall cost of water. In fact, the main contribution of this work is to show that integrating backup systems (DG, BSS, and WST) always leads to lower levelized cost of water (LCOW).

Conventional RO plants operate at quasi-constant feed pressure and quasi-constant flow rate, while direct coupling to Renewable Energy (RE) sources require modulation of power consumption and thus modulation of hydraulic parameters. In fact, manufacturers of RO membranes usually give guarantees for their products under recommended steady conditions [5]. Despite these manufacturers restrictions, researchers have tested power modulation on pilot projects, and their conclusions ranged from no deterioration [6,7] to improved performance [8,9] of the membranes under variable operation. This improved performance is explained by improved diffusion and reduced concentration polarization resulting from increased turbulence under fluctuating pressure and flow rates inside the membranes. An investigation by Richards et al. [10] evaluated the effects of irradiation transients on the RO performance, by varying the solar input power level and transient occurrence frequency. They reported good overall performance, noting positive effects of a varying feed pressure level on the membrane's performance. The authors in Ref. [11] analyzed the operation data over 14-years of an intermittently operated RO plant (~9 h/d) and concluded that daily shutdowns and start-ups did not cause additional problems in the desalination plant, indicating that intermittent operation of BWRO desalination plants is feasible over the long term. The permeability of RO membranes declines with usage, Freire-Gormaly et al. [12] compared intermittent and continuous operations with regards to RO membrane fouling for brackish water and concluded that the decline of the membrane permeability can be reduced in intermittent operation with a permeate water rinse before shutdown period. The same authors studied the effect of components sizing of a PV-RO system [13] and concluded that neglecting membranes fouling in such studies would result in under-sized systems. In our work, we did not include the fouling simulation as it is not part of the main objectives of our research and would not affect a variable RO system more than it affects a constant

operation RO system.

The modulation of RO power requires the operation of the RO membranes in varying pressure and flow conditions. The study of these variable conditions leads to the concept of safe operating window (SOW), first proposed by Feron back in 1985 [14]. In a more in-depth analysis, Pohl et al. [15] used the ROSA software (predecessor of the software WAVE) to build the SOW of a commercial membrane by varying its operating conditions. Pohl et al. found out that a constant permeate recovery strategy would be the best choice for a variable RO operation, as it allows low specific energy consumption (SEC) values over a large power operating range, while constant feed pressure strategy is only beneficial when the system operates around its nominal power. Park et al. [16] detailed a method to construct experimentally the SOW for any membrane and any feed water salinity and compared different operating strategies. Although the authors measurements confirmed that a constant recovery strategy is the most efficient one as suggested by Pohl et al. [15], they argued that such operation strategy increases system complexity. The authors of [17] installed a test rig using and RO system with a split-feed flow configuration. They tested different strategies and concluded that constant brine flow strategy offers the widest operation range and lowest SEC, contrarily to previous studies. Differences between these results are explained by the fact that different number of membranes per pressure vessel are considered, and variations in membrane characteristics studied, including permeability coefficients and feed spacer geometries affect optimization results as noted in Ref. [18].

More recent studies have tackled the variable RO operation conditions. The authors in Ref. [19] coupled a portable nano-filtration unit with PV panels, batteries, and a water tank, and compared variable pressure operation with fixed pressure, and concluded that there is a 20% reduction in yearly costs using variable operation. From the design side of the problem, the authors pre-designed some of the system elements, fixing the battery capacity, NF system size, and only optimizing the number of PV panels used. In Ref. [20] the authors analyzed the economic benefit of installing intermittently operated RO plants coupled with renewable energies in coastal areas of Australia and concluded that desalination plants are particularly suitable for load-shifting and may reduce LCOE by 43% and required utility grid capacity by 29%. A thorough study presented in Ref. [21] assesses the cost effectiveness of using wind turbines with a flywheel to operate a standalone RO system with hourly water requirements. The authors modulated the RO operation such that permeate water concentration was fixed and concluded that variable operation reduces water cost by about 14% compared to an on-off strategy.

Research papers published on the topic of variable RO operation have predominantly either focused on the short term (transients, hours) operation of a stand-alone PV-RO (and sometimes storage) [17,22,23] without including it in a full techno-economic context with seasonal variations or have focused on system economics [24], omitting detailed operation parameters. As a result, it is not yet clear if and where variable operation of RO systems is beneficial.

In our previous work [25], we simulated a microgrid supplying both water and electricity to a remote community, where the RO specific power consumption represented an average value of about 2.28 kWh/m^3. The RO plant was operated using a rule-based controller, i.e. turning it on when excess solar energy is available, or when the water level inside the tank drops below minimum. In this work, we developed a flexible and accurate RO system model that accounts for hydraulic and mechanical variability affecting power consumption and cost estimation. The RO plant model was integrated with models of a PV plant, a battery, and a diesel generator using the method of dynamic programming (DP) to determine the hourly level of operation over a year. The two-dimensional method [27] was extended to calculate the power mix of three subsystems: The RO plant, the diesel generator, and the battery. This upgrade allowed us to assess the variable operation of the RO system as presented in this paper. The objective is to minimize the cost of system operation accounting for diesel fuel usage, and battery degradation. We used ordinal optimization (OO) to examine the design search space of different sizes of the RO, PV, water tanks, and diesel generator, and select the ones to yield a minimum levelized cost of water. The design search space is large, but it is quickly and exhaustively examined using a simple model. The different designs are thus assessed and then ranked in increasing cost order. A reduced number of designs, as predicted by the OO theory, are then assessed using an accurate model to simulate the system on an hourly basis for all the days of a year and deduce an accurate system cost. This approach relies on the fundamental tenet of OO, which states that order obtained through the simple model is robust to noise introduced by the simulation using the simple model. The simple model samples the year using only 48 days and allows three operational levels of the RO plant and three levels of the diesel generator (DG). The accurate model allows for more DG and RO power levels, e.g. 5 to 7 levels for each. Using OO, we significantly reduce the number and complexity of the simulation runs needed to obtain a system design. The Optimal sizing and operational results are presented for five different case studies, with the objective of minimizing the yearly cost of operation of water production.

Section II presents the general design of the system used, with a description of the problem solving process. Section III outlines the developed models of each of the system components, with an emphasis on the detailed RO system model. The simulation results and discussions are provided in section IV followed by section V, which summarizes the conclusions of our study.

2. Problem formulation

The topology of the proposed system is shown in Fig. 1. The proposed system consists of a microgrid with the following components: diesel generators, batteries, solar panels, RO plant, and water tanks.

A power management and control system are used to operate the battery storage and the RO plant. The power level of the RO system is dictated by varying the operation frequency of its pumps, and by controlling the position of the concentrate pressure valve. This controller also manages the charging and discharges powers of the battery and turns on or off the diesel generator in a way to guarantee system stability. If the batteries are full, then excess solar energy power is dumped (not produced by shifting the MPPT voltage of the PV plant). The operation thus described can be challenging if one needs to operate the system with the objective of minimizing the specific cost of water. Furthermore, the system itself must consist of components with sizes selected to minimize the investment cost. The objective is to select a set of components sizes and operate them somewhat as described in a way to minimize the specific cost of water production.

The proposed hybrid system is composed of a variety of complex components, with non-linear operation regimes, varying efficiencies, and restrictions on allowable operating ranges. To name a few, safe RO system operation is limited to a window of input/output conditions that restricts operating range.

The set of pumps included in the RO system have varying efficiencies depending on the chosen hydraulic operating points, which in turn have an effect on the desalted water output flow and salinity. In addition, the shutdown and startup of RO systems should respect minimum up and down times for the sake of membranes longevity and to allow backwash cleaning of the membranes. Diesel generators and battery storage systems have non-linear efficiencies, while solar radiation variability adds an additional layer of complexity.

In order to make realistic evaluations of such a system, the use of detailed models of its components is essential. The detailed models of the various components, described below, were integrated into the DP-based simulation, based on hourly data points.

2.1. Ordinal optimization for components sizing (OO)

The OO theory provides a probabilistic framework for reducing the search space and the computational effort involved in ranking the different alternatives. OO is based on the idea that the relative order of different alternatives in a decision problem is robust with respect to
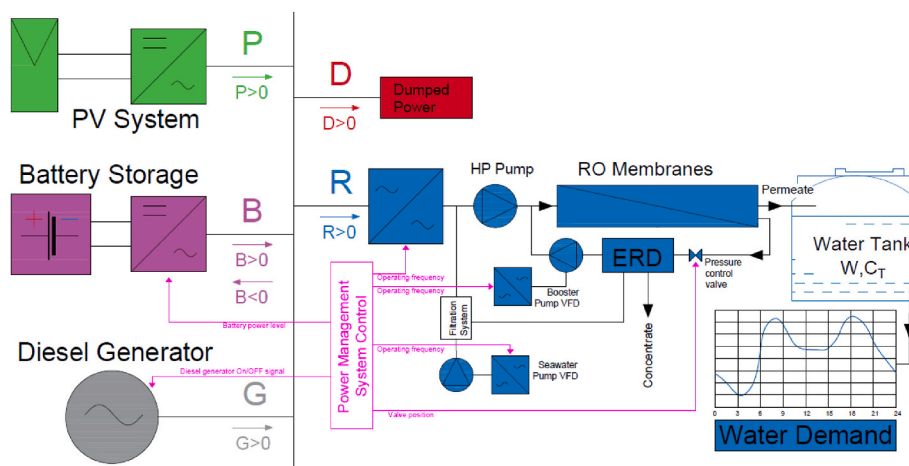

Fig. 1. Topology of system with power control signals (Adapted from Ref. [25]).

estimation noise. This implies that if a set of alternatives is very approximately evaluated and ordered according to this approximate evaluation, then there is high probability that the actual good alternatives can be found in the top-s estimated good choices.

Jabr et al. [26] used OO to locate and size distributed generators on power distribution-grid nodes. The OO formulation used in this work is closely based on their approach. A similar approach was used by Karaki et al. [27] in sizing the components of a fuel cell car. The overall sizing optimization logic is summarized in Fig. 2. The steps for OO implementation are described in the following paragraphs.

Reduce the Search Space: let Θ represent the population of all designs, and Λ represents the population of the top α-percent designs in Θ. If we randomly pick N designs in Θ, the probability that at least one of these designs is in Λ is $1 - (1 - \alpha)^N$. If this probability is desired to be at least P, then N should be chosen as follows [28]:

$$N \geq \frac{\ln(1 - P)}{\ln(1 - \alpha)} \tag{1}$$

Choosing $P = 99.9\%$, and $\alpha = 0.3\%$, then N should be at least 2300. In reality, the choice of the N alternatives is enhanced by a heuristic choice based on our knowledge of the water and electricity needs and associated component sizes. Thus, N is an upper limit for the number of designs that respect P.

Rank the Alternative Designs: a simple model of the system is applied on all N alternative designs of the reduced search space, then these are ranked according to their year costs.

Find the Size of the top-s Designs: let S denote the subset of the top-s alternative designs among the above ordered N designs using the simple model and let the actual top-g designs denote the good enough subset G, that is, the truly good enough designs are the top-g alternatives among the accurately ordered N designs. By assuming an infinite variance of the estimation noise of the simple model relative to the accurate

model, it is possible to compute the value s such that at least k truly good enough alternatives are in S with a given value of the alignment probability:

$$AP(k) = Prob(|G \cap S| \geq k) = \sum_{i=k}^{\min(g,s)} \frac{\binom{g}{i}\binom{N-g}{s-i}}{\binom{N}{s}} \tag{2}$$

If we choose $k = 1$, the value of s that gives $AP(1) \geq 0.975$ is the number of top-s designs to be chosen among the N designs, ordered using the simple model, with a 97.5% chance that at least 1 of these s-designs is among the truly top-g designs. In our case, choosing $N = 2304$ and $g = 115$ (5% of N), the s value for $AP(1) \geq 0.975$ is 72 designs.

Rank the Top-s Designs with an Accurate Model: now that we have a small set of designs to test (top-s designs), we will use an accurate model to determine a cost of operation for each of them and finally pick the best of the top-s designs.

2.2. Operation optimization

With a given mix of component sizing, different operating power levels of the battery storage, the diesel generator, and the RO system can be used to optimize costs. The objective is to minimize the yearly cost of the system defined as follows:

$$\min_{n=1...N} \left\{ \sum_j A_j I_j(n) + O_c(n) + M_c(n) \right\} \tag{3}$$

$$O_c(n) = \min \left\{ \sum_{i=1}^{T} [\varphi_G(G_i) + \varphi_B(B_i)] \right\} \tag{4}$$

where $\varphi_G(G_i)$ is a quadratic curve relating fuel consumption costs and electric power generated, and $\varphi_B(B_i)$ is a cost measure of battery degradation. Both functions are defined in Section III. The term $\sum_j A_j I_j(n)$ is the sum of the annualized investment costs of each of the system components, $O_c(n)$ is the yearly operation cost and $M_c(n)$ is the yearly maintenance cost for design n. The above objective function is subject to the following constraints. The power balance equation is given by:

$$G_i + B_i + P_i = R_i + D_i \tag{5}$$

The battery state of charge and the water volume in the tank are given by:

$$SOC_i = SOC_{i-1} - \frac{Q_B(B_i)}{C_{bat}}\Delta t \tag{6}$$

$$W_i = W_{i-1} + (Q_{Pi} - Q_{Di})\Delta t \tag{7}$$

where $Q_B(B_i)$ is the internal energy rate change of the battery when the battery is delivering a power B_i, and the rest of the variables defined in the diagrams of Figs. 1 and 4. The set of inequality constraints arise from the physical capacities of the components are given by:

$$SOC_{min} \leq SOC_i \leq SOC_{max} \tag{8}$$

$$G_{min} \leq G_i \leq G_{max}$$

$$B_{min} \leq B_i \leq B_{max}$$

$$R_{min} \leq R_i \leq R_{max}$$

$$W_{min} \leq W_i \leq W_{max}$$

$$D_i \geq 0$$

The diesel generator and RO system power levels, G_i and R_i, are both discretized in our 3D dynamic programming approach. For each pair of
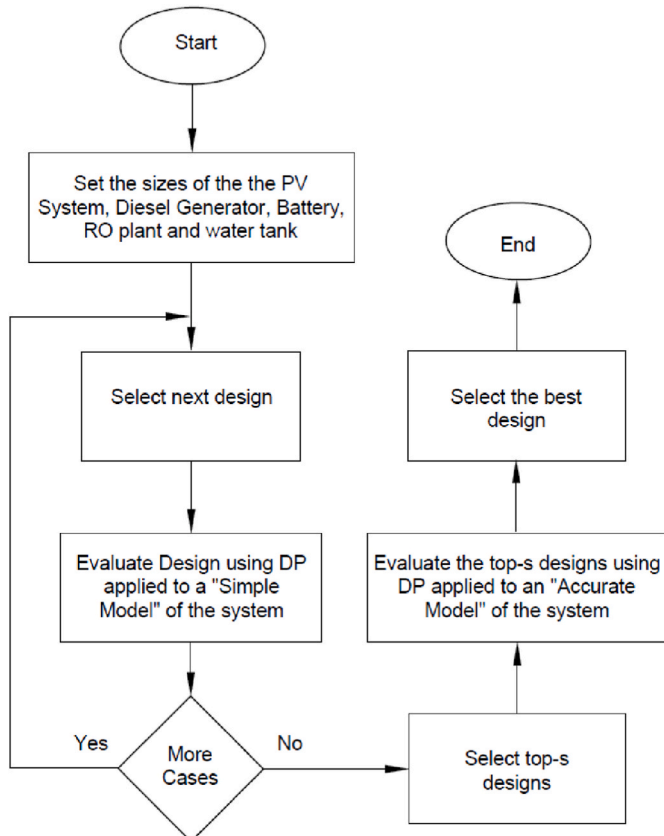

Fig. 2. Ordinal Optimization of components sizes for minimum cost.

values, the required power from the battery is calculation from power balance equation (5). The dumped power Di is usually zero unless the battery is fully charged.

2.3. Combined sizing and operation optimization

Our problem may be looked at as two interrelated optimization tasks, one being the sizing choices of the components mix, and the other being the search for the best operation corresponding to each particular mix. A large pool of system components sizes is chosen, and a simple model calculation is performed, first using hourly data of 48 days to represent the whole year, and very rough discretization of the diesel generator and RO system power levels, with only 3 different levels allowed (0%, 50%, and 100%).

Even though an interval of smaller length than 48 days could be used as simple model, this length was chosen in order to account for battery state of charge and its effects on sizing. A limited set of the best component mixes identified using the simple model are ranked and simulated with the accurate model, using hourly data of 365 days, and 5 different power levels. This formulation provides a probabilistic framework that greatly reduces the computation time needed without affecting the solution. To validate the choice of the simple model we performed the simulations using this model first, ranked the designs, and then re-simulated all combinations using the accurate model, and found out that the simple model ranking actually gives results that are very close to the accurate model results. In Table 1, the example of a simulation with 10 different system sizing combinations compares the rankings obtained using both the simple and the accurate model.

The rank number allocated in the simple model is compared to that allocated by the accurate model, using both a variable RO operation mode and a fixed operation mode. We note that system designs highly ranked in the simple model are also being highly ranked in the accurate model, validating the OO approach used.

This good alignment demonstrate that the ranking made using the simple model is reliable and allows the relaxation of the percentage of good-enough subset that should be accurately simulated.

3. System modelling

3.1. Photovoltaic system

The solar PV generator was simulated using PVSyst [29]. The simulation was done using a 1000kWp system facing south and tilted to optimal year-round production (20° tilt), and irradiation and weather data for Beirut-Lebanon. The output of the simulation was tabulated as MPPT current and MPPT voltage as a function of irradiation and ambient temperature, using conventional solar ground-mount systems. This table is then used in MATLAB in scaled up or down formats as per the different solar system sizes considered, using interpolation between data points. This approach allows a more accurate simulation than the theoretical approach we had used in our previous work [25] as it takes into consideration all details of a typical solar systems such as module temperature variations, light induced degradation, mismatching between solar panels, cabling voltage drops, inverter efficiencies, low light performance, and soiling.

Table 1
Simple and accurate model ranking comparisons.

Rank in Accurate Model	1	2	3	4	5	6	7	8	9	10
Rank in Simple Model – Fixed RO	3	1	2	5	4	6	7	9	8	10
Rank in Simple Model – Variable RO	2	3	4	1	5	7	6	9	8	10

3.2. Battery storage

Battery storage was simulated as a Li-ion battery, using the internal charge model described in our previous work [25], which was first used by Karaki et al. [30] for the simulation of a fuel cell hybrid electric vehicle, scaling it up or down as required by the different battery sizes considered.

The ageing model of the battery system can be made more or less complex as per the required details needed in the simulation. Weitzel et al. [31] described a sophisticated modeling method for battery ageing that divides battery ageing into two components: the total amount of energy cycled through the battery, and battery calendrical ageing, both being a function of the depth of discharge (DOD). Weitzel's model requires the simulation of a plethora of battery parameters such as temperature, charge rate and DOD. In the work presented here, we opted for a simpler, yet representative model, which considers that half of the battery investment is lost in calendrical ageing, and the other half is lost in energy cycling.

The total expected battery energy over its lifetime (E_{life}) is calculated using the battery capacity (E_B) expressed in kWh, the *DOD* and the expected number of cycles (N_{DOD}) at the given *DOD* published by battery manufacturer:

$$E_{life} = E_B DOD N_{DOD} \tag{9}$$

The cyclical ageing (δ_B), in per unit, is calculated as the sum of the delivered energy by the battery (positive output power only) divided by E_{life}:

$$\delta_B = \frac{\sum_{i=1}^{T_{year}} max(B_i, 0) \, \Delta h}{E_{life}} \tag{10}$$

The cost of cyclical ageing φ_B is calculated as the per unit loss times half of the battery investment cost (C_B) while the cost of the calendrical ageing is calculated as annuity factor ($A_{battery}$) times half of C_B.
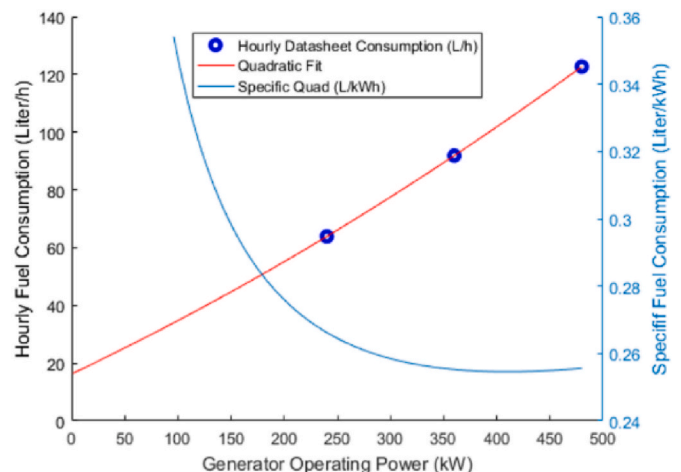
$$\varphi_B = \left(\delta_B + A_{battery} \right) \frac{C_B}{2} \tag{11}$$

3.3. Diesel generator

Backup diesel generators fuel consumption can be modeled by a quadratic fit to manufacturer data.

$$\varphi_G(G_i) = a_0 + a_1 \, G_i + a_2 G_i^{\,2}$$

Consumption levels are usually given by manufacturers for operation at 50%, 75% and 100% of nominal power. Fig. 3 shows the fuel consumption of a CAT 600kVA, 480 kW diesel generator based on

Fig. 3. Diesel generator fuel consumption.

manufacturer data. The specific consumption value (l/kWh) is minimal at around 85% of nominal power. The yearly investment cost of the diesel generators is annualized using A_{10}. Different diesel generator sizes are considered in the simulations using scaled up or down consumption parameters.

3.4. Reverse osmosis

RO-systems are designed as a one-pass configuration for usual domestic water use but can be designed as two-pass configurations for higher water quality if required by specific industrial processesA detailed model of the RO plant has been developed in this work, considering the additional power requirements of the seawater intake pump and the filtration system. It uses the efficiency curves of the various pumps in order to take into account the different operation levels of the RO plant and its effect on the water quality, quantity, and water cost. Commercially available equipment commonly installed in industrial RO plants have been chosen, and their technical sheets used, to make accurate simulations of the RO system's operating regimes.

A one-stage RO system unit has been designed, using 10 pressure vessels, each containing 8 RO membranes, shown in Fig. 4. The RO membrane chosen is a membrane used for single pass designs, and high rejection rates. It has an active area of 41 m^2, maximum operating pressure of 83 bar, and a nominal permeate flow rate of 37.5 m^3/h [32]. The high pressure (HP) pump is chosen to operate at 60 m^3/h and 50 bar [33], and the booster pump (BP) at 50 m^3/h and 2 bar [34]. The seawater intake (SWI) pump needed is a 110 m^3/h and 4 bar [35], and a rotary pressure exchanger is used as energy recovery device (ERD) capable of handling 45–70 m^3/h. In the pressure exchanger element, the pressurized brine comes in direct contact with the low-pressure feed stream where the energy is transferred to the feed stream at a very high efficiency (92%–98% depending on manufacturers [36, 37]). The brine stream is at a lower pressure than the feed water stream, and some additional pressure losses occur across the pressure exchanger, compensated for by the booster pump.

The input-output data of the membranes are simulated in WAVE [38] at different operation levels of the feed flow, feed pressure and input water temperatures. The output of WAVE simulation is tabulated in MATLAB and subsequently coupled with the detailed simulation of the RO plant, using the different pumps hydraulic curves (head-flow-efficiency).

The total RO system power is equal to the sum of HP, BP and SWI required powers, which are calculated separately for each operation level. The following power equation is used for all pumps to calculate required electric pump power:

$$P_{elec} = \frac{\rho g H Q}{3.6 \times 10^6 \mu_p \mu_d} \quad (12)$$

where.

P_{elec}: AC electric power supplied to the pump motor (kW)
ρ: density of sea water (1025 kg/m^3)
g: gravitational constant
H: total dynamic head (m)
Q: water flow in (m^3/h)
μ_p: pump efficiency (as per efficiency curve)
μ_d: motor drive efficiency (94%)

The following mass and power balance relations are used.

- The flow supplied by the HP pump is equal to the RO system feed flow minus the ERD flow (which is in turn equal to the concentrate flow),
- HP Pump head is equal to the pressure vessel input pressure minus the HP pump suction pressure.
- Booster pump flow is equal to the ERD flow as the two elements are working in series.
- Booster pump head is equal to the feed pressure minus the recovered pressure from the concentrate minus the booster pump suction pressure (pressure at the output of the filter)
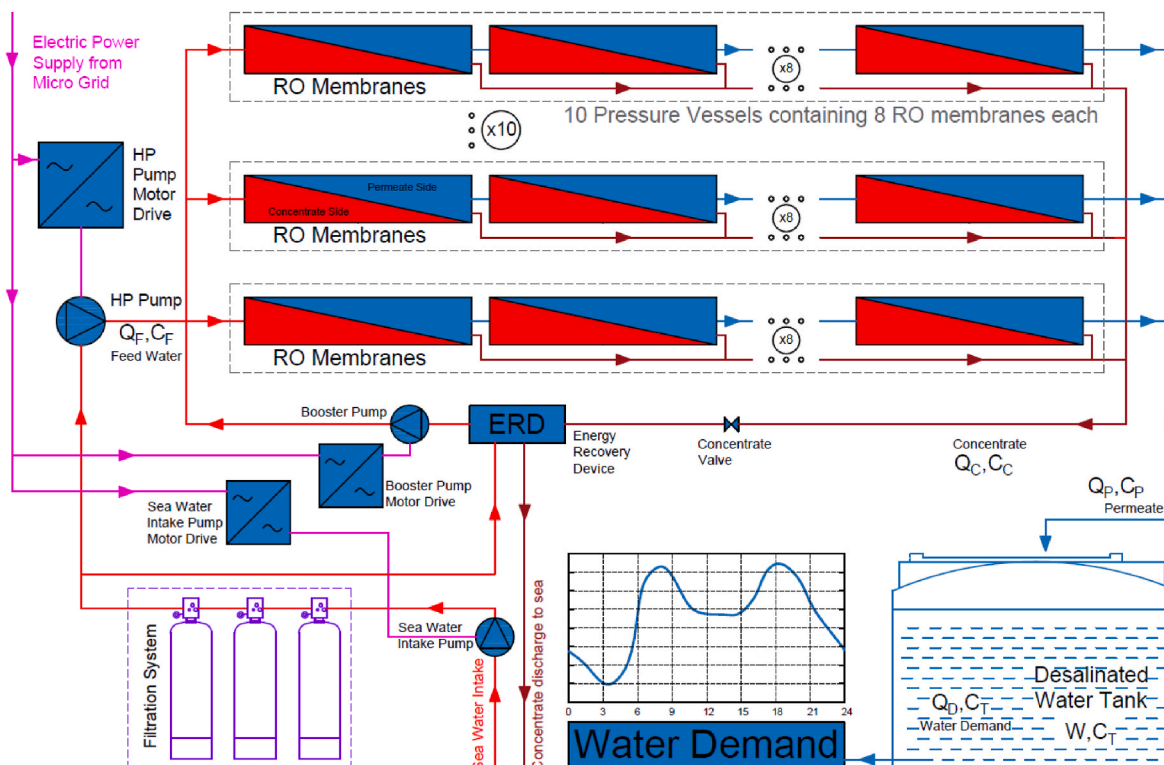

Fig. 4. Simulated RO system design.

- SWI pump flow is equal to the pressure vessels feed flow
- SWI pump head is equal to the input pressure of the filtration system.

Seasonal variation in the seawater temperature directly affects the efficiency of the RO system. The higher the water temperature, the higher the recovery rate under the same feed pressure and flow (and thus same power consumption). For example, in the Mediterranean Sea, water temperature varies between 12 °C in January and 27 °C in August [39]. To estimate the effect of these variations, simulations in WAVE were performed at temperatures of 12, 22 and 27 °C. The energy consumption difference between a feed water of 27 and 12 °C was determined to be around 2.9%, and that between 27 and 22 °C to be 1.1%. These variations can be integrated into the system simulation in the future but have not been taken into consideration in this paper. All data shown in this paper correspond to an average feed water temperature of 22 °C. In Ref. [40], the authors analyzed the effects of using the feed water of the RO plant to cool down the PV panels, increasing both PV and RO systems efficiencies. They concluded that every 1% increase in RO feed temperature results in 1% reduction of required RO pressure.

Fig. 5 shows the operating points of the RO system simulated in WAVE. These points were chosen based on a feed pressure discretization of 5 bar and feed flow discretization of 10 m3/h. The acceptable operating points are marked with an "×" symbol, while non-acceptable operating points are colored. The reason for non-feasibility of the colored operating points comes from hydraulic limitations and permeate quality requirements as explained in the legend.

Interpolation was used to characterize the system operation parameters between the above-simulated operating points. Fig. 6a shows isolines of specified water recovery ratios with steps of 5%. Fig. 6b shows the calculated isolines of specific energy consumption in kWh/m^3, by dividing the plant's power consumption in kW by the corresponding permeate flow rate in m^3/h. Fig. 6c shows isolines of the RO electric power consumption.

As shown in Fig. 6c, each power level of the RO plant can be associated with a continuum of feed water pressure and feed flow sets. Thus, we need to choose an operation strategy that associates each RO power level with a unique set of head-flow values. Once those strategies are defined, each power level of the RO system is translated to a unique set of hydraulic parameters, namely the feed pressure and flow, the permeate flow rate and concentration, among others. The different operating strategies are described below.

- **Constant Feed Pressure**: Membrane manufacturers highly insist on limiting operational pressure variations [5], which would suggest a preference for constant pressure operation. Unfortunately, such a strategy results in small margins of power variation as shown in Fig. 7a. In this strategy, only the feed pressure is fixed to 45 bars while feed flow rate is varied according to allocated power level. Power variation within the SOW range from 85 to 120 kW.
- **Minimum specific energy consumption**, allowing large power level variations, but also results in high variations of feed pressure as shown in Fig. 7b. In this strategy, all RO system states are varied in a way to follow the minimum SEC (normal to the isolines of Fig. 6b). Power variation within the SOW range from 80 to 180 kW.
- **Constant RO water recovery rate**, a compromise strategy allowing large power variations with relatively low pressure modulation, as shown in Fig. 7c. In this strategy, only the RO recovery rate is fixed while feed pressure and flow rates are varied according to allocated power level. In practice, applying this strategy requires varying the speed of the water pumps to regulate flow rate while controlling the concentrate valve at the same time to regulate system pressure. Power variation within the SOW range from 90 to 180 kW.

Fig. 6c shows that the 50% constant recovery rate strategy restricts operational levels to only very high-power values, while the 45% constant recovery rate strategy allows large variations of power. A lower recovery rate is not considered as it results in higher water intake and filtration costs, and low usage level of the investment. As a result, the 45% fixed recovery rate strategy was chosen and used subsequent sections.
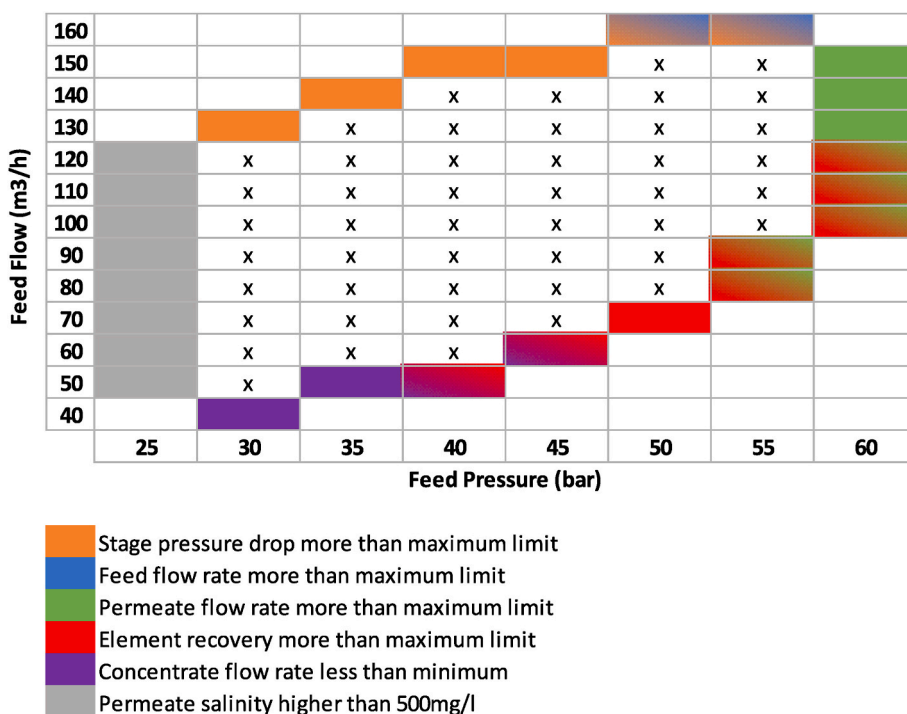

Feed Flow (m3/h)	25	30	35	40	45	50	55	60
160								
150						x	x	
140				x	x	x	x	
130			x	x	x	x	x	
120		x	x	x	x	x	x	
110		x	x	x	x	x	x	
100		x	x	x	x	x	x	
90		x	x	x	x	x		
80		x	x	x	x	x		
70		x	x	x	x			
60		x	x	x				
50		x						
40								

Feed Pressure (bar)

- Stage pressure drop more than maximum limit
- Feed flow rate more than maximum limit
- Permeate flow rate more than maximum limit
- Element recovery more than maximum limit
- Concentrate flow rate less than minimum
- Permeate salinity higher than 500mg/l

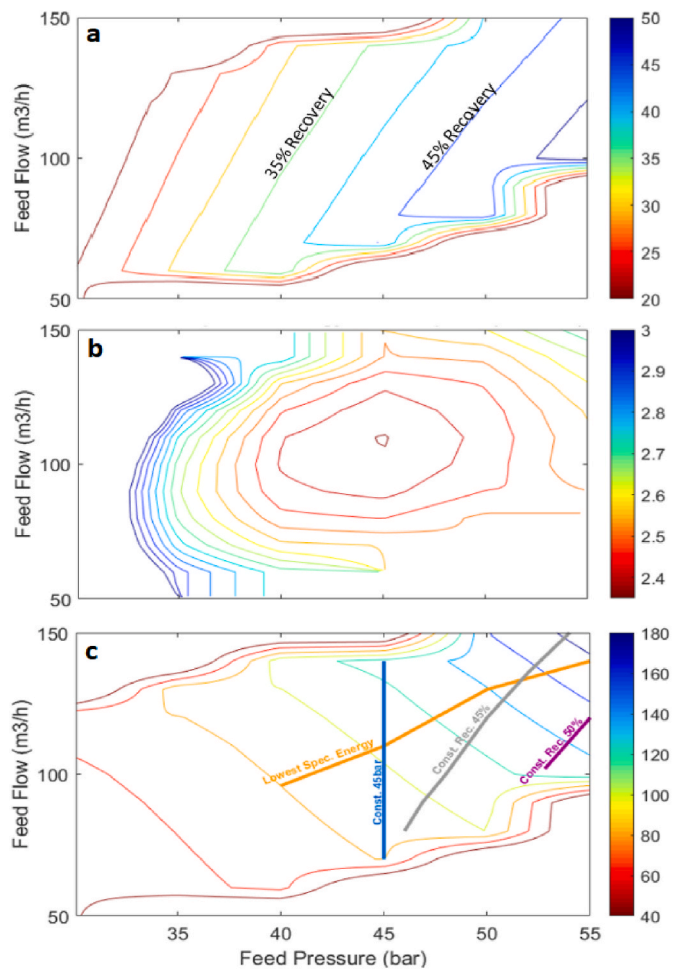**Fig. 5.** Operating points from WAVE.

Fig. 6. RO System model (a) isolines of water recovery (%), (b) isolines of specific energy consumption (kWh/m3), and (c) isolines of power consumption with strategy lines overlay (kW).

4. Simulation results

4.1. Case studies

Different synthetic case studies were considered to cover different water profiles. A "residential" water profile where the water load is distributed throughout the day, peaking early in the morning and in the evening, and slightly lower during weekends. Weighting Coefficients were used with the residential profile as shown in Table 3. An "Industrial" profile adapted from Ref. [41] representing water use in a large beef packing plant, where weekends have a very low water use compared to weekdays. A "constant" year-round water load to represent a desalination that supplies a constant flow rate to a water network. A "Day only" profile where constant flow rate is supplied for 9h during daytime only (8am to 5pm) was considered to test if such water load shifting to day hours only would enhance the benefits of variable RO operation. Finally, an "Agricultural" water load profile was synthetically built in a way to mimic solar power profile on a typical sunny day, and was weighted with seasonal coefficients (Table 3) adapted from a study representing irrigation of an olive orchards in the Mediterranean [42]. These load profiles are plotted in Fig. 8. It should be noted that all scenarios were scaled in a way that yearly consumption is the is exactly the same, 730,000m3 per year (averaging 2000m3/d) (Table 2).

Investment costs for each of the system components are annualized over their expected lifetimes using an interest rate of 5%. The PV system, the water storage, and the battery [43] systems are annualized over 25
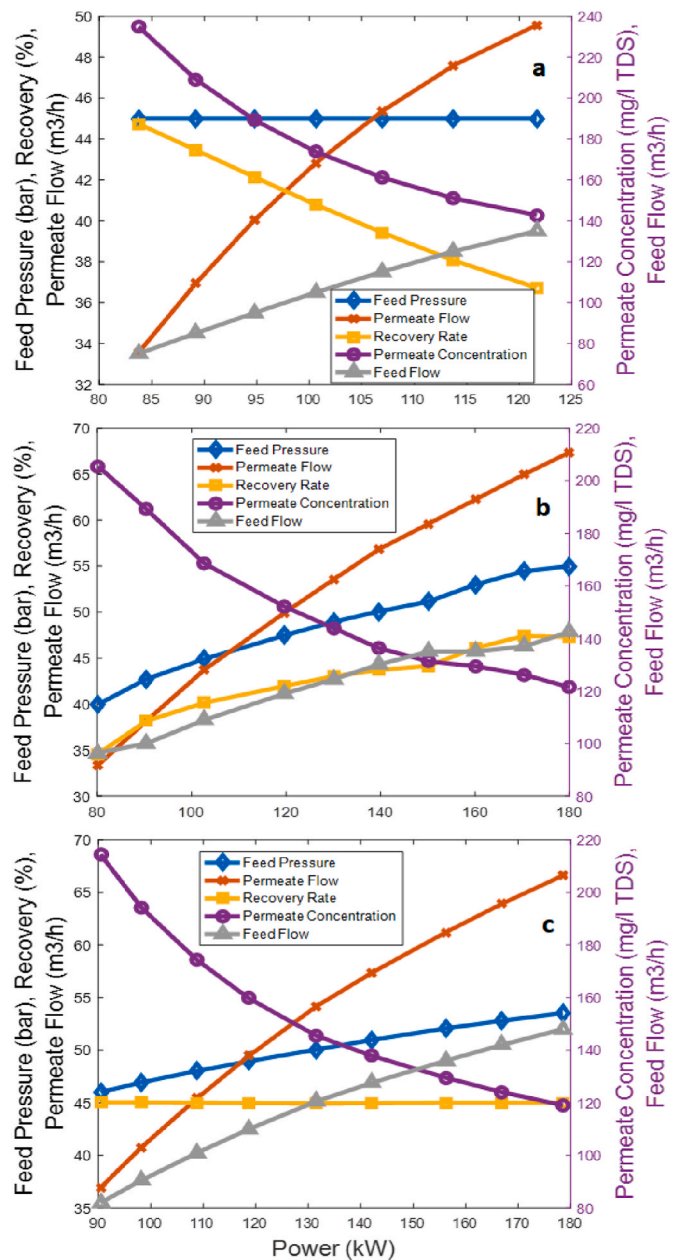

Fig. 7. Operational parameters of different operation strategies a) Fixed pressure 45 bars, b) Lowest SEC, c) Fixed recovery rate 45%.

years, while the diesel generator is annualized over 10 years and the RO system over 20 years. Capital investment costs, annuity factors and maintenance costs used in the simulation are given in Table 4.

The RO plant's minimum up time is fixed to 10 h and a minimum down time of 10h, to ensure the system stability and to allow backwashing of the RO membranes. Diesel generator's minimum up and down time are both set to 2 h. Using the constant recovery rate strategy of 45%, RO operation parameters are determined for each power level, including the permeate flow, which feeds the water tank.

A fixed 94% efficiency is considered for the motor drives as a worst-case scenario efficiency for part-load operations [49]. A fixed 95% efficiency was used for the ERD (minimum efficiency warranted by ERD supplier). Considering fixed efficiencies for the ERD and motor drives is justified by the fact that the variation of their efficiencies is minimal.
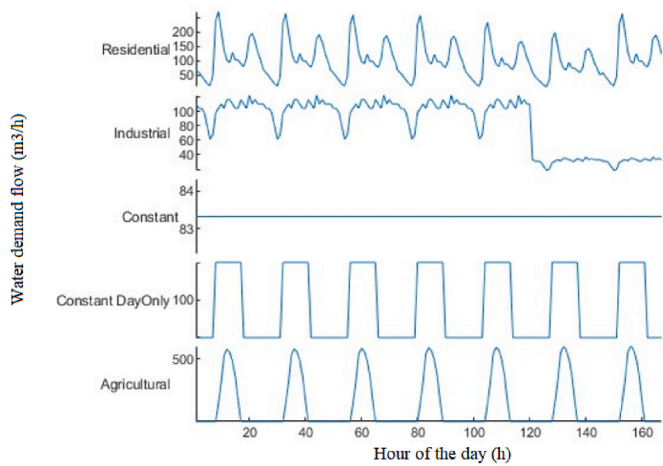
Fig. 8. Plot of one week of the different water demand profiles.

Table 2

Water demand profiles of different case studies considered.

Demand profile	Description	Average Daily Load
Residential	Water demand peaking at 9am and 9pm, with a relatively low flat day use	2000m3
Industrial	High quasi constant load from 8am to 4am, with a small dip between 4am and 8am	2000m3
Constant	Constant all day and night	2000m3
Day Only	Constant for 9h only during daytime, zero at night	2000m3
Agricultural	A hypothetical irrigation load that follows typical solar power profile	2000m3

4.2. Analysis of different component combinations

Each case study was simulated under five different component compositions as detailed in Table 5.

The yearly costs of the optimal solutions found for each combination are shown in the stacked columns graphs for each case study Figs. 9–13 while LCOW values are shown in Fig. 14. In all five case studies considered, the LCOW is the lowest using combinations C4 and C5, followed by C1, C3 and C2 respectively.

In C2 and C3, the RO system is solely powered from PV, and as such, can only operate during day hours with high enough solar resource. Given that PV power slowly builds up in the morning, peaks at noon and later diminishes, and in order to supply the required water demand, the RO, WST and PV systems are excessively oversized to make use of an unstable solar resource in the short periods of sun hours. Such increase

in system sizes results in very high annuity and maintenance costs, and leads to high LCOW values, ranging between 1.76 and $2.37/m^3$. The number of RO system startups per year ranges between 286 and 411 occurrences. Available but unused solar energy (dumped solar fraction) ranges between 71 and 88%, which is a direct result of the excessive PV system oversizing (except for agricultural case study, where this fraction is 47–66%, cf. discussion below).

In C4 and C5, the introduction of backup energy systems (DG and BSS) into the power mix allows the usage of a smaller RO system, WST and PV generator, overcoming much of the effects of PV power intermittency. With C4 and C5, RO system sizes capable of supplying the required water demand are 54–71% smaller than those required in C2 and C3, PV sizes are 59%–80% smaller, and WST sizes are 76–98% smaller (except in the agricultural case study). These tremendous reductions of component sizes naturally lead to lower LCOW which ranges between 0.97 and $1.52/m^3$. The number of RO system startups is reduced to half or less of that with C2 and C3. The fraction of energy supplied by diesel in C4 and C5 ranges between 10 and 13.5% only, meaning that solar is still supplying 86.5–90% of the RO energy consumption. Dumped solar fraction are reduced to a range between 35 and 43% (except in the agricultural case study, where this fraction is 28–32%).

In C1, the RO system is solely powered by a diesel generator, without PV, which means that it can operate at any time of the day, under a steady state (fixed) regime. As a result, the RO system size is at its minimum, reducing the RO annuity and maintenance cost, while diesel cost is at its maximum. In C1, diesel fuel cost ranges between 51 and 56% of the total yearly cost (except in the agricultural case study where

Table 5

Different system compositions simulated.

	RO Fixed with DG, without BSS and without PV	RO Fixed with PV, without BSS and without DG	RO Variable with PV, without BSS and without DG	RO Fixed with BSS and DG and PV	RO Variable with BSS, DG and PV
Composition Number	C1	C2	C3	C4	C5
With Solar Generator		X	X	X	X
With Battery Storage				X	X
With Diesel Generator	X			X	X
Fixed RO Operation	X	X		X	
Variable RO Operation			X		X

Table 3

Seasonal weighting coefficients for residential and agricultural profiles.

	JAN	FEB	MAR	APR	MAY	JUN	JUL	AUG	SEP	OCT	NOV	DEC
Residential	63%	60%	63%	66%	70%	75%	91%	100%	97%	88%	79%	70%
Agriculture	0%	0%	53%	65%	65%	82%	100%	100%	65%	53%	0%	0%

Table 4

Investment, annuity factors and maintenance costs of the system components.

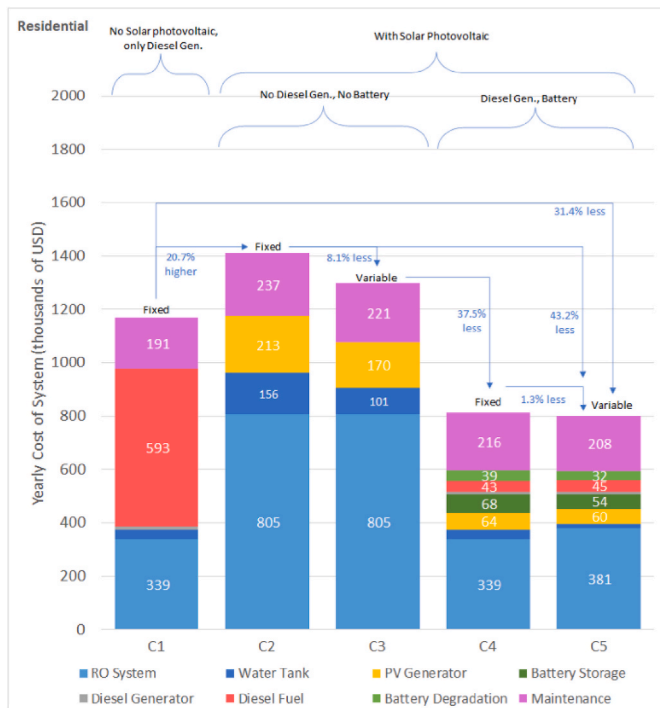| Component	Units	Unit Cost (USD)	Annuity (Years/Rate)	Annuity Factor	Maintenance (USD)	Running Costs (USD)	References
Water Storage Tank	(m3)	220	(25/5%)	0.07095	1% of investment		[21]
Diesel Generator	(kW)	250	(10/5%)	0.1295	0.5$/h	Diesel Fuel 1.2$/L	[44, 45]
Battery Storage	(kWh)	400	(25/5%) half (cf. III-B)	0.07095	1% of investment	Degradation	[46], market survey
Solar Generator	(kWp)	600	(25/5%)	0.07095	1% of investment		[44], market survey
RO Nominal Permeate Flow	(m3/d)	2000	(20/5%)	0.08024	0.25$/m3		[47, 21, 48]

Fig. 9. Residential yearly costs.
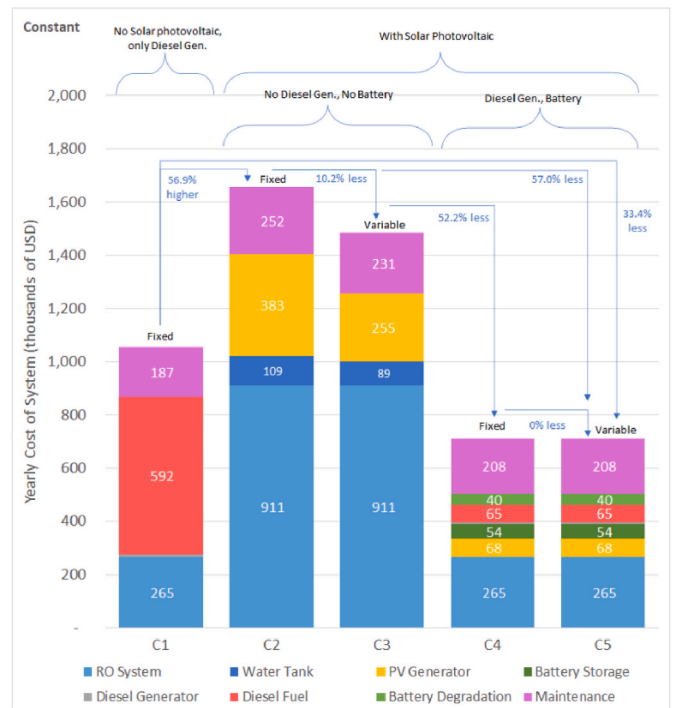
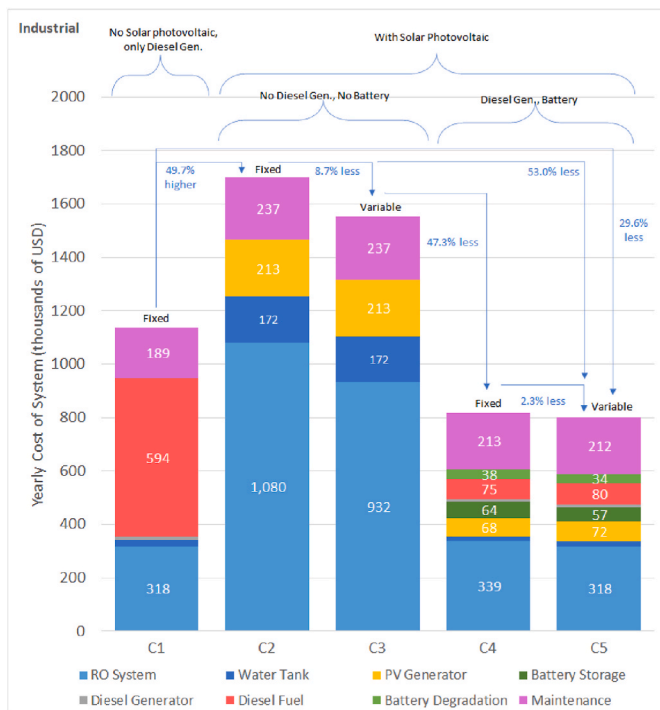

Fig. 11. Constant flow yearly costs.
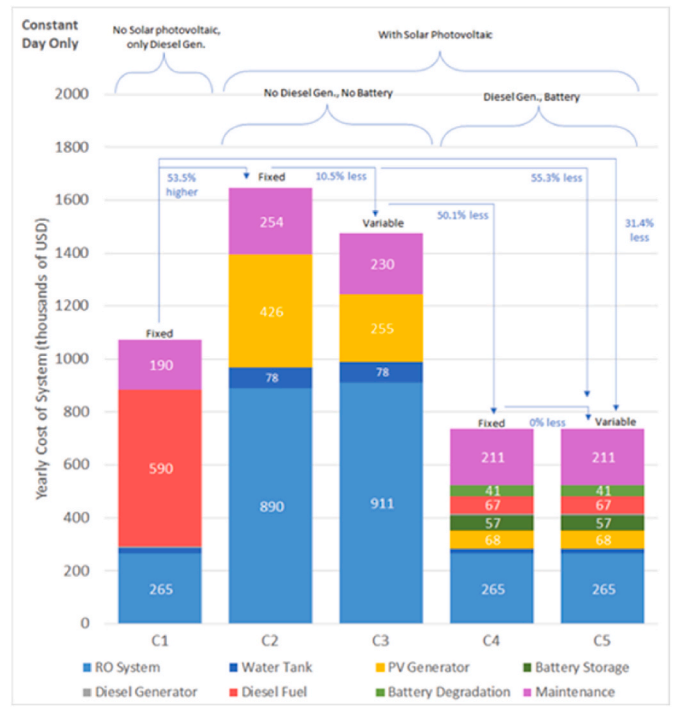

Fig. 10. Industrial yearly costs.

Fig. 12. Constant flow day only yearly costs.

it is 41%). LCOW ranges between 1.44 and $1.60/m^3 (except in agricultural case study where it is $1.98/m^3). The number of RO system startups is similar to that of C4 and C5.

Concerning the agricultural case study, no irrigation of orchards is needed in January, March, November and December, while irrigation peaks in summer month. Considering that similar yearly water needs are used in all case studies, RO system size for agricultural use should be much larger than that in other case studies. On the other, the high

summer water demand coincides with high summer solar resources, leading to smaller WST, smaller BSS, and smaller fractions of dumped PV power. The increased costs due to larger RO system is much higher than the savings resulting from smaller WST and BSS, which results in significantly higher LCOW for this case study.

We conclude that C4 and C5 combinations are to be favored when considering the supply of energy to an RO plant that cannot be supplied by grid power. C4 is 36–57% cheaper than C2. Interestingly enough, C1
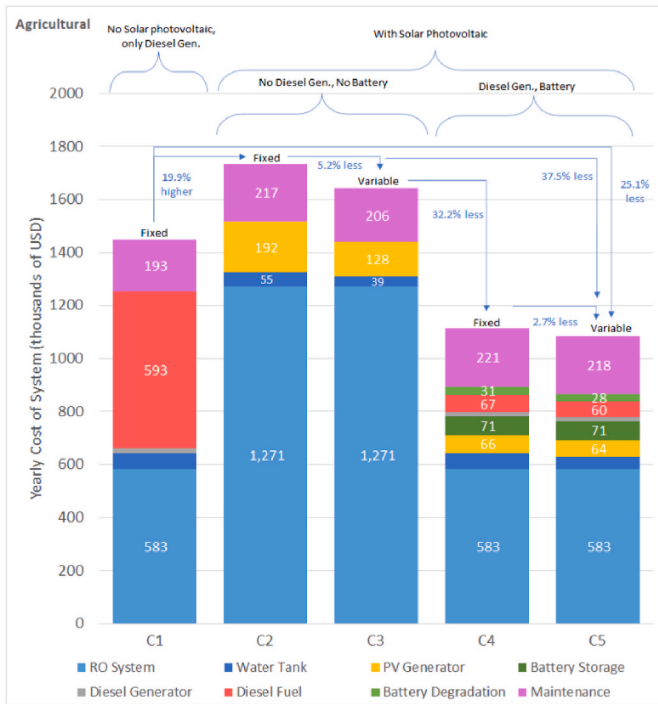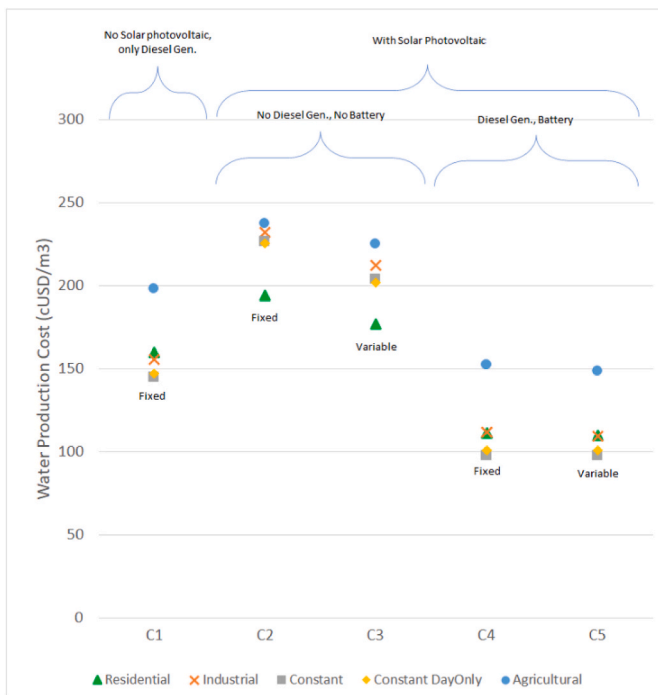
Fig. 13. Agricultural yearly costs.

Fig. 14. Levelized cost of water for the considered case studies.

is more cost effective than C2 and C3. This means that as long as CO2 emissions are not taxed, supplying an RO system with solar power without DG and BSS is more expensive than supplying it using diesel fuel (20–57% more expensive). These values are obtained using a diesel cost of $1.2/liter, and would certainly evolve if diesel prices changes.

4.3. Analysis of the variable RO operation

The only difference between C2 and C3 being that C3 is allowed to

vary the RO power level (within SOW) while C2 only uses a fixed power level equal to nominal RO power. Yearly cost savings attributed to variable operation are seen by comparing C2 to C3 where DG and BSS are not used. Similar comparison between C4 and C5 applies to the case where DG and BSS are used. Table 6 summarizes these savings.

When no energy backup systems are used, modulating the RO power level significantly reduces yearly costs. These savings come from the fact that the RO plant will be modulating its power level whenever solar resource is not enough to run at full power, yet enough to operate within its SOW, or else when the WST is full. Typical winter and summer behavior is shown in Fig. 15 for C3 in the constant case study. Looking at these graphs, it is clear that the benefit from variable RO operation is almost null during most of the day. In fact, the conditions needed for RO power modulation occur during morning and evening times, and during cloudy days, but never during strong sun hours. Under strong sun hours, the RO plant is runs at its nominal rate, especially that C3 always boosts an excessively oversized PV system as discussed in section I.B above.

Fig. 16 shows the frequency of RO operation levels for C2/C3, and for C4/C5 for all case studies considered. The large modular operation around 51% in constant day-only under C3 mostly represents reduction of power level during summer caused by a full tank condition and as such doesn't represent savings attributed to variable operation. Such condition doesn't show under the constant case study as the WST level is reduced during the nights, and then filled back up during the day.

Overall, savings shown in Table 6 between C2 and C3 are attributed to the reduction in required system component sizes in C3, either through a smaller solar generator, a smaller WST or a smaller RO system, or a mix of those. These savings vary with the profiles of daily and seasonal water demand. To better understand the effect of the demand profiles, Table 7 shows the RO system annuity cost portion out of the total yearly costs for all case studies and combinations considered. This portion is clearly the largest between all cost centers and is a direct result of the high RO capital costs.

In fact, with a value of $2000/(m^{3}d^{-1}) as shown in Table 4, RO CAPEX is very high relatively to other components CAPEX, in a way that it becomes economically not effective to install a large RO system and then modulate its power level to match solar resources. On the contrary, with the current cheap costs of PV systems, oversizing the PV generator in a way to allow maximum usage of the RO plant becomes more optimal. This observation explains the lower percentage of savings seen in the agricultural case study between C2 and C3, as the RO CAPEX represents on its own 77% in C3, in addition to the lower utilization time (RO plant being off in during 4 months of the rainy season).

The very low or null savings between C4 and C5 shown in Table 6 are also explained by the high RO CAPEX relatively to other components of the system. The inclusion of DG and BSS gives so much operation flexibility, such that optimal solutions always tend to minimize the RO system size to a middle point between that needed for the most demanding periods of the year and the less demanding parts of the year. This is particularly shown in the 0% savings between C4 and C5 in the constant and constant day-only case studies. An extract of winter and summer operation under C5 is shown in Fig. 17. The optimal solution found under C5 ends up being running the RO plant at a fixed power level equal to nominal power level, leading to an exact same behavior as in C4. During winter, the diesel generator kicks in whenever the BSS level low (20%) and let then turns off when solar power is available. In

Table 6
Savings on yearly costs resulting from variable operation.

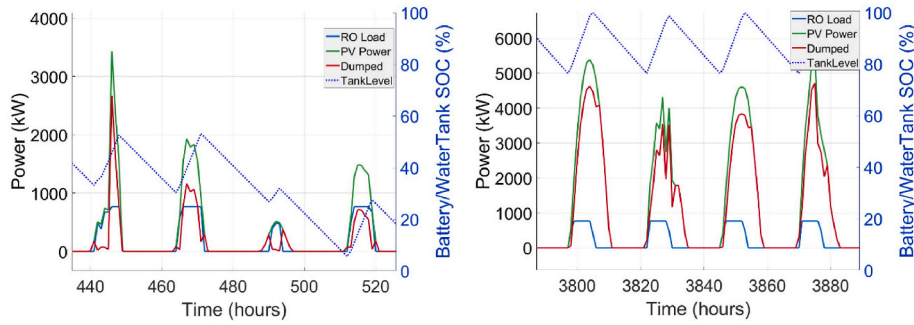|	Using C3 instead of C2	Using C5 instead of C4
Residential	8.1%	1.3%
Industrial	8.7%	2.3%
Constant	10.2%	0.0%
Constant day only	10.5%	0.0%
Agricultural	5.2%	2.7%

Fig. 15. Extract of typical winter (left) and summer (right) days under C3 in the Constant case study.
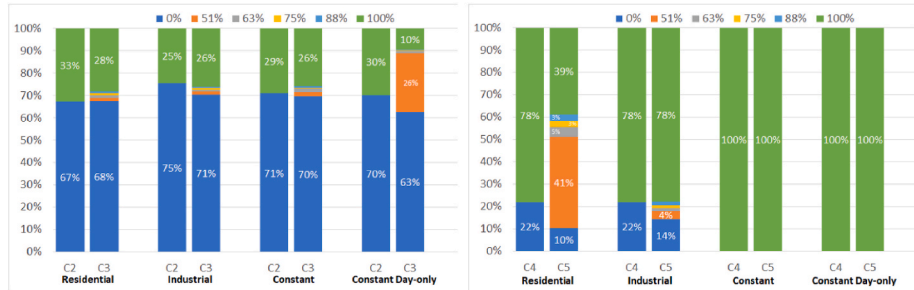

Fig. 16. Frequencies of RO power operation levels under C2 and C3 (left) and under C4 and C5 (right).

Table 7
RO annuity portion of total yearly cost.

	C1	C2	C3	C4	C5
Residential	29%	57%	62%	42%	48%
Industrial	28%	63%	60%	41%	40%
Constant	25%	55%	61%	37%	37%
Constant day only	25%	54%	62%	36%	36%
Agricultural	40%	73%	77%	52%	54%
Average	**29%**	**61%**	**64%**	**42%**	**43%**

summer, the diesel generator is not run at all, as the BSS stores enough power during the day to keep the fixed full level operation of the RO plant.

The relatively small savings attributed to variable operation shown for agricultural, industrial, and residential case studies (2.7%, 2.3%, and 1.3% respectively) come from the slight RO oversizing caused by the seasonal variation in the agricultural and residential case studies and the weekend low load in the industrial case study. With a slightly larger than needed RO plant during low load periods, variable operation kicks in and makes use of any small amount of solar power available. This is clarified in.

Simply put, the current CAPEX costs of RO systems are high enough not to permit variable operation from being economically attractive whenever backup energy sources are possible.

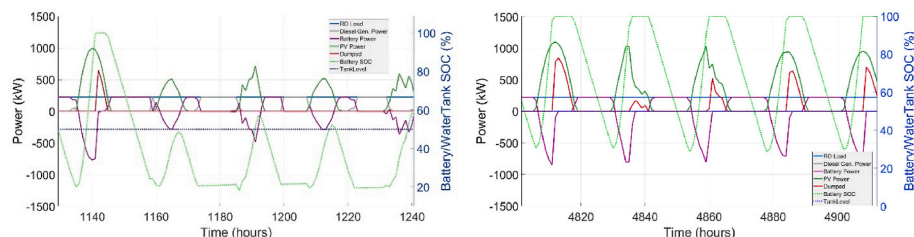Following Table 8 shows main results under C5 for all case studies.

System reliability, or ability to supply the specified demand throughout the operating period, is built in the Ordinal Optimization process. When a particular design is simulated, using the simple model, and the energy not supplied (ENS) is large because of inability to supply the required demand, then that design is penalized in proportion. On the other hand, oversized designs would yield larger costs and as a result are also likely to be rejected as they have a higher order in the ordinal optimization process.

A sensitivity analysis would not have significantly changed the conclusions on the merit of the different scenarios as long as prices changes are within reasonable range. For example, PV prices have to increase ten folds to make scenarios C4 or C5 more expensive than Scenario C1 relying on DG operation only. In another example, let us note that the PV sizes in C4 and C5 are 33% the PV size of C2. Therefore, a large increase in the PV prices would make C4 and C5 more favorable. Even a large drop in the PV price of 50% would still keep the optimal designs of Scenarios C4 and C5 more favorable that those of C2 and C3. From an operational point of view, the system stability against load variations is guaranteed by the presence of a diesel generator, which can be run more or less as needed.

5. Conclusion

In this work, we developed a flexible and accurate RO system model and integrated it with models of a PV plant, a battery, and a diesel generator using the method of dynamic programming (DP) to minimize

Fig. 17. Extract of typical winter (left) and summer (right) days under C5 in Constant case study.

Table 8
Main results under C5.

			Residential	Industrial	Constant	Constant Day only	Agricultural
Component Sizes	Water Storage Tank	(m3)	800	1200	100	1200	3000
	Diesel Generator	(kW)	270	270	270	225	450
	Battery Storag	(kWh)	3800	4000	3800	4000	5000
	Solar Generator	(kWp)	1400	1700	1600	1600	1500
	RO Nominal Permeate Flow	(m3/d)	2878	2398	2000	2000	4397
Annuity costs	Water Storage Tank	(1000 USD)	12.5	18.7	1.6	18.7	46.8
	Diesel Generator	(1000 USD)	8.7	8.7	8.7	7.3	14.6
	Battery Storage	(1000 USD)	53.9	56.8	53.9	56.8	71.0
	Solar Generator	(1000 USD)	59.6	72.4	68.1	68.1	63.9
	RO System	(1000 USD)	381.3	317.8	265.0	265.0	582.5
Investment Annuity		(1000 USD)	516.0	474.4	397.3	415.9	778.7
Investment Value		(1000 USD)	7355.5	6911.5	5871.9	6182.7	10,932.5
O&M Costs	Diesel Fuel Spent	(1000 USD)	44.8	80.0	65.4	67.2	59.5
	Battery Degradation	(1000 USD)	32.2	34.1	40.3	41.5	27.8
	Maintence Cost	(1000 USD)	208.3	212.0	208.1	211.4	218.4
Yearly System Cost		(1000 USD)	**801.3**	**800.5**	**711.1**	**735.9**	**1084.5**
Indicators	Count RO Yearly Startups	(Occurences)	176	76	–	–	421
	Generator Running Time	(Hours)	909	1282	1131	1233	570
	Solar Fraction	(%)	92.5	86.8	89.1	88.7	90.1
	Diesel Fraction	(%)	7.7	13.5	11.0	11.2	10.0
	Dumped Solar	(%)	29.8	43.6	38.0	35.5	28.6
Water Cost	RO Energy Consumed	(MWh)	1883	1945	1956	1956	1937
	Water Produced	(m3)	730,176	729,814	730,000	730,000	731,435
	Specific Energy Consumption	(kWh/m3)	2.58	2.67	2.68	2.68	2.65
	Energy Cost	(USD/MWh)	425.6	411.5	363.6	376.2	560.0
	LCOW	(USD/m3)	**1.10**	**1.10**	**0.97**	**1.01**	**1.48**

the cost of system operation, accounting for diesel fuel usage and battery degradation. We used ordinal optimization (OO) to examine the large design search space quickly but exhaustively using a simple model. We then ranked the different designs in increasing cost order and assessed a reduced number of designs using an accurate model that simulates the system on an hourly basis for all the days of a year. This approach relies on the fundamental tenet of OO: "order is robust to noise introduced by the simple model". The simple model samples the year using only 48 days and uses only three operational levels of the RO plant and diesel generator (DG).

The Optimal sizing and operational results are presented for five different case studies, with the objective of minimizing the yearly cost of operation of water production. The variable operation of an RO plant solely powered by solar PV was demonstrated to reduce yearly costs by about 5–10% depending on water demand profiles. The addition of a diesel generator and a battery storage system to the energy mix reduces costs by 36–57%, but almost negates the effectiveness of variable operation. The savings attributed to variable operation decrease to a range between 0 and 2.7%. Diesel fuel-based operation without solar is found to be more cost effective than using PV-RO without backup energy systems.

These results depend on the cost factors used in the simulation and may be enhanced by a sensitivity analysis on the diesel fuel price, the different prices of each of the system components and their respective maintenance costs. They can also be enhanced by the inclusion of components yearly degradation factors in order to account for any forecasted losses of system efficiencies, and by the inclusion of seasonal variations in feed water temperature. Applying this simulation to different locations with different solar irradiance patterns, and the application of different minimum startup and shutdown times would also help understand their respective effects on variable operation.

Financial disclosure

None reported.

CRediT authorship contribution statement

Adnan Zein: Conceptualization, Methodology, Software, Writing. and. **Sami Karaki:** Conceptualization, Methodology, Software, Writing, Supervision, Reviewing. and. **Mahmoud Al-Hindi:** Supervision, Reviewing.

Declaration of competing interest

The authors declare that they have no known competing financial interests or personal relationships that could have appeared to influence the work reported in this paper.

References

[1] M. Castro, M. Alcanzare, E. Esparcia, J. Ocon, A comparative techno-economic analysis of different desalination technologies in off-grid islands, Energies 2261 (2020) 13.

[2] D. Borge-Diez, F.J. García-Moya, P. Cabrera-Santana, E. Rosales-Asensio, Feasibility analysis of wind and solar powered desalination plants: an application to islands, Sci. Total Environ 764 (2021) 142878.

[3] B. Giovanni, B. Annamaria, F. Cesare, G. Giovanni, P. Adolfo, Supporting the sustainable energy transition in the canary islands: simulation and optimization of multiple energy system layouts and economic scenarios, Frontiers in Sustainable Cities 3 (2021).

[4] H. Nassrullah, S.F. Anis, R. Hashaikeh, N. Hilal, Energy for desalination: a state-of-the-art review, Desalination 491 (2020) 114569.

[5] Dow Chemicals, FILMTEC reverse osmosis membranes technical manual [Online]. Available: https://www.dupont.com/content/dam/dupont/amer/us/en/water-solutions/public/documents/en/RO-NF-FilmTec-Manual-45-D01504-en.pdf, June 2022. (Accessed 1 August 2022).

[6] A. Abufayed, Performance characteristics of a cyclically operated seawater desalination plant in Tajoura, Libya 156 (2003).

[7] F. Latorre, S. Báez, A. Gotor, in: Energy performance of a reverse osmosis desalination plant operating with variable pressure and flow, 366, 2015.

[8] V. Subiela, J. Fuente, G. Piernavieja, B. Peñate, in: Canary Islands Institute of Technology (ITC) experiences in desalination, 7, 2009.

[9] N. Al-Bastak, A. Abbas, Periodic operation of a reverse osmosis water desalination unit, Taylor France Group. 33 (16) (1998) 2531–2540.

[10] B. Richards, D. Capão, W. Früh, A. Schäfer, in: Renewable energy powered membrane technology Impact of solar irradiance fluctuations on performance of a brackish water reverse osmosis system, 156, 2015.

[11] A. Ruiz-García, I. Nuez, Long-term intermittent operation of a full-scale BWRO desalination plant, Desalination489 (2020) 114526.

[12] M. Freire-Gormaly, A. Bilton, Impact of intermittent operation on reverse osmosis membrane fouling for brackish groundwater desalination systems, J. Membr. Sci. (583) (2019) 220–230.

[13] M. Freire-Gormaly, A. Bilton, Design of photovoltaic powered reverse osmosis desalination systems considering membrane fouling caused by intermittent operation, Renew. Energy (135) (2019) 108–121.

[14] P. Feron, in: Use Of Windpower In Autonomous Reverse Osmosis Seawater Desalination, 9, 1985.

[15] R. Pohl, M. Kaltschmitt, R. Holländer, in: Investigation of different operational strategies for the variable operation of a simple, 249, 2009.

[16] B. Richards, G. Park, T. Pietzsch, A. Schäfer, in: Renewable energy powered membrane technology: Safe operating window of a brackish water desalination system, 468, 2014.

[17] M.T. Mito, X. Ma, H. Albuflasa, P.A. Davies, Variable operation of a renewable energy-driven reverse osmosis system using model predictive control and variable recovery: towards large-scale implementation, Desalination 532 (2022) 115715.

[18] A. Ruiz-García, I. Nuez, Simulation-based assessment of safe operating windows and optimization in full-scale seawater reverse osmosis systems, Desalination 533 (2022) 115768.

[19] S. Modarresi, B. Abada, S. Sivaranjani, L. Xie, S. Chellam, Planning of survivable nano-grids through jointly optimized water and electricity: the case of Colonias at the Texas-Mexico border, Appl. Energy 278 (2020) 115586.

[20] M. Heihsel, S.M.H. Ali, J. Kirchherr, M. Lenzen, Renewable-powered desalination as an optimisation pathway for renewable energy systems: the case of Australia's Murray–Darling Basin, Environ. Res. Lett. 14 (2019) 124054.

[21] J.A. Carta, P. Cabrera, Optimal sizing of stand-alone wind-powered seawater reverse osmosis plants without use of massive energy storage, Appl. Energy 304 (2021) 117888.

[22] A. Jiang, J. Wang, L.T. Biegler, W. Cheng, C. Xing, Z. Jiang, Operational cost optimization of a full-scale SWRO system under multi-parameter variable conditions ,Desalination, 355, (2015), 124 -140.

[23] J. Leijon, D. Salar, J. Engström, M. Leijon, C. Boström, Variable renewable energy sources for powering reverse osmosis desalination, with a case study of wave powered desalination for Kilifi, Kenya, Desalination 494 (2020) 114669.

[24] S. Loutatidou, N. Liosis, R. Pohl, T.B. Ouarda, H.A. Arafat, Wind-powered desalination for strategic water storage: techno-economic assessment of concept, Desalination 408 (2017) 36–51.

[25] A. Zein, C. Ghabech, S. Karaki, Optimization of a solar photovoltaic micro grid for electricity and desalinated water production, in: 4th International Conference on Renewable Energies for Developing Countries (REDEC), 2018.

[26] R. Jabr, B. Pal, Ordinal Optimisation Approach for Locating and Sizing of Distributed Generation, 2009.

[27] S. Karaki, R. Dinnawi, R. Jabr, R. Chedid, F. Panik, Fuel Cell Hybrid Electric Vehicle Sizing Using Ordinal Optimization, 2015.

[28] Y. Luo, M. Guignard, C. Chen, A hybrid approach for integer programming combining genetic algorithms, Linear Program. Ordinal. Optimization. 12 (2001).

[29] PVSyst, PVSyst scientific publications section [Online]. Available: https://www.pvsyst.com/scientific-publications/, 2020, 2022.

[30] S. Karaki, R. Jabr, R. Chedid, F. Panik, Optimal Energy Management of Hybrid Fuel Cell Electric Vehicles, 2015.

[31] T. Weitzel, M. Schneider, C. Glock, F. Lober, S. Rinderknecht, Operating a storage-augmented hybrid microgrid considering battery aging costs, J. Clean. Prod. 188 (2018) 638–654.

[32] Lenntech, Dow filmtec SW30XLE-440i [Online]. Available: https://www.lenntech.com/Data-sheets/Dow-Filmtec-SW30XLE-440i.pdf, 2021.

[33] FLOWSERVE, HP pump MSH-065-B [Online]. Available: https://www.flowserve.com/en/products/products-catalog/pumps/between-bearings-pumps/horizontal-multistage-single-case-msh/, 2019. (Accessed 6 February 2019).

[34] FLOWSERVE, BP pump 3HPX7-TOP [Online]. Available: https://www.flowserve.com/en/products/products-catalog/pumps/overhung-pumps/api-process-pumps-hhpx/, 2019. (Accessed 6 February 2019).

[35] FLOWSERVE, SWI pump 4HPX12-TOP [Online]. Available: https://www.flowserve.com/en/products/products-catalog/pumps/overhung-pumps/api-process-pumps-hhpx/, 2019. (Accessed 6 February 2019).

[36] Danfoss, ERD iSave. https://www.danfoss.com/en/products/hpp/energy-recovery-devices/, 2021.

[37] energy recovery, PX Q300. https://energyrecovery.com/resource/px-q-series/, 2021.

[38] Dupont, WAVE user manual. https://www.dupont.com/Wave/Default.htm, 2021.

[39] C. Richardson, H. Kennedy, C. Duarte, D. Kennedy, S. Proud, Age and growth of the fan mussel Pinna nobilis from south-east Spanish Mediterranean seagrass (Posidonia oceanica) meadows, Mar. Biol. (133) (1999) 205–212.

[40] C. Koutsou, E. Kritikos, A. Karabelas, M. Kostoglou, Analysis of temperature effects on the specific energy consumption in reverse osmosis desalination processes, Desalination 476 (2020) 114213.

[41] S. Li, R.M.M. Ziara, B. Dvorak, J. Subbiah, Assessment of water and energy use at process level in the U.S. beef packing industry: case study in a typical U.S. large-size plant, J. Food Process. Eng. 41 (2018), e12919.

[42] G. Todde, L. Murgia, P.A. Deligios, R. Hogan, I. Carrelo, M. Moreira, A. Pazzona, L. Ledda, L. Narvarte, Energy and environmental performances of hybrid photovoltaic irrigation systems in Mediterranean intensive and super-intensive olive orchards, Sci. Total Environ. 651 (2019) 2514–2523.

[43] Saft Batteries, Intensium max 20 high energy [Online]. Available: https://www.saftbatteries.com/products-solutions/products/intensium%C2%AE-max-20-high-energy-nmc, 2022.

[44] H. Masrur, H. Howlader, M. Elsayed Lotfy, K. Khan, J. Guerrero, T. Senjyu, Analysis of techno-economic-environmental suitability of an isolated microgrid system located in a remote island of Bangladesh, Sustainability 12 (2020) 2880.

[45] H. Mehrjerdi, Modeling and optimization of an island water-energy nexus powered by a hybrid solar-wind renewable system, Energy 197 (2020) 117217.

[46] C.D. R.-G, et al., A siting and sizing optimization approach for PV–Battery–Diesel hybrid systems, IEEE Trans. Ind. Appl. 54 (2018) 2637–2645.

[47] C. Upeksha, B. Christian, Learning curve for seawater reverse osmosis desalination plants: capital cost trend of the past, present, and future, Water Resour. Res. 53 (2017) 10523–10538.

[48] S. Bhojwani, K. Topolski, R. Mukherjee, D. Sengupta, M.M. El-Halwagi, Technology review and data analysis for cost assessment of water treatment systems, Sci. Total Environ. 651 (2019) 2749–2761.

[49] U.S. Department of Energy, Adjustable speed drive part-load efficiency DOE/GO-102012-3730, Energy Efficiency Renewable Energy. (2012). https://www.energy.gov/sites/prod/files/2014/04/f15/motor_tip_sheet11.pdf.

BIBLIOGRAPHY

Abufayed, A. (2003). Performance characteristics of a cyclically operated seawater

    desalination plant in Tajoura, Libya. *156*.

Al-Bastak, N., & Abbas, A. (1998). Periodic Operation of a Reverse Osmosis Water

    Desalination Unit. *Taylor & Francis Group, 33*(16), 2531-2540.

Bhojwani, S., Topolski, K., Mukherjee, R., Sengupta, D., & El-Halwagi, M. M. (2019).

    Technology review and data analysis for cost assessment of water treatment systems.

    Science of The Total Environment.

Borge-Diez, D., García-Moya, F. J., Cabrera-Santana, P., & Rosales-Asensio, E. (2021).

    Feasibility analysis of wind and solar powered desalination plants: An application to

    islands. *Science of The Total Environment*.

Carta, J. A., & Cabrera, P. (2021). Optimal sizing of stand-alone wind-powered seawater

    reverse osmosis plants without use of massive energy storage. *Applied Energy*.

Castro, M., Alcanzare, M., Esparcia, E., & Ocon, J. (2020). A Comparative Techno-

    Economic Analysis of Different Desalination Technologies in Off-Grid Islands.

    Energies .

CAT DG C18-600. (2023). Retrieved from CAT:

    https://www.cat.com/en_US/products/new/power-systems/electric-power/diesel-

    generator-sets/1000027412.html

Cazenave, A., & Jaber, B. (2001). Recent sea level change in the Mediterranean Sea revealed

    by topex/poseidon satellite altimetry. *Geophysical Research Letters, 28*(8), 4.

Danfoss. (2021). ERD iSave. https://www.danfoss.com/en/products/hpp/energy-recovery-

    devices/.

Dow Chemicals. (2022, June). *FILMTEC Reverse Osmosis Membranes Technical Manual.*

    Retrieved August 01, 2022, from

https://www.dupont.com/content/dam/dupont/amer/us/en/water-solutions/public/documents/en/RO-NF-FilmTec-Manual-45-D01504-en.pdf

Dupont. (2021). WAVE user manual. https://www.dupont.com/Wave/Default.htm.

energy recovery. (2021). PX Q300. https://energyrecovery.com/resource/px-q-series/.

Feron, P. (1985). USE OF WINDPOWER IN AUTONOMOUS REVERSE OSMOSIS SEAWATER DESALINATION. *9*.

Fleer, J., Zurmühlen, S., Meyer, J., Badeda, J., Stenzel, P., Hake, J.-F., & Sauer, D. U. (2018). Techno-economic evaluation of battery energy storage systems on the primary control reserve market under consideration of price trends and bidding strategies. *Journal of Energy Storage*, 345-356.

FLOWSERVE. (2019). *BP Pump 3HPX7-TOP*. Retrieved Feb 06, 2019, from https://www.flowserve.com/en/products/products-catalog/pumps/overhung-pumps/api-process-pumps-hhpx/

FLOWSERVE. (2019). *HP Pump MSH-065-B*. Retrieved Feb 06, 2019, from https://www.flowserve.com/en/products/products-catalog/pumps/between-bearings-pumps/horizontal-multistage-single-case-msh/

FLOWSERVE. (2019). *SWI Pump 4HPX12-TOP*. Retrieved Feb 06, 2019, from https://www.flowserve.com/en/products/products-catalog/pumps/overhung-pumps/api-process-pumps-hhpx/

Freire-Gormaly, M., & Bilton, A. (2019). Design of photovoltaic powered reverse osmosis desalination systems considering membrane fouling caused by intermittent operation. *Renewable Energy*(135), 108-121.

Freire-Gormaly, M., & Bilton, A. (2019). Impact of intermittent operation on reverse osmosis membrane fouling for brackish groundwater desalination systems. *Journal of Membrane Science*(583), 220-230.

Ghazi, Z. M., Rizvi, S. W., Shahid, W. M., Abdulhameed, A. M., Saleem, H., & Zaidi, S. J. (2022). An overview of water desalination systems integrated with renewable energy sources. *Desalination, 542*.

Giovanni, B., Annamaria, B., Cesare, F., Giovanni, G., & Adolfo, P. (2021). Supporting the Sustainable Energy Transition in the Canary Islands: Simulation and Optimization of Multiple Energy System Layouts and Economic Scenarios. *Frontiers in Sustainable Cities*.

Heihsel, M., Ali, S. M., Kirchherr, J., & Lenzen, M. (2019). Renewable-powered desalination as an optimisation pathway for renewable energy systems: the case of Australia's Murray–Darling Basin. *Environmental Research Letters*.

Helveston, J., He, G., & Davidson, M. (2022). Quantifying the cost savings of global solar photovoltaic supply chains. *Nature*, 83-87.

Jabr, R., & Pal, B. (2009). Ordinal optimisation approach for locating and sizing of distributed generation.

Jiang, A., Wang, J., Biegler, L. T., Cheng, W., Xing, C., & Jiang, Z. (2015). Operational cost optimization of a full-scale SWRO system under multi-parameter variable conditions. *Desalination*.

Karaki, S., Dinnawi, R., Jabr, R., Chedid, R., & Panik, F. (2015). Fuel Cell Hybrid Electric Vehicle Sizing using Ordinal Optimization.

Koutsou, C., Kritikos, E., Karabelas, A., & Kostoglou, M. (2020). Analysis of temperature effects on the specific energy consumption in reverse osmosis desalination processes. *Desalination,*.

Latorre, F., Báez, S., & Gotor, A. (2015). Energy performance of a reverse osmosis desalination plant operating with variable pressure and flow. *366*.

Leijon, J., Salar, D., Engström, J., Leijon, M., & Boström, C. (2020). Variable renewable
     energy sources for powering reverse osmosis desalination, with a case study of wave
     powered desalination for Kilifi, Kenya. *Desalination*.

Lenntech. (n.d.). *Dow Filmtec SW30XLE-440i.* Retrieved 2021, from
     https://www.lenntech.com/Data-sheets/Dow-Filmtec-SW30XLE-440i.pdf

Li, S., Ziara, R. M., Dvorak, B., & Subbiah, J. (2018). Assessment of water and energy use at
     process level in the U.S. beef packing industry: Case study in a typical U.S. large-size
     plant. *Journal of Food Process Engineering*.

Loutatidou, S., Liosis, N., Pohl, R., Ouarda, T. B., & Arafat, H. A. (2017). Wind-powered
     desalination for strategic water storage: Techno-economic assessment of concept.
     Desalination,.

Luo, Y., Guignard, M., & Chen, C. (2001). A hybrid approach for integer programming
     combining genetic algorithms, linear programming and ordinal optimization. *12*.

Masrur, H., Howlader, H., Elsayed Lotfy, M., Khan, K., Guerrero, J., & Senjyu, T. (2020).
     Analysis of Techno-Economic-Environmental Suitability of an Isolated Microgrid
     System Located in a Remote Island of Bangladesh. *Sustainability* .

Mehrjerdi, H. (2020). Modeling and optimization of an island water-energy nexus powered
     by a hybrid solar-wind renewable system. *Energy*.

Mito, M. T., Ma, X., Albuflasa, H., & Davies, P. A. (2022). Variable operation of a
     renewable energy-driven reverse osmosis system using model predictive control and
     variable recovery: Towards large-scale implementation. *Desalination,*.

Mobarra, M., Rezkallah, M., & Ilinca, A. (2022). Variable Speed Diesel Generators:
     Performance and Characteristic Comparison. *ENERGIES, 15*.

Modarresi, S., Abada, B., Sivaranjani, S., Xie, L., & Chellam, S. (2020). Planning of survivable nano-grids through jointly optimized water and electricity: The case of Colonias at the Texas-Mexico border. *Applied Energy*.

Nassrullah, H., Anis, S. F., Hashaikeh, R., & Hilal, N. (2020). Energy for desalination: A state-of-the-art review. *Desalination*.

Pohl, R., Kaltschmitt, M., & Holländer, R. (2009). Investigation of different operational strategies for the variable operation of a simple. *249*.

PVSyst. (2020). *PVSyst scientific publications section*. Retrieved 2022, from https://www.pvsyst.com/scientific-publications/

Richards, B., Capão, D., Früh, W., & Schäfer, A. (2015). Renewable energy powered membrane technology Impact of solar irradiance fluctuations on performance of a brackish water reverse osmosis system. *156*.

Richards, B., Park, G., Pietzsch, T., & Schäfer, A. (2014). Renewable energy powered membrane technology: Safe operating window of a brackish water desalination system. *468*.

Richardson, C., Kennedy, H., Duarte, C., Kennedy, D., & Proud, S. (1999). Age and growth of the fan mussel Pinna nobilis from south-east Spanish Mediterranean seagrass (Posidonia oceanica) meadows. *Marine Biology*(133), 205-212.

Rodríguez-Gallegos, C. D., Gandhi, O., Yang, D., Alvarez-Alvarado, M. S., Zhang, W., Reindl, T., & Panda, S. K. (2018). A Siting and Sizing Optimization Approach for PV–Battery–Diesel Hybrid Systems. *IEEE Transactions on Industry Applications*.

Rosales-Asensio, E., García-Moya, F., Borge-Diez, D., & Colmenar-Santos, A. (2022). Stress Mitigation of Conventional Water Resources in Water-Scarce Areas Through the Use of Renewable Energy Powered Desalination Plants: An Application to the Canary Islands. Springer, Cham.

Ruiz-García, A., & Nuez, I. (2020). Long-term intermittent operation of a full-scale BWRO desalination plant. *Desalination,.*

Ruiz-García, A., & Nuez, I. (2022). Simulation-based assessment of safe operating windows and optimization in full-scale seawater reverse osmosis systems. *Desalination.*

Saft Batteries. (n.d.). *Intensium Max 20 High Energy*. Retrieved 2022, from https://www.saftbatteries.com/products-solutions/products/intensium%C2%AE-max-20-high-energy-nmc

Subiela, V., Fuente, J., Piernavieja, G., & Peñate, B. (2009). Canary Islands Institute of Technology (ITC) experiences in desalination. *7.*

Sunny Tripower Core1. (2022). Retrieved from SMA: https://www.sma.de/en/products/solarinverters/sunny-tripower-core1

Todde, G., Murgia, L., Deligios, P. A., Hogan, R., Carrelo, I., Moreira, M., . . . Narvarte, L. (2019). Energy and environmental performances of hybrid photovoltaic irrigation systems in Mediterranean intensive and super-intensive olive orchards. *Science of The Total Environment.*

U.S. Department of Energy . (2012). Adjustable Speed Drive Part-Load Efficiency DOE/GO-102012-3730 . Energy Efficiency and Renewable Energy https://www.energy.gov/sites/prod/files/2014/04/f15/motor_tip_sheet11.pdf.

Upeksha, C., & Christian, B. (2017). Learning Curve for Seawater Reverse Osmosis Desalination Plants: Capital Cost Trend of the Past, Present, and Future. *Water Resources Research.*

Weitzel, T., Schneider, M., Glock, C., Lober, F., & Rinderknecht, S. (2018). Operating a storage-augmented hybrid microgrid considering battery aging costs. *Journal of Cleaner Production, 188*, 638-654.

Zein, A., Ghabech, C., & Karaki, S. (2018). Optimization of a Solar Photovoltaic Micro Grid for Electricity and Desalinated Water Production. *4th International Conference on Renewable Energies for Developing Countries (REDEC)*.